Identification of novel regulators of growth angle control in Arabidopsis lateral roots and shoots

Martina De Angelis

Submitted in accordance with the requirements for the degree of
Doctor of Philosophy

The University of Leeds
School of Biology
Centre for Plant Sciences

March 2023

The candidate confirms that the work submitted is her own and that appropriate credit has been given where reference has been made to the work of others.

To Barbara and Vittoria

Acknowledgements

I'd like to start thanking my supervisor Stefan for believing in me since the very start, supporting me when the road was bumpy and sharing my enthusiasm for every achievement, no matter how small.

Thanks to Suruchi for being an incredible mentor, sharing her experience with me and helping me in and out the lab.

Thanks to Marta for her valuable guidance and for being a friend during my first months in Leeds.

Thanks to Adam for being the best lab companion I could possibly have asked for, for listening to all my lab-(and non lab)-related problems, achievements and nonsense, cheering me up and sharing the ups and downs of my PhD journey.

Thanks also to Fay and Sibo for being always supportive and caring and for sharing, to quote the great sage, moments of *living not just breathing.*

I honestly feel blessed to have been part of this amazing group.

On the outside of the lab now…I really want to thank my partner Stuart for always being loving and patient with me. I'm at loss of words to describe how I wouldn't really be here now without him.

Thanks to Imelda for always rooting for me and keeping me safe whenever I felt the ground was slipping beneath my feet. She is a major shareholder of this company.

Thanks to my sister Giulia for being my best friend, sharing the good and bad days and sending me all the best videos of our little zoo back at home.

And last but not least, thanks to my parents for always supporting me and believing in me. Their hard work made all of this possible for me to pursue, I'm forever grateful to them.

Abstract

The angle of growth of root and shoot branches is a key determinant of plant architecture. Arabidopsis lateral roots and shoots grow maintaining non-vertical gravitropic setpoint angles (GSAs) for a considerable part of the plant life (Digby and Firn, 1995). Non-vertical GSAs are the result of two counteracting auxin-dependent components: the gravitropic response, responsible for auxin flux to the lower side of the organ, and the antigravitropic offset (AGO), responsible for auxin flux to the upper side (Roychoudhry *et al.*, 2013). In lateral roots, this auxin transport is mediated by PIN3 and PIN7, which localization to the upper and lower side of the columella cells is controlled by their phosphorylation status (Grones *et al.*, 2018; Roychoudhry *et al.*, 2019). PIN3 dephosphorylation by PP2A/RCN1 phosphatase determines the protein to localise to the lower side of the columella cells, mediating the gravitropic auxin flux (Roychoudhry *et al.*, 2019). In lateral shoots, the molecular regulation of non-vertical GSAs has been suggested to be the same of lateral roots, with PIN3, PIN4 and PIN7 mediating auxin fluxes from the endodermis to the sides of the stem (Rakusová *et al.*, 2011; Roychoudhry *et al.*, 2013; Bennett *et al.*, 2016). During my PhD I identified two novel regulators of lateral root GSAs working in antagonism with RCN1. Their proposed role in membrane trafficking suggests their possible regulation of PIN localization at the upper side of the columella cells. Furthermore, I described a new phase of lateral shoot development preceding the setting of the GSA, and identified three novel putative regulators of the stem ad-abaxial polarity during early development. Taken together my results have advanced our understanding of growth angle control in shoot and root branches, for growth angles set both dependently and independently of gravity.

Table of Contents

List of Tables

List of Figures

Abbreviations

AGO – Antigravitropic offset

AM – Axillary meristem

ANOVA – Analysis of variance

ARF – Auxin responsive factor

ARF – Adenosine diphosphate (ADP) ribosylation factor

ARF-GEFs – ADP ribosylation factor-GDP/GTP exchange factors

BR – Brassinosteroid

CK – Cytokinins

CME – Clathrin-mediated endocytosis

DMSO - Dimethyl sulphoxide

EMS – Ethyl Methane Sulfonate

ER – Endoplasmic reticulum

GA – Gibberellic acid

GSA – Gravitropic setpoint angle

IAA – Indole-3-acetic acid

LRC – Lateral root cap

LZY – LAZY1-LIKE

PAT – Polar auxin transport

PP2A – Phosphatase 2A

RCN1 – Roots curl in NPA 1

SEM – Standard error of mean

SNPs – Single nucleotide polymorphisms

SOR – Suppressor of *rcn1*

WGS – Whole genome sequencing

WT – wild type

Chapter 1. General Introduction

Higher plants are characterized by a great variety of shapes, both above- and below-ground. An important component of this variation in plant form is the non-vertical angle of growth of lateral roots and shoots. Indeed, this laterally spreading growth is a critical adaptation that allows plants to optimise the capture of nutrients, water and light from their surrounding environment (Digby and Firn, 1995). Lateral shoots and roots are often maintained at specific angles with respect to gravity, independently of other parts of the plant. To define these growth angles, Digby and Firn first introduced the concept of gravitropic setpoint angles (GSAs), i.e. an angle maintained by an organ as a consequence of gravitropism (Digby and Firn, 1995). According to the GSA concept, organs that are maintained at the vertical, such as primary roots and shoots, have GSAs of 0° and 180°, respectively. Lateral branches, that maintain non-vertical growth independently of the main root and shoot, have, instead, GSAs between these two extremes. As both vertical and non-vertical GSAs are maintained with respect to gravity, gravitropism plays a crucial role in their maintenance. Taking vertical GSAs as an example, in *Arabidopsis thaliana* (Arabidopsis) when a primary root is moved away from its vertical GSA, the gravitropic response causes the root to bend downward and restores, in a few hours, its vertical GSA. An interesting characteristic of the gravitropic response is its angle-dependence. Firstly defined by Sachs, angle-dependence describes the relationship between the angle an organ is reoriented away from its GSA and the strength of its gravitropic response (Sachs, 1882). According to Sachs, the gravitropic response is proportional to the sine of the reorientation angle (Sachs, 1882). For this reason, the hypothesis was named Sine Law. In Arabidopsis the Sine Law has been shown to be valid for primary roots reoriented at angles between 20° and 90° from the vertical (Mullen *et al.*, 2000). However, for reorientation above 90° the Sine Law is not suited to describe the root graviresponse and a more complex relationship between angle of reorientation and gravitropic response needs to be investigated (Sageman-Furnas, 2016; Thomas, 2017).

1.1 Gravity perception and signal transduction

The perception of gravity in roots and shoots occurs in specialized cells containing dense, starch-filled plastids, also known as amyloplasts, that sediment in response to gravity and function as statoliths (Nakamura, Nishimura and Morita, 2019). These gravity sensing cells are found in the root-cap columella and shoot endodermis in dicotyledons, and pulvini cells in leaves and tillers of monocots (Song *et al.*, 1988; Sack, 1991). Several studies have shown that the physical and molecular removal of these tissues determine the suppression of the gravitropic response, demonstrating their fundamental role in gravity-sensing (Juniper *et al.*, 1966; Blancaflor, Fasano and Gilroy, 1998; Fukaki and Tasaka, 1999). In line with this, mutants impaired in starch biosynthesis and amyloplast formation are also defected in their gravitropic responses (Kiss, Hertel and Sack, 1989). According to the starch-statolith hypothesis, changes in the direction of gravity lead the statoliths to relocate to the new lower side of the cell, triggering the gravitropic response (Ottenschläger *et al.*, 2003). In the last 30 years several models have been proposed to explain the molecular mechanisms behind the signal transduction immediately following statolith sedimentation, but at the moment such mechanisms are still largely unknown. In some early models, actin filaments were proposed to be responsible for transferring the force generated by statolith sedimentation to putative mechanosensitive channels present on the plasma membrane or the endoplasmic reticulum (ER) (Sievers *et al.*, 1991; F. Baluška and K.H. Hasenstein, 1997; Yoder *et al.*, 2001). According to this theory, activation of these channels would determine the release of ions, most likely calcium, translating the statolith physical signal into a molecular one. However, later studies demonstrated that drug-induced disruption of the actin cytoskeleton did not impair gravitropism, but rather determined an enhanced gravitropic response in both shoots and roots (Yamamoto and Kiss, 2002; Hou, Mohamalawari and Blancaflor, 2003). Furthermore, it has been shown that the force applied by statoliths to cell membranes is not the central physical trigger of the gravitropic response, but rather changes in statolith position in the gravity-sensing cells (Chauvet *et al.*, 2016; Bérut *et al.*, 2018). Regardless of the puzzling evidence about its involvement in statolith sedimentation and signal transduction, actin is still a fundamental part of the cell cytoskeleton and is likely to play a role in the early stages of gravitropism. For example, actin has been shown to interact with two DnaJ-like proteins, ALTERED RESPONSE TO GRAVITY 1 (ARG1) and its paralog ARG1-LIKE2 (ARL2) in

a complex with HEAT SHOCK COGNATE PROTEIN 70-1 (HSC70-1) (Sedbrook, Chen and Masson, 1999; Harrison and Masson, 2008). Loss-of-function mutants of ARG1 and ARL2 show altered gravitropism, determined by impairment in the signal transduction pathway downstream of statolith sedimentation (Sedbrook, Chen and Masson, 1999; Guan *et al.*, 2003). A role of the Translocon of Outer Membrane of Chloroplasts (TOC) complex has also been suggested in relationship to ARG1 and ARL2 (Stanga *et al.*, 2009). According to this model, two members of the TOC complex, TOC132 and TOC75, located into the statolith membrane, may interact directly with a putative transducer positioned on the plasma membrane or the ER. Alternatively, TOC132 and 75 may mediate the insertion into the statolith outer membrane of an unknown protein that, similarly, would interact with the transducer. In this case, the position of the transducer would be controlled by ARG1 and ARL2. Interestingly, using immunoprecipitation coupled with mass spectrometry, a possible interaction of LAZY1 family proteins LAZY1-LIKE 2 (LZY2) and LZY3 with TOC75 and HSC70-1 was also recently suggested (Furutani *et al.*, 2020). LZY proteins are important factors required for gravitropism in both shoots and roots. If these interactions can be confirmed, it will provide an exciting link between statolith sedimentation and the downstream events leading to shoot and root gravitropic response.

1.2 Auxin distribution in primary roots and shoots

Auxin is a hormone involved in the control of a plethora of plant developmental and growth responses. Together with its biosynthesis, homeostasis and catabolism, auxin distribution in both shoots and roots highly depends on its active polar transport, also referred as PAT (polar auxin transport) (Goldsmith, 1977). Generally, auxin is transported from shoot to roots mainly though the vasculature (Petrášek and Friml, 2009). In a vertically growing root, auxin travelling through the vasculature reaches the root tip and, once in the columella, is redistributed laterally and then shootward through the lateral root cap (LRC) and epidermis. From the epidermis auxin then re-enters the vasculature and is transported back to the root tip (Fig. 1.1A). This transport pattern is also known as “reverse fountain” and ensures the maintenance of the auxin maxima and minima across the root that regulate the meristem zonation and function (Sabatini *et al.*, 1999; Benková *et al.*, 2003; Blilou *et al.*, 2005). In primary roots growing at their vertical GSA, auxin transport from the columella to the sides of the organ is maintained symmetrical. Similarly, in

primary stems, the main rootwards auxin flux in the vasculature is accompanied by a symmetrical lateral transport in and out the vasculature (Fig. 1.1A) (Bennett *et al.*, 2016). Upon gravistimulation, the lateral transport of auxin to the sides of both shoots and roots becomes asymmetric, with auxin being re-directed towards the lower side of the organ (Fig. 1.1B). Here, auxin accumulation regulates cell expansion causing primary roots to bend downward and primary shoots to bend upwards restoring their vertical GSAs. The ability of the asymmetric distribution of auxin to trigger the tropic response responsible for restoring root and shoot vertical growth was first described in the Cholodny-Went hypothesis (Went, 1926; Cholodny, 1927). The opposite tropic responses elicited by auxin depend on its ability to inhibit and induce cell elongation on the lower side of, respectively, the primary root and the primary shoot when subjected to gravistimulation (Kögl, Haagen-Smit and Erxleben, 1934; Bonner and Koepfli, 1939).

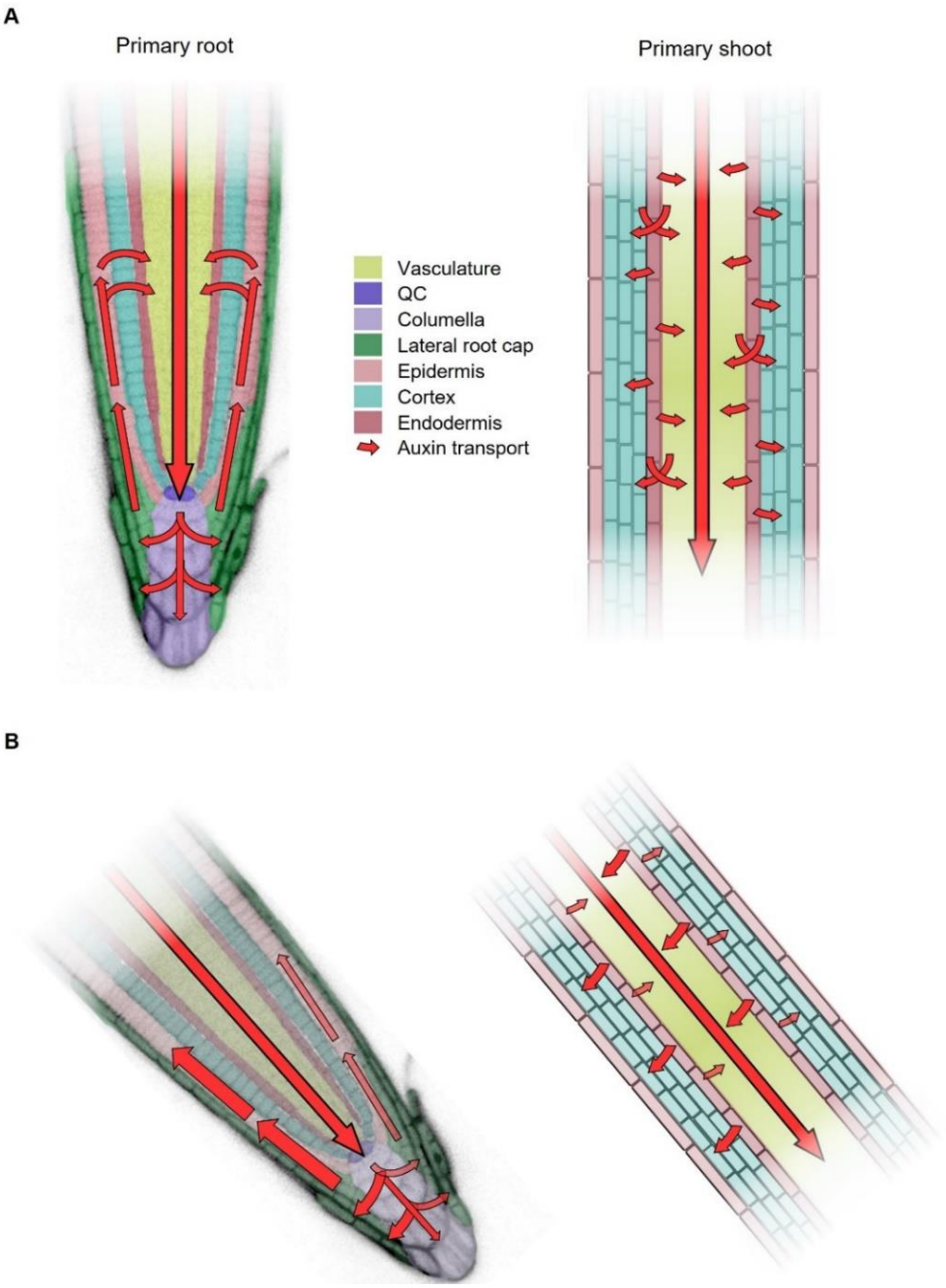

Figure 1.1: Auxin transport in primary roots and shoot

A) Schematic representation of vertically growing primary root and primary shoot. Auxin distribution in both organs is symmetrical. B) Schematic representation of a primary root and a primary shoot after being reoriented away from the vertical. In this case, auxin is asymmetrically redistributed towards the lower side of the organ. Arrow thickness represent the magnitude of auxin transport.

1.3 Auxin transport by PIN proteins

As described in figure 1.1, the gravitropic response could not exist without the fine regulation of auxin redistribution across primary roots and shoots. In Arabidopsis, auxin is actively transported by different classes of carriers. AUXIN1/LIKE-AUX1 (AUX1/LAX) are the major auxin influx carriers (Swarup and Bhosale, 2019), while few members of the P-GLYCOPROTEIN/ATP-BINDING CASSETTE B4 (PGP/ABCB) transporters and PIN-FORMED (PIN) proteins are responsible for auxin efflux from the cell (Geisler *et al.*, 2017). PIN efflux carriers are responsible for the polar transport of auxin and, not surprisingly, play a fundamental role in GSA regulation and gravitropism (Blilou *et al.*, 2005). In primary roots, PIN1 is the main PIN protein responsible for auxin transport to the root tip, localising basally in the vasculature, while PIN3, PIN4 and PIN7 are expressed in the columella and maintain an apolar distribution when the root is growing vertically, exporting auxin laterally (Jiří Friml *et al.*, 2002; Blilou *et al.*, 2005). In the epidermis and lateral root cap (LRC), PIN2 localise apically and determine the shootward auxin flux (Blilou *et al.*, 2005). Finally, PIN2, PIN3 and PIN7 expression in the layers between the epidermis and vasculature determines the re-entry of auxin in the vasculature (Blilou *et al.*, 2005). Although less characterised, PINs are believed to play a similar role in gravitropism and GSA maintenance in Arabidopsis primary and lateral shoots (Fig.1.2).

Upon gravistimulation, PIN3 and PIN7 polarize to the lower side of the columella cells and redirect auxin export to the lower side of the root (Jiří Friml *et al.*, 2002; Kleine-Vehn *et al.*, 2010). PIN ability to change subcellular localization during gravistimulation is regulated by specific post-translational modifications at the cytoplasmic domain of the protein. Although the precise 3D structure and mode of action of PIN proteins still remains elusive, analysis of the amino acid sequence suggests multiple transmembrane domains at both the amino and carboxy-terminal ends of the protein and a central cytoplasmic loop (Zwiewka *et al.*, 2019). Furthermore, recent evidence supports a model where PIN proteins form homodimers and transport auxin outside the cell via an elevator-type mechanism (Ung *et al.*, 2022). Regardless of the precise structure and mode of auxin transport of PIN proteins, it has been shown that phosphorylation of specific residues in the cytoplasmic loop controls both PIN polarity and activity (Barbosa, Hammes and Schwechheimer, 2018). Several studies have shown that serine residues of the loop are phosphorylated by members of the AGCVIII serine/threonine

kinase family including the PINOID (PID)/WAG1/WAG2 and D6 protein kinase (D6PK) clades, controlling both PIN polarity and activity (Zourelidou *et al.*, 2014; Barbosa, Hammes and Schwechheimer, 2018). Given the important role phosphorylation has in PIN regulation, much work has been focused on uncovering the residues in the loop responsible for the PIN polarity switch (Dhonukshe *et al.*, 2010; Huang *et al.*, 2010; Ganguly, Lee and Cho, 2012; Grones *et al.*, 2018). For instance, three serine residues (S316, S317 and S321) in PIN3 are targets of all AGCVIII kinases (Grones *et al.*, 2018), while two serine residues (S215 and S283) are mainly phosphorylated by D6PK (Zourelidou *et al.*, 2014). Once phosphorylated, the hydrophilic loop of PIN proteins can be dephosphorylated by the action of protein phosphatases. In Arabidopsis, PROTEIN PHOSPHATASE 2A (PP2A) and 6 (PP6) are responsible for the removal of PIN phosphate residues. PP2A and PP6 are holoenzymes formed by a catalytic subunit and two regulatory subunits (A and B), and influence PIN distribution working in antagonism to PID kinase (Michniewicz *et al.*, 2007; Dai *et al.*, 2012; Uhrig, Labandera and Moorhead, 2013). The analysis of loss-of-function of kinases and phosphatases involved in PIN phospho-status, together with localization analysis of PIN3 phospho-mutants supports a model where upon gravistimulation, dephosphorylated PIN3 is targeted to the lower membrane of columella cells and mediate auxin redistribution to the lower side of the primary root (Grones *et al.*, 2018).

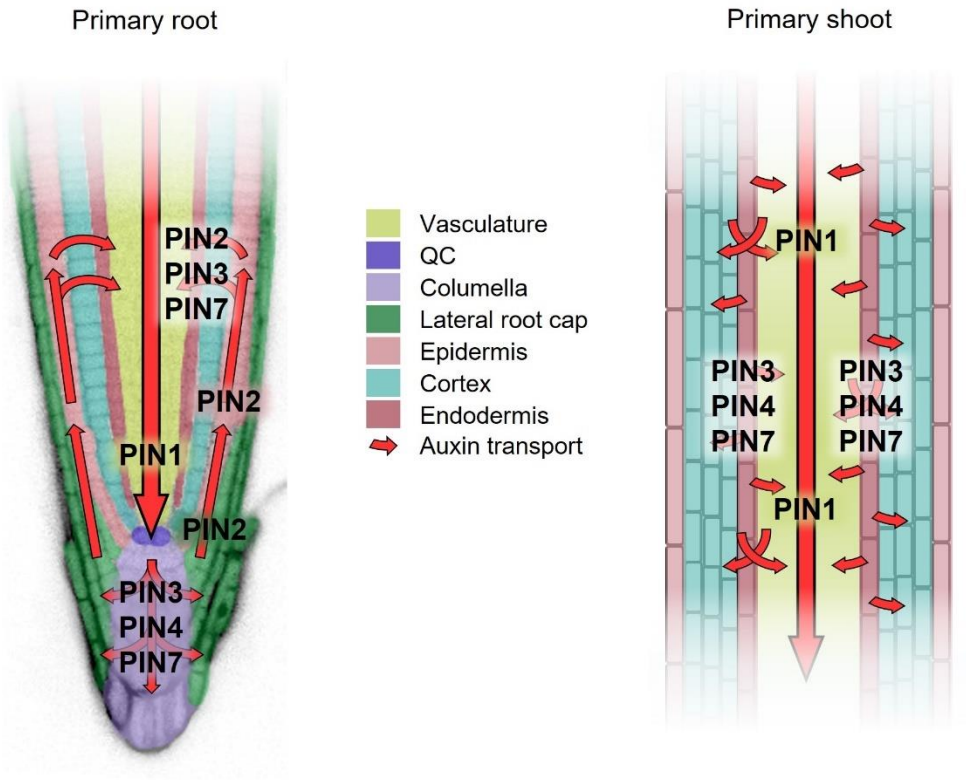

Figure 1.2: PIN expression across the primary root and shoot

Schematic representation of PIN polar transport of auxin across the primary root and primary shoot.

1.4 PIN membrane trafficking

The phosphorylation status of PIN proteins determines their subcellular localization by the membrane trafficking system responsible for protein endo and transcytosis (Glanc, Fendrych and Friml, 2018; Marhava, 2022). PIN proteins are currently proposed to dynamically cycle between the plasma membrane and the endomembranes, although the precise molecular basis of PIN secretion and cycling are still to be completely elucidated (Cheng and Wang, 2022). From the plasma membrane PIN proteins can be recycled via clathrin-mediated endocytosis (CME) (Dhonukshe *et al.*, 2007; Kitakura *et al.*, 2011). CME is determined by the formation of vesicle at the plasma membrane coated in lattice-like structures formed by clathrin (Narasimhan *et al.*, 2020). Lipid composition of the plasma membrane can influence PIN endocytosis both by affecting clathrin-coated vesicle formation and by establishing plasma membrane domains where proteins involved in PIN endocytosis are recruited (Ischebeck *et al.*, 2014; Pan *et al.*, 2020). After forming, the PIN-containing vesicles are sorted by members of the small

GTPases ADP RIBOSYLATION FACTOR (ARF) family (Kjos *et al.*, 2018). ARF proteins cycle between an inactive GDP-bound state and an active GTP-bound state. In the activated state, ARFs interact with coated vesicles and connect them to the cytoskeleton where they are transported to their destination (Kjos *et al.*, 2018). ARF GDP/GTP EXCHANGE FACTORS (ARF-GEFs), as the name suggests, mediate the GDP to GTP exchange on ARF proteins, activating them (Kleine-Vehn, Dhonukshe, *et al.*, 2008). The ARF-GEF GNOM and its homologous GNOM-LIKE1 (GNL1) have been shown to regulate PIN endocytosis and recycling in roots (Steinmann *et al.*, 1999; Geldner *et al.*, 2003; Doyle, Haeger, Vain, Rigal, Viotti, Łangowska, Ma, Friml, N. v. Raikhel, *et al.*, 2015). Interestingly, recent work has shown that RCC1-like domain (RLD) proteins interact with GNOM and are likely involved in endomembrane trafficking (Wang *et al.*, 2022). RLD proteins have also been shown to interact with members of the LZY family (Furutani *et al.*, 2020). Four members of LZY family, LZY1-4, have been all shown to regulate gravitropism in a redundant way in both shoots and roots (Taniguchi *et al.*, 2017; Yoshihara and Spalding, 2017). It has been suggested that this regulation is mediated by LZYs recruitment of RLD proteins to the plasma membrane of columella cells towards the direction of gravity (Furutani *et al.*, 2020). In this model, upon gravistimulation, the LZY-dependent polarization of RLDs determines the subsequent asymmetric distribution of PIN3, which leads to asymmetric auxin redistribution and gravitropic response. The previously mentioned possible interaction between LZYs and TOC75 and HSC70-1 could represent a potential link between statolith sedimentation and PIN-dependent asymmetric redistribution of auxin.

1.5 Auxin signalling

In the nucleus, members of TRANSPORT INHIBITOR RESPONSE1/AUXIN SIGNALLING F-BOX (TIR1/AFB) family act as auxin receptors (Dharmasiri *et al.*, 2005; Kepinski and Leyser, 2005). TIR1/AFB proteins are subunits of the SCF complex (SKIP, CULLING, F-BOX), responsible for recognising proteins to mark for degradation via ubiquitylation (Salehin, Bagchi and Estelle, 2015). Once in the nucleus, auxin acts as a molecular glue stabilising the interaction between the TIR1/AFBs and their substrates, the transcriptional repressors AUXIN/INDOLE-3-ACETIC ACID (AUX/IAA) (Ulmasov *et al.*, 1997). The auxin-dependent recruitment of AUX/IAAs to the SCF complex determines their ubiquitylation and consequent degradation by the proteasome (Tan *et*

al., 2007). AUX/IAAs inhibit the transcription of genes regulated by the AUXIN RESPONSE FACTOR (ARF) family, directly binding ARF proteins recruited to their target promoters rather than physically interacting with DNA sequences (Tiwari, Hagen and Guilfoyle, 2004). AUX/IAA interaction with ARF proteins determines the recruitment of a family of corepressors named TOPELESS (TPL), which in turn recruit chromatin remodelling factors that stabilise gene repression (Szemenyei, Hannon and Long, 2008). AUX/IAA degradation releases ARF proteins from repression and allows them to regulate the expression of auxin responsive genes (Fig. 1.3).

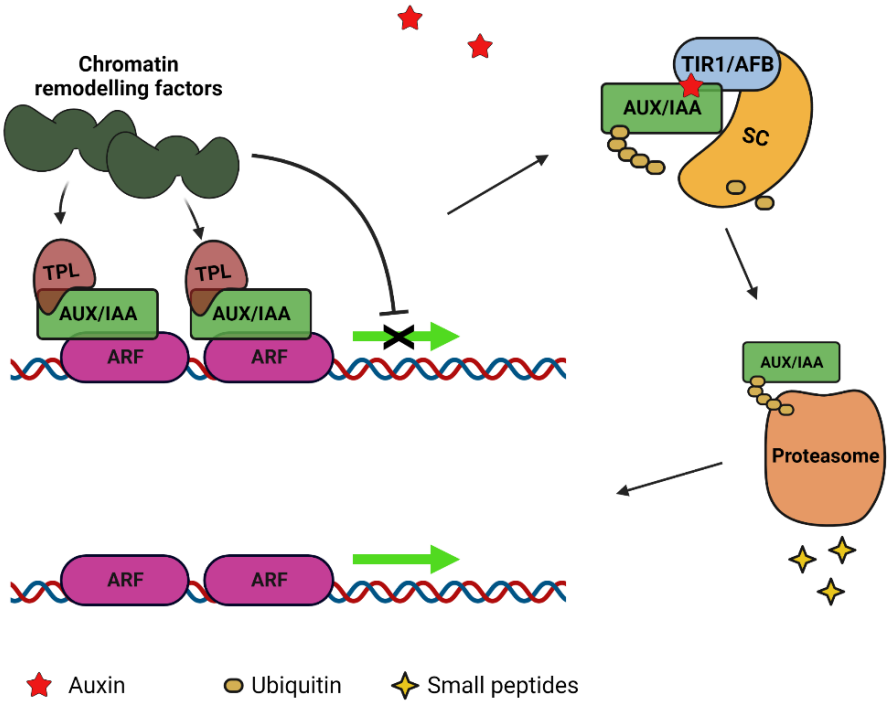

Figure 1.3: Auxin Signalling

Schematic representation of the canonical auxin signalling pathway. ARF transcription factors bind auxin-responsive elements on the promoters of auxin-regulated genes. AUX/IAAs interact with ARFs and recruit on the promoters TPLs corepressors and chromatin remodelling factors to repress gene transcription. In presence of auxin, AUX/IAAs are targeted by TIR1/AFB-SCF complex, ubiquitylated and sent to degradation via proteasome. Green arrows indicate to the direction of transcription.

Although auxin canonical signalling pathway is described here simplistically, auxin responses do not work solely as an on/off switch of transcription. In Arabidopsis there are 6 TIR1/AFB receptors, 23 ARF proteins and 29

AUX/IAA repressors, which show tissue-specific expression across the plant and specific interaction preferences (Paponov *et al.*, 2008; Vernoux *et al.*, 2011; Li *et al.*, 2016). ARFs also show different affinities for specific promoter sequences and can form homo- and heterodimers (Bargmann *et al.*, 2013). In addition, some ARFs work as transcriptional repressors and might compete for the same promoters ARF activators regulates (Leyser, 2018). Finally, auxin-mediated activation of transcription via ARFs is often regulated by negative feedbacks, with the same ARFs activating the transcription of their AUX/IAA repressors (Leyser, 2018). The makeup of the auxin pathway machinery will therefore determine the cell-specific output of the auxin response.

The recent evidence of the existence of noncanonical auxin signalling pathways further increases the possible complexity of the auxin response. For example, ARF3/ETTIN (ETT) is an ARF that mediates a non-canonical auxin response involved in leaf polarity and floral development (Sessions *et al.*, 1997; Takahashi *et al.*, 2013). ETT protein lacks the AUX/IAA-interacting domain, known as PB1 domain, and mediates auxin signalling independently from the canonical TIR1/AFB pathway (Sessions *et al.*, 1997; Simonini *et al.*, 2016, 2017). Recent work has suggested that one of ETT modes of action involves ETT direct association with TPLs (Kuhn *et al.*, 2020). Similarly to the canonical auxin signalling pathway, ETT-bound TPLs recruit chromatin remodelling factors and mediate transcriptional repression. When levels of auxin increased in the nucleus, auxin can directly bind ETT, destabilising its interaction with TPLs. TPL disassociation from ETT consequently determines the activation of transcription of ETT target genes (Kuhn *et al.*, 2020). Another non-canonical auxin signalling pathway involves a possible non-transcriptional role of TIR1/AFB involved in auxin inhibition of cell elongation and, being of relevance for the gravitropic response, will be discussed below (Fendrych *et al.*, 2018).

1.6 Auxin regulation of cell elongation

The ability of auxin to regulate many aspects of plant growth is based on the specific responsiveness of the cell. For this reason, the spatial and temporal context of a cell is a fundamental factor to determine the cell behaviour in presence of auxin. This is particularly relevant during gravitropism, where despite sharing the same mechanisms of statolith sedimentation leading to

the accumulation of auxin to the lower side of the organ, auxin drives opposite growth responses in root and shoot cells.

Auxin-induced cell elongation in the shoot is also known as acid growth. During this process, the acidification of the apoplast leads to cell wall loosening, allowing the expansion of the cell protoplast by turgor pressure (Rayle and Cleland, 1970; Ruck *et al.*, 1993). Auxin is able to activate the plasma membrane H^+-ATPases (AHAs), which acidify the apoplast by pumping H^+ cations outside the cell (Rayle and Cleland, 1980). AHA protein activation is determined by the interaction with 14-3-3 proteins (Baunsgaard *et al.*, 1998). This interaction depends on the phosphorylation of a C-Terminal threonine residue of the AHA proteins (Fuglsang *et al.*, 1999; Kanczewska *et al.*, 2005; Takahashi, Hayashi and Kinoshita, 2012). Phosphorylation of AHA C-Terminal threonine residue is made possible thanks to the auxin induction, via its canonical signalling pathway, of the SMALL AUXIN UP-REGULATED RNA (SAUR) expression (Spartz *et al.*, 2012; Fendrych, Leung and Friml, 2016). It has been shown that SAUR19 determines the phosphorylation and subsequent activation of AHA proteins by negatively regulating type 2C phosphatases, which are responsible for the dephosphorylation of AHA C-Terminal end (Spartz *et al.*, 2014). Together with cell wall loosening, acidification of the apoplast leads to the antiport of K^+ inside the cell, which further induces cell expansion through the increase of the cell turgor (Claussen *et al.*, 1997; Tode and Lüthen, 2001).

Similarly to the shoot, in roots auxin inhibition of cell expansion is accompanied by changes in apoplastic pH. Upon gravistimulation, auxin redistribution to the lower side of the primary root triggers a rapid increase of the surface pH (Zieschang, Kohler and Sievers, 1993; Monshausen *et al.*, 2011). This increase of apoplastic pH is coupled with a decrease in cytoplasmic pH, suggesting movement of protons across the plasma membrane (Monshausen *et al.*, 2011). It has been proposed that the auxin-dependent apoplast alkalization on the lower side of the gravistimulated primary root is mediated by a cytoplasmic calcium signal travelling from the root tip to the elongation zone (Monshausen *et al.*, 2011). The loss-of-function mutant of CNGC14, a member of CYCLIC NUCLEOTIDE-GATED CHANNEL (CNGC) family, shows loss of calcium dynamics on the lower side of gravistimulated primary roots (Shih *et al.*, 2015). Interestingly, *cngc14* primary roots show attenuated and delayed apoplastic alkalization and a delayed gravitropic response (Shih *et al.*, 2015). This evidence suggests a role of

CNGC14 in generating a calcium signal during the graviresponse, which leads to the alkalinization of the apoplast and inhibition of cell elongation on the lower side of primary roots. Differently from shoots, auxin-mediated growth inhibition in roots happens too fast to be explained by changes in gene expression linked to the canonical auxin signalling pathway. It has been shown that auxin treatments determine inhibition of growth in primary roots in less than 30 seconds, while the earliest TIR1-dependent gene expression response is detected after 15 minutes from auxin application (Fendrych *et al.*, 2018). This suggests that the rapid growth inhibition detected in roots might be mediated by a noncanonical fast-acting auxin pathway. Recently it has been proposed a non-transcriptional role for TIR1/AFBs in mediating this rapid auxin response, excluding the existence of an unknown auxin receptor (Scheitz, Lüthen and Schenck, 2013; Fendrych *et al.*, 2018). Although there are contrasting evidence on the participation of TIR1/AFBs to the gravitropic calcium signal and subsequent alkalization of the apoplast leading to the cell growth inhibition (Monshausen *et al.*, 2011), the continuous development of new imaging tools and techniques, and the improvement of cytoplasmic and apoplastic sensors emerging in recent years will help elucidate the molecular mechanisms behind auxin-induced fast inhibition of cell elongation.

1.7 Regulation of non-vertical GSAs

The standard model of gravitropism involving the starch-statolith hypothesis and Cholodny-Went model provides a ready explanation for the maintenance of vertical GSAs in primary roots and shoots, but on its own cannot account for non-vertical GSAs in branches. Differences between vertical and non-vertical growth could be caused by a change in the perception of gravity such that even if the branch is not at the vertical, it is maintained at a state of equilibrium in which graviresponse is not triggered. Alternatively, lateral branches might share the same mode of gravity perception as primary roots and shoots but the consequent graviresponse is prevented from moving the branch to the vertical by another, counteracting mechanism. To distinguish between the two possibilities, experiments involving clinorotation have been used to good effect. Clinorotation induces an omnilateral gravitational stimulus to the plant that prevents the statoliths from sedimenting stably within the gravity-sensing cells and thus determining orientation within the gravity field (Fig. 1.4). Primary roots that have not been subject to gravistimulation continue to grow straight when deprived of a stable reference to gravity under

clinorotation (Roychoudhry *et al.*, 2013). Under these same conditions, lateral roots show a pronounced outward/upward bending (Roychoudhry *et al.*, 2013). This observation suggests that lateral roots do not maintain non-vertical GSAs via a change in perception of gravity as otherwise they would, like primary roots, continue to grow straight under clinorotation. The behaviour of lateral roots indicates the activity of another growth force that acts against the underlying gravitropic response of the branch to maintain the non-vertical growth. This offset mechanism has been named antigravitropic offset (AGO) and acts to counteract the gravitropic response, generating stable gravity-dependent growth at non-vertical angles (Roychoudhry *et al.*, 2013, 2017). Interestingly, lateral roots ceased to bend outward/upward after few hours of clinorotation, suggesting that also the AGO is set and maintained with respect to gravity (Roychoudhry *et al.*, 2013).

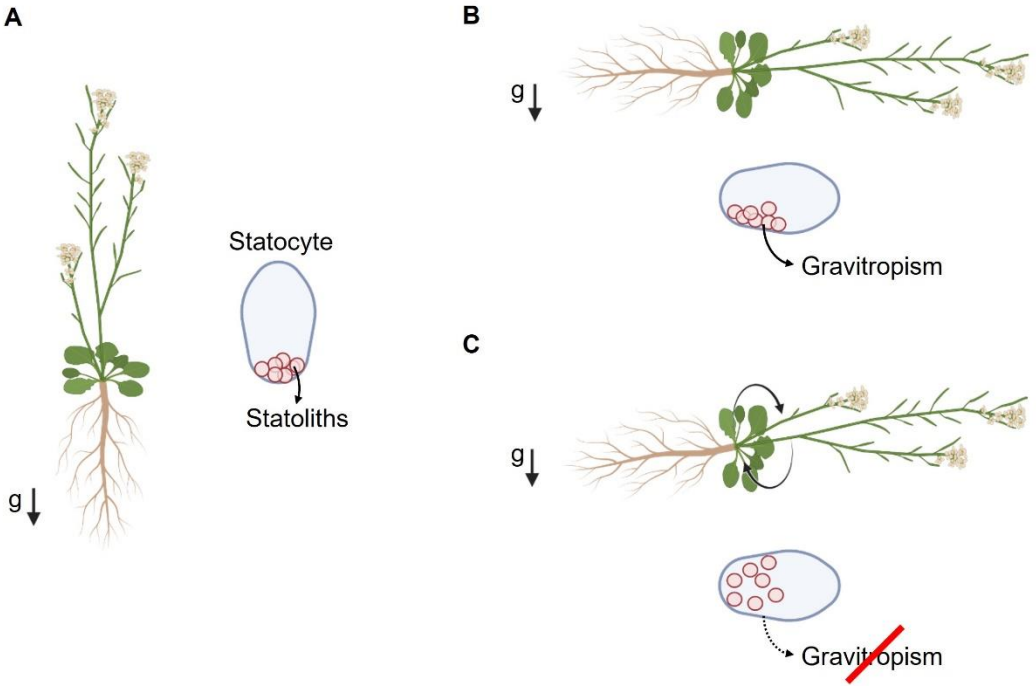

Figure 1.4: Clinorotation suppresses gravity perception

Schematic representation of statolith sedimentation in primary organs during normal growth (A), reorientation (B), and clinorotation (C). Statolith sedimentation signals the position of the organ with respect to gravity. During normal growth, statoliths sediment at the bottom of the statocytes of primary root and shoot (A). Upon reorientation statoliths sediment to the new lower side of the cell, triggering the gravitropic response that will restore root and shoot GSA (B). During clinorotation, the continuous revolving of plants prevents statoliths from sedimenting, suppressing plant ability to perceive the direction of gravity and the downstream processes maintaining the correct plant orientation (C). Black arrows indicate the direction of gravity, g = gravity

The molecular basis of the interaction between gravitropism and antigravitropism has been established in the context of the Arabidopsis lateral root (Roychoudhry *et al.*, 2013). Lateral roots growing at their GSA show no asymmetry in auxin levels on the upper and lower sides of the lateral root. Here, the AGO is responsible for the auxin export to the upper side of the root while gravitropic response regulates the transport of auxin to the lower side (Fig. 1.5). A crucial difference between these two opposing auxin transport components is that while upward, AGO-mediated auxin flux is constant for a given GSA, downward, gravitropic auxin flux is highly dynamic and depends on the root orientation (Roychoudhry *et al.*, 2019). In this way, stable growth with respect to gravity occurs when gravitropic and antigravitropic auxin fluxes are in equilibrium. If the lateral root is moved above its GSA, the magnitude of gravitropic auxin flux relative to the AGO increases, causing the lateral root to bend downward and restore its GSA (Fig. 1.5) (Roychoudhry and Kepinski, 2015). Similarly, if the lateral root is moved below its GSA, the magnitude of the gravitropic component decreases leading the AGO-dependent auxin flux towards the upper side to become prominent with respect to the lower auxin transport, causing the upward bending of the lateral root (Fig. 1.5) (Roychoudhry and Kepinski, 2015). According to this model, variation in cell expansion in root lower side is responsible for both downward and upward tropic growth. Indeed, it has been shown that cells in the elongation zone of the lower side of the gravistimulated lateral root are shorter when the root is bending downward and longer when it is bending upward, compared to the upper side of the organ, where cell length stays relatively constant (Roychoudhry *et al.*, 2019).

Similarly to primary roots, PIN3, PIN4 and PIN7 are expressed in the columella cells of lateral roots and play an essential role in regulating non-vertical GSAs (Guyomarc'h *et al.*, 2012; Roychoudhry *et al.*, 2019) Recent work has shown that also in lateral roots phosphorylation of PIN3 cytoplasmic loop regulates the protein localization in the columella cells (Roychoudhry *et al.*, 2019). Phosphorylated PIN3 is targeted to the upper side of the columella and contributes to AGO-dependent auxin flux, while dephosphorylated PIN3 is targeted to the lower side and contributes to the gravitropic-dependent auxin flux (Roychoudhry *et al.*, 2019). In addition to this, it has been shown that PIN3 dephosphorylation is controlled by the phosphatase PP2A/RCN1 (Roychoudhry *et al.*, 2019). LZY proteins and their RLD interactors have also been shown to be necessary for PIN3 regulation, contributing to the gravitropic

auxin flux to the lower side of the lateral root (Furutani *et al.*, 2020). Taken together this suggests that the gravitropic component regulating non-vertical GSAs shares similar molecular mechanisms with the gravitropic response in primary roots.

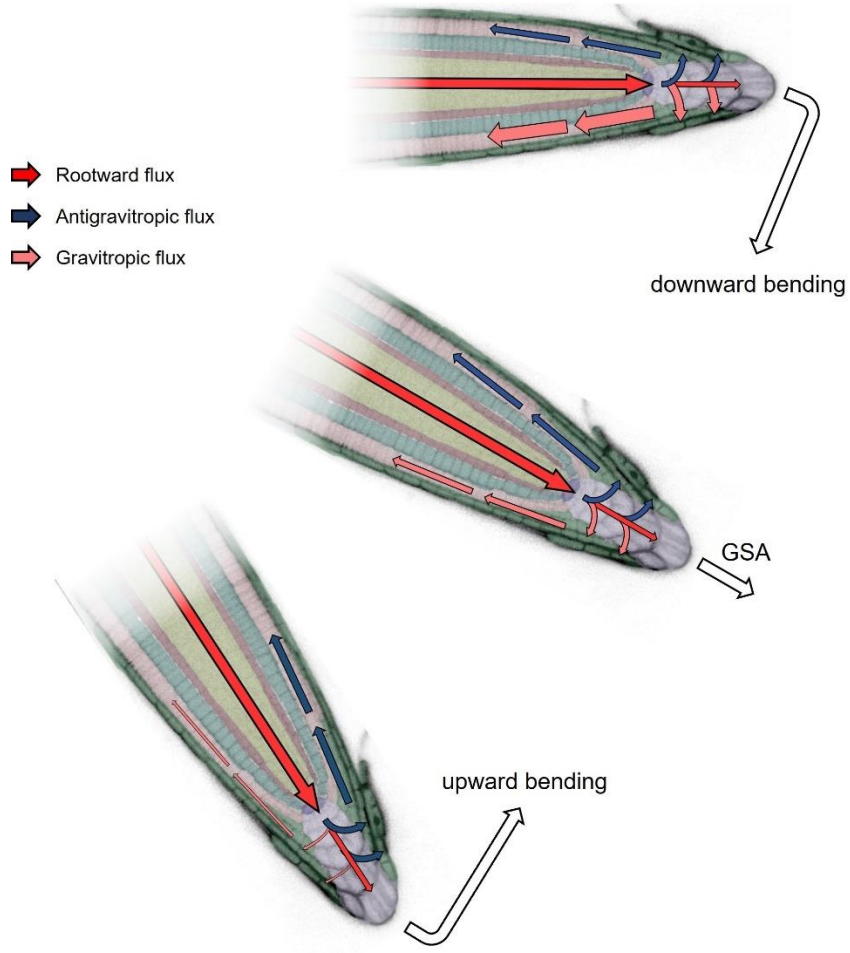

Figure 1.5: Auxin distribution in lateral roots

Schematic representation of auxin distribution in a lateral root growing at its GSA and moved below or above the GSA. White arrows represent the direction of growth. Thickness of arrows represent the magnitude of the auxin transport.

Similarly to lateral roots, shoot branches also maintain non-vertical GSAs thanks to the activity of an AGO counteracting the inherent negative gravitropic response in the branch (Roychoudhry *et al.*, 2013). Lateral shoots originate by the activity of axillary meristems (AMs) (Wang and Jiao, 2018) and, after a phase of elongation not yet characterised, set and maintain non-vertical GSAs. Consistent with this, when clinorotated, lateral branches also

show an outward/downward bending, in line with the action of a constant AGO at the upper side of the organ (Roychoudhry *et al.*, 2013). In addition, similarly to lateral roots, mutants with higher levels of auxin or a greater sensitivity to auxin show more vertical GSAs, while those with lower auxin levels or auxin sensitivity show more horizontal GSAs (Roychoudhry *et al.*, 2013). As in the root, PIN3, PIN4 and PIN7 are important to maintain the GSA of shoot branches, with *pin3pin4* and *pin3pin4pin7* showing more horizontal lateral shoot GSAs (Bennett *et al.*, 2016). In contrast, lateral roots of *pin3pin4* and *pin3pin4pin7* mutants show variable GSA phenotypes, with just a percentage of the roots showing more horizontal growth angles (Rosquete *et al.*, 2013). Taken together, these observations indicate that while GSA control in shoot branches shares fundamental similarities with that in the root, the underlying molecular basis of GSA regulation may be different.

1.8 Project Aims

Previous work on lateral root and shoot GSA maintenance has established a basic mechanistic framework for GSA control in which gravitropic response is counteracted by an antigravitropic offset mechanism (AGO) (Roychoudhry *et al.*, 2013). In lateral roots, the maintenance of non-vertical GSAs is mainly based on the control of auxin export from the columella cells (Roychoudhry *et al.*, 2019). For this reason, the molecular mechanisms regulating the polarity of PIN proteins in the columella are of critical importance. Strong evidence supports a model where the PP2A/RCN1 phosphatase is responsible for controlling PIN3 polarity via the dephosphorylation of the cytoplasmic loop, while it is less clear which kinases are involved in PIN3 phosphorylation (Roychoudhry *et al.*, 2019). In addition, recent studies on the role of LZY proteins have advanced our knowledge on the components forming the trafficking machinery involved in the gravitropic-dependent distribution of PIN3 at the plasma membrane (Taniguchi *et al.*, 2017). Although the recent progress that has been made in understanding GSA maintenance in lateral roots, regulators of the antigravitropic auxin efflux mediated by PIN3 and PIN7 are still unknown. For this reason, this project aimed to fill this gap by uncovering uncharacterised GSA regulators working in antagonism to RCN1/LZY1 gravitropic control of PIN3.

Although the molecular details of GSA maintenance in lateral shoots are yet to be uncovered, shoot branches shared the same basic mechanisms of gravity-perception and auxin distribution controlled by gravitropism and AGO

of lateral roots (Fukaki and Tasaka, 1999; Roychoudhry *et al.*, 2013). Conversely to lateral roots though, early stages of development preceding the setting of the GSA have not yet been studied and characterised. With this project I aimed to lay the groundwork for a better understanding of the initial stages of lateral shoot development and their contribution to the final branch shape.

The specific aims of this project were:

- To characterise novel regulators of lateral root GSA control working in antagonism with RCN1, performing a suppressor screening on the *RCN1* loss-of-function mutant *rcn1-1*
- To phenotypically characterise the early stages of lateral shoot development
- To uncover molecular regulators of the early stages of lateral shoot development using transcriptomic analysis

Chapter 2. Materials and Methods

2.1 Plants lines and growth conditions

2.1.1 Plant lines

Table 2.1 List of plant lines used in this project

Plant line	Background	Source
Columbia (Col-0)		Kepinski lab
Col-3		NASC
Wasilewskija (Ws-0)		Kepinski lab
rcn1-1	Ws-0	S. Roychoudhry, Kepinski lab
rcn1-6	Col-0	NASC (SALK_059903)
rcn1sor1	Ws-0	This project
rcn1sor2	Ws-0	This project
rcn1sor3	Ws-0	This project
rcn1sor4	Ws-0	This project
proton1	Col-0	NASC (SALK_117261)
map70-2	Col-0	NASC (SALK_060997)
kuk	Col-0	NASC (SALK_019083)
lrr-k	Col-0	NASC (SALK_006948)
perk15	Col-0	NASC (SALK_020345)
abhy	Col-0	NASC (SALK_062093)
o-ft	Col-0	NASC (SALK_152459)
net2b	Col-3	NASC (SAIL_2_F03C1)
lot-2	Col-0	NASC (SALK_130228)
anp3	Col-0	NASC (SALK_081990)
nov	Col-0	NASC (SALK_053496)
far1	Col-0	NASC (SALK_031652)
phs	Col-0	NASC (SALK_034519)

errp	Col-0	NASC (SALK_208480)
c2dp	Col-0	NASC (SALK_200658)
hsl1	Col-0	NASC (SALK_141756)
o-gt	Col-0	NASC (SALK_083047)
drb5	Col-0	NASC (SALK_031307)
rcn1map70	Col-0	This project
rcn1drb5	Col-0	This project
rcn1net2b	Col-0; Col-3	This project
rcn1errp	Col-0	This project
rcn1o-ft	Col-0	This project
rcn1far1	Col-0	This project
rcn1c2dp	Col-0	This project
rcn1anp3	Col-0	This project
rcn1lot-2	Col-0	This project
rcn1perk15	Col-0	This project
rcn1lrr-k	Col-0	This project
rcn1abhy	Col-0	This project
pgm1	Col-0	M. Del Bianco, Kepinski lab
lzy1	Col-0	Kepinski lab
scr-3	Col-0	NASC
tac1	Col-0	S. Roychoudhry, Kepinski lab
pin3pin4pin7	Col-0	T. Bennett, University of Leeds
PIN3::PIN3:GFP (pin3)	Col-0	S. Roychoudhry, Kepinski lab
PIN7::PIN7:GFP (pin7)	Col-0	S. Roychoudhry, Kepinski lab
PIN4::PIN4:GFP (pin4)	Col-0	S. Roychoudhry, Kepinski lab
CYCB1;1::GUS	Col-0	C. West, University of Leeds
CYCD3;1::GUS	Col-0	J. Murray, Cardiff University

CYCD3;2::GUS	Col-0	J. Murray, Cardiff University
CYCD3;3::GUS	Col-0	J. Murray, Cardiff University
ahk1ak2	Col-0	T. Bennett, Leeds
ahk2ahk3	Col-0	T. Bennett, Leeds
ahk3ahk4	Col-0	T. Bennett, Leeds
ipt3ipt5ipt7	Col-0	T. Bennett, Leeds
rock1	Col-0	T. Bennett, Leeds
rock2	Col-0	T. Bennett, Leeds
arf4	Col-0	L. Østergaard, JIC
ett-3	Col-0	L. Østergaard, JIC
arf4ett-3	Col-0	This project
agl71	Col-0	NASC (SALK_132739)
agl72	Col-0	NASC (GK-799A05)
agl71agl72	Col-0	This project
35S::TCP1	Col-0	This project

2.1.2 Seed sterilization

Arabidopsis seeds were surface sterilised using either chlorine gas or 20% v/v bleach solution before being plated. Seeds sterilised with chlorine gas were collected in open microcentrifuge tubes, placed inside a desiccator under a fume hood, and exposed to chlorine gas for 2 to 3 hours. Chlorine gas was created adding 3 ml of 37% hydrochloric acid to 100 ml of liquid bleach. After the exposure, seeds were ventilated for 1 hour in a laminar flow hood. Seeds sterilised with bleach were soaked in 20% bleach solution for 20 minutes and subsequently washed with sterile water for 5 times in a laminar flow hood.

2.1.3 Plant growth media preparation

Arabidopsis seeds were plated on 120 mm square petri dishes containing 45 ml of sterile Arabidopsis thaliana salt (ATS) medium containing 1% w/v sucrose and 0.8% w/v plant agar (Duchefa Biochemie). For auxin sensitivity experiments, seeds were plated in 9 cm round dishes containing 25 ml of sterile ATS medium. ATS medium was prepared using concentration of

macronutrients and micronutrients shown in Table 2.2 as set-out by (Wilson *et al.*, 1990).

Table 2.2: Preparation of ATS media

Macronutrients	**mM**
Potassium dihydrogen monophosphate (KH_2PO_4), pH 5.5	2.5
Potassium nitrate (KNO_3)	5
Calcium nitrate ($Ca(NO_3)_2$)	2
Magnesium sulphate ($MgSO_4$)	2
Micronutrients	**µM**
Iron ethylenediaminetetraacetic acid (Fe-EDTA)	50
Orthoboric acid (H_3BO_4)	70
Manganese chloride ($MnCl_2$)	14
Sodium chloride (NaCl)	10
Copper sulphate ($CuSO_4$)	0.5
Zinc sulphate ($ZnSO_4$)	1
Sodium molybdate ($NaMoO_4$)	0.2
Cobalt chloride ($CoCl_2$)	0.01

2.1.4 Plant growth conditions

After being plated, seeds were stratified at 4°C for 48 hours. Plates were then incubated vertically in a plant growth room under long day photoperiod (16 h day) at 20-22 °C, with 60% humidity and light intensity of ~120 µmol/m^2s^{-1} from white fluorescent tubes. For auxin sensitivity experiments, seedlings were left grow in 9 cm round dishes for 5 days before being moved to 120 mm square dishes on ATS supplied with DMSO or 50 nM indole-3 acetic acid (IAA) dissolved in DMSO. For shoot phenotype analysis, seeds were sown in soil (Petersfield No.2) in p24 potting trays or 9 cm square pots, stratified at 4°C for 48 hours and then moved in growth rooms or greenhouses under long day photoperiod (16 h day) at 20-25°C.

2.1.5 Arabidopsis transformation by floral dipping

Arabidopsis plants were grown in 9 cm square pots for 21-28 days prior transformation, with each square pot containing 5 plants. Two to three pots were transformed with the same construct. A day before transformation, a 5 ml liquid culture derived from a single colony of *Agrobacterium tumefaciens*,

transformed with the desired construct, was used to inoculate two 250 ml of liquid Luria-Bertani (LB) media containing gentamycin (25 μg/ml), rifampicin (100 μg/ml) and spectinomycin (70 μg/ml). The culture was grown overnight at 28°C shaking at 140 RPM. Agrobacterium cells were isolated by centrifugation at 6000 RPM at room temperature and resuspended in 250 ml of sucrose solution (5% w/v sucrose, 10 mM MgCl2•6H2O, 10% v/v Silwet Vac in Stuff®). Arabidopsis inflorescences were dipped in the sucrose solution for 2-3 minutes. After dipping, plants were sealed in autoclave bags for 2-3 days and then left grown for 4-6 weeks before T_1 seeds were harvested.

2.1.6 Selection of transgenic plant with seed coat fluorescence

Seeds successfully transformed with ALLIGATOR-III (pALL-III) vector containing the gene of interest, showed GFP fluorescence in the seed coat. T_1 seeds were screened for seed coat fluorescence using an OLYMPUS® SZX12 stereo microscope with a GFP filter, then sown, left self and produce T_2 lines.

2.2 Bacteria growth conditions and transformation

2.2.1 *Escherichia Coli* growth conditions

Transformed *Escherichia Coli* (E. Coli) were grown on solid LB media (Luria-Bertani: tryptone 10 g/l, NaCl 10 g/l, yeast extract 5 g/l, 1.5% w/v agar) supplied with appropriate antibiotics, overnight at 37°C. For E. Coli transformed with pALL-III vectors LB media was supplied with Spectinomycin (70 μg/ml). E. Coli transformed with pENTR™ /D-TOPO™ (Thermo Scientific) vectors were grown on LB supplied with Kanamycin (40 μg/ml). Single E. Coli colonies were inoculated in 5 ml of liquid LB, with the appropriate antibiotics, overnight at 37°C shaking at 200 RPM.

2.2.2 E. Coli transformation

30 μl frozen aliquots of NEB® 5-alpha and One Shot™ TOP10 chemically competent E. coli cells were thawed on ice for 10 minutes. The cells were then inoculated with 1-5 μl plasmid DNA at a concentration between 15-100 ng/ml and kept on ice for 30 minutes. After that, cells were heat-shocked at 42°C for 45 seconds and then moved on ice for 2 minutes. The cells were then inoculated with 1 ml of LB and left recovering at 37°C for 1-1.5 hours while shaking at 200 RPM. After recovery, cells were pelleted, resuspended in 100

μl of LB and plated on LB agar supplied with the appropriate antibiotics. Plates were incubated at 37°C overnight.

2.2.3 *Agrobacterium tumefaciens* growth conditions

Transformed *Agrobacterium tumefaciens* (A. tumefaciens) cells, strain GV3101, were grown on solid LB media supplied with gentamycin (25 μg/ml), rifampicin (100 μg/ml) and spectinomycin (70 μg/ml) at 28°C for 2-3 days. Single A. tumefaciens colonies were then inoculated in 5 ml of liquid LB supplied with the same antibiotics and left growth at 28°C shaking at 140 RPM for 1-2 days. 2 ml of inoculum were then added to 250 ml of liquid LB in 1 l flasks, containing the same antibiotics, and incubated at 28°C shaking at 140 RPM overnight.

2.2.4 A. tumefaciens transformation

100 μl frozen aliquots of chemically competent A. tumefaciens were inoculated with up to 1 μg of plasmid DNA and heat-shocked at 37°C for 5 minutes. The cells then were inoculated with 1 ml of ice-cold LB and left recovering at 28°C shaking at 140 RPM for 3-4 hours. After recovery, the cells were pelleted, resuspended in 100 μl of liquid LB and plated on LB agar supplied with gentamycin (25 μg/ml), rifampicin (100 μg/ml) and spectinomycin (70 μg/ml). The plates were incubated at 28°C for 2-3 days.

2.2.5 Preparation of A. tumefaciens competent cells

A. tumefaciens cells (strain GV3101) from a glycerol stock were streaked on LB agar plates containing gentamycin (25 μg/ml) and rifampicin (100 μg/ml) and incubated at 28°C for 2-3 days. Single colonies were inoculated in 5 ml of liquid LB with the same antibiotics and incubated at 28°C shaking at 140 RPM overnight. The inoculum was then added to 100 ml of liquid LB inside 500 ml flasks and incubated at 28°C shaking until the cells reached a period of steady-state growth (measured using a spectrophotometer, OD_{600} = 0.6-1). The inoculum was then centrifuged at 6000 RPM at 4°C for 20 minutes. The pellet was then resuspended in 2 ml of ice-cold $CaCl_2$ (20 mM) solution and 100 μl aliquots were frozen in liquid nitrogen and stored at -80°C.

2.3 Molecular biology

2.3.1 Genomic DNA extraction from A. thaliana leaves

To genotype Arabidopsis plants, a young leaf for each plant was collected in sterile microcentrifuge tubes and frozen. The leaf tissue was then grinded to

a fine powder with a pestle and suspended in 200 µl of Edward's Buffer (200 mM Tris-HCl (pH7.5), 250 mM NaCl, 25 mM EDTA, 0.5% SDS (sodium dodecyl sulphate)). The solution was centrifuged at 13000 RPM for 5 minute at room temperature. The supernatant was transferred to a new microcentrifuge tube and 1 volume of isopropanol was added. Tubes were inverted and left resting for 5 minutes at room temperature and then centrifuged again at 13000 RPM for 5 minutes. The supernatant was discarded and the pellet washed once with 70% Ethanol. The pellet was then left drying in a flow hood. After drying, 50 µl of sterile water was added to each sample and the DNA was stored at -20°C.

2.3.2 PCR

GoTaq® G2 DNA polymerase kit (Promega) was used for genotyping Arabidopsis T-DNA insertional lines, while Phusion® High-Fidelity DNA Polymerase kit (NEB) was used for cloning CDS of *TCP1*, *AGL71* and *AGL72* genes. Both kits were used as per the manufacturer's instruction. The following set-up reaction and thermocycler conditions were used (Table 2.3-5) Primers used are listed in (Table 7.4 and 7.5).

Table 2.3: PCR reagents

GoTaq® G2 DNA polymerase kit reagents	**Phusion® High-Fidelity DNA polymerase kit reagents**	**µl**
dH_2O	dH_2O	12.4
5X Green GoTaq buffer	5X Phusion HF buffer	4
Forward primer (10 µM)	Forward primer (10 µM)	1
Reverse primer (10 µM)	Reverse primer (10 µM)	1
dNTP (10 mM)	dNTP (10 mM)	0.4
GoTaq	Phusion Taq	0.2

Table 2.4: Thermocycle conditions to genotype T-DNA insertion lines

Step	Temperature	Time	Cycles
Initial denaturation	95°C	2 min	1
Denaturation	95°C	30 sec	30
Annealing	58°C	30 sec	
Extension	72°C	1 min	
Final extension	72°C	5 min	1

Table 2.5: Thermocycle conditions to amplify CDS for TOPO cloning

Step	Temperature	Time	Cycles
Initial denaturation	95°C	2 min	1
Denaturation	95°C	30 sec	30
Annealing	58-64°C	30 sec	
Extension	72°C	25-40 sec	
Final extension	72°C	5 min	1

2.3.3 Agarose gel electrophoresis

PCR products were analysed using agarose gel electrophoresis. Agarose was dissolved in 1X Tris-acetate-EDTA (TAE) buffer at a concentration of 1% w/v, and Gel Red Nucleic Acid Stain was added at a concentration of 1X. For genotyping of T-DNA insertion lines, 8 µl of PCR product per sample was directly loaded to the gel, while 1 µl of 6X Orange DNA loading dye was added to 5 µl of PCR products amplified with Phusion Taq before loading them to the gel. A voltage of 80 V was applied in 1X TAE running buffer using Bio-Rad gel tanks. Gels were left running for ~30 minutes. A UV trans-illuminator was used to visualise DNA bands after the run.

2.3.4 PCR purification

PCR products generated for cloning were purified using QIAquick PCR Purification Kit (Qiagen). Before loading the samples to the column, pH of PCR products was adjusted to ≤ 7.5 adding 10 µl of sodium acetate (3 M) at

pH 5.0. Purified DNA samples were eluted in 30 µl of EB buffer (10 mM Tris-HCl at pH 8.5). DNA was quantified using a nanodrop.

2.3.5 TOPO cloning

Entry vectors containing CDS of *TCP1, AGL71* and *AGL72* were obtained using pENTR™/D-TOPO™ cloning kit. Purified PCR products and TOPO® vector were incubated together in a 1:1 ratio as the following set-up reaction (Table 2.6, Fig. 2.1).

Table 2.6: pENTR/TOPO cloning reagents

Reagent	µl
Purified PCR product	0.5-4
Salt solution (1.2 M NaCl, 0.06 M $MgCl_2$)	1
TOPO vector	1
Water	up to 5

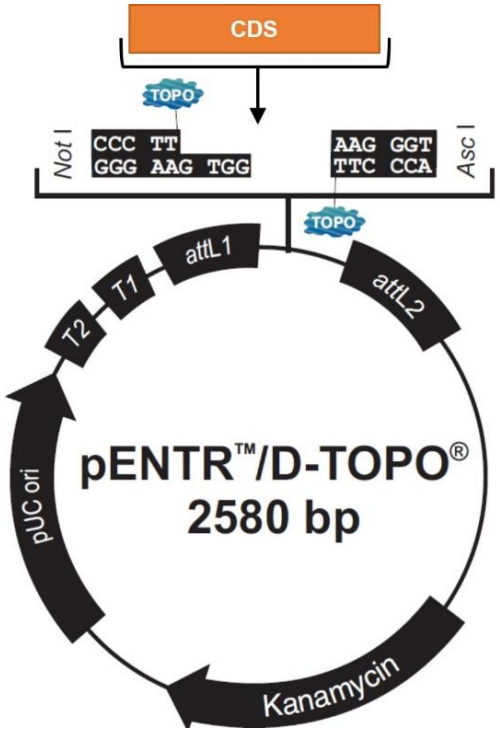

Figure 2.1: pENTR/D-TOPO vector

Schematization of pENTR/D-TOPO entry vector, showing the site of insertion of the gene on interest between the attL sites. In orange is represented the CDS of *TCP1*, *AGL71* and *AGL72* genes inserted in the vector during TOPO cloning reaction.

The reaction was incubated 5 minutes at room temperature and then used to transform One Shot® TOP10 chemically competent E. coli, that were plated of LB agar supplied with Kanamycin (40 μg/ml) and left grow. Four colonies per entry vector were chosen and each inoculated in 5 ml liquid LB containing Kanamycin (40 μg/ml). Miniprep was performed to extract plasmid DNA from the cultures and plasmid concentrations were measured using a nanodrop. To check the correct sequence and insertion of the CDS, all plasmids were sent to sequence.

2.3.6 Gateway Cloning

Gateway™ LR cloning system was used to generate expression clones of *TCP1*, *AGL71* and *AGL72* CDS. Such system allows entry vectors, containing sequences of interest flanked by attL sites, to recombine with destination vectors containing attR sites. The recombination determines the insertion of the sequence of interested in the destination vector. Generated pENTR entry vectors, containing CDS of *TCP1, AGL71* and *AGL72* genes flanked by attL sites were recombined with pALL-III destination vector using the following set-up reaction (Table 2.7, Fig. 2.2).

Table 2.7: Gateway Cloning reagents

Reagent	µl
Entry vector (10 fmoles)	1-7
Destination vector (20 fmoles)	1
LR Clonase™ II Plus Enzyme Mix	2
Tris-EDTA (TE) buffer, pH 8.0	up to 8

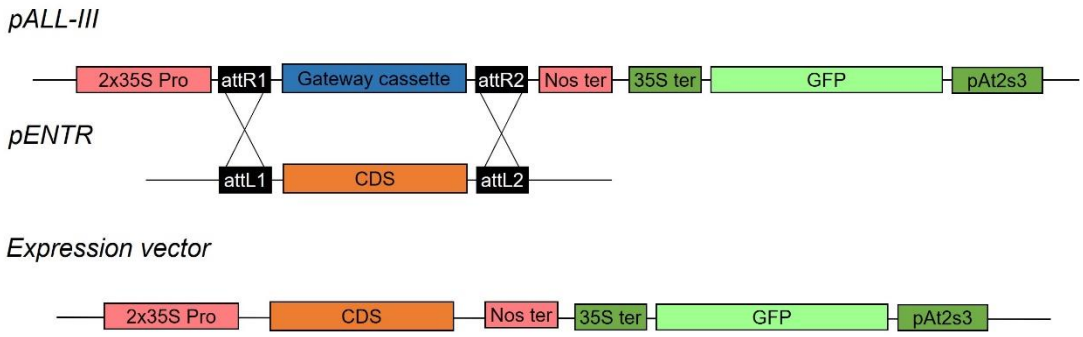

Figure 2.2: Gateway recombination

Schematization of Gateway reaction between attL sited of pENTR containing CDS of *TCP1, AGL71* and *AGL72* genes and pALL-III destination vector. The Expression vector shown the result of the recombination.

The reaction was incubated overnight at 25°C. To stop the recombination, 1 μl of Proteinase K solution was added to the reaction, which then was incubated at 37°C for 10 minutes. 5 μl of the reaction was then used to transform chemically competent E. Coli cells. E. Coli cells were then plated on LB agar supplied with spectinomycin (70 μg/ml) and left grow. Four colonies per expression vector were chosen and each inoculated in 5 ml liquid LB containing spectinomycin and left grow. Miniprep was performed to extract plasmids from the cultures and plasmid concentrations were measured using a nanodrop. To check successful recombination, expression vectors were digested with specific enzyme and send to sequence. The vectors were used to transform A. tumefaciens cells.

2.3.7 Plasmid miniprep

Plasmid isolation from bacteria was carried out using Plasmid Mini Kit® (Qiagen). 5 ml liquid culture was centrifuged for 5 minutes at 3500 RPM to pellet the bacteria. Bacteria lysis and plasmid ligation to the spin column was performed as for manufacturer's instructions. Isolated plasmids were eluted in 50 ml of Elution buffer and concentrations were measured using a nanodrop.

2.3.8 PCR colony

5 colonies of transformed E. Coli growing on LB agar plates were separately picked with sterile toothpicks and resuspended in 5 µl of sterile water. 2 µl of each resuspended colony were then used as DNA template for PCR, with the initial denaturation step at 95°C set for 5 minutes rather than for 2. At the end of the reaction, PCR products were run on a 1% w/v agarose gel.

2.3.9 Plasmid digestion

Plasmid digestion was carried out using restriction enzymes from NEB. Each reaction was performed using 1 μl of enzyme, 2 μl of 10X rCutSmart buffer, 1-5 μl of DNA (1 μg) and sterile water up to 20 μl. The reaction was incubated at 37°C for 1-16 hours. The digested product was run on a 1% w/v agarose gel.

2.3.10 GUS staining

Section of shoot growing lateral shoots at different developmental stages were fixed in ice with acetone 90% for 40 minutes. After that, the sections were washed twice in 100 mM phosphate buffer at pH 7 (Na_2HPO_4 + NaH_2PO_4) and incubated in Gus solution (100 mM phosphate buffer, 0.5 mM $K_3Fe(CN)_6$, 0.5 mM $K_4Fe(CN)_6$, 0.5-1 mg/ml X-Gluc dissolved in DMSO, 0.1% Triton X-100). Samples were then vacuumed for 10 minutes and left at 37°C overnight. The samples were then washed in 100% ethanol and cleared using a 3:1 solution of methanol and acetic acid. Samples were stored in 70% ethanol. Images were taken using a Zeiss Scope A1 microscope with an Axiocam 305 colour camera.

2.3.11 Total RNA extraction and cDNA synthesis

Lateral shoots of Arabidopsis at different developmental stages were sectioned under a stereoscope. The adaxial and abaxial side of the lateral shoot were collected in different tubes and frozen in liquid nitrogen. Sections from three different plants were pooled together as one biological replicate for a total of three biological replicates. Total RNA was extracted using E.Z.N.A. plant RNA kit (Omega bio-tek). Before eluting RNA from binding columns, on-membrane DNase I digestion was performed to eliminate DNA from the sample. Quantity and quality of total RNA extracted were assessed using a bioanalyzer (Agilent). Complementary DNA (cDNA) was synthesized from 1 μg of total RNA per sample using a SuperScript™ VILO™ cDNA Synthesis Kit according to the manufacturer's instructions.

2.3.12 Real-Time quantitative PCR

cDNA of each sample was diluted 1:10^3 and SsoFast™ EvaGreen® Supermix (Bio-rad) was used for real-time quantitative PCR (qPCR). 1 μl of diluted cDNA and 14 μl of reaction mix containing forward and reverse primers (10 μM) and SsoFast supermix (1X) were used per reaction. A 96-well plate was loaded with three biological replicates for sample, each loaded in triplicate (technical

replicates). For each couple of primers a standard curve was calculated pooling cDNA from each sample and using 1:4 serial dilutions. qPCR was performed using Bio-Rad's CFX96 Real-Time PCR system in accordance with the cycling conditions instructed in the SSoFast Eva Green Supermix protocol. A melt-curve was carried out for each amplicon at the end of every qPCR. Based on the results of the three technical repeats for three biological replicates, quantification of various mRNA expression levels relative to the transcript of the housekeeping genes *ELONGATION FACTOR 1*α (*EF1*α) and *ACTIN2* (*ACT2*) was determined as described by (Taylor *et al.*, 2019), comparing the expression of each gene of interest with the two housekeeping genes using the geometric mean. Primers used are listed in (Table 7.6).

2.3.13 RNA sequencing

Total RNA samples containing $\geq$ 2μg of RNA, with RIN (RNA integrity number) > 6.0 and Nucleic Acid 260/280 ratio of 1.8-2.2 were submitted in triple biological replicate to Azenta/GENEWIZ for RNA sequencing and data analysis (Table 2.8).

Table 2.8: Total RNA quality control

Sample		Concentration (ng/μl)	RNA Integrity Number
Adaxial	#1	123	9.4
	#2	92	9.6
	#3	140	9.6
Abaxial	#1	133	9.7
	#2	75	9.9
	#3	146	9.8

RNA sequencing was carried out using Illumina NovaSeq system with 2x150 bp sequencing and 10M read pairs configuration. Data quality and analysis was performed by Azenta/GENEWIZ applying the following steps. Quality Score was used to check the quality of sequencing. As shown in Table 2.9, all the biological replicates sent to sequence reach a quality score > 30, indicating 1 in 1000 probability of incorrect base call during the sequencing.

Table 2.9: Sample sequencing statistics

Sample		Number of reads	Mean Quality Score
Abaxial	#1	27,911,589	35.25
	#2	25,065,952	34.99
	#3	31,358,263	35.00
Adaxial	#1	38,319,083	34.57
	#2	18,929,066	34.80
	#3	23,662,765	35.12

To remove adapter sequences and nucleotides with poor quality, reads were trimmed using Trimmomatic v.0.36. Trimmed reads were mapped to the *Arabidopsis thaliana* TAIR10 reference genome using STAR aligner v2.3.2b. featureCounts from the Subread package v.1.5.2 was used to calculate unique gene hit counts, which were reported using the gene_id feature in the annotation file. Unique reads that fell within exon regions were counted. Table 2.10 shows the statistics of the mapping process.

Table 2.10: Mapping statistics

Sample		Total mapped reads	% mapped reads	% unique reads
Abaxial	#1	25,687,033	98.58	88.53
	#2	17,317,402	98.55	87.91
	#3	21,125,142	98.60	88.19
Adaxial	#1	21,906,844	98.64	88.46
	#2	27,136,228	98.67	87.12
	#3	30,965,110	98.21	88.19

Distribution of read counts were analysed by plotting the raw counts and the normalized counts (Fig. 2.3 A). Counts were normalized for sequencing yield between samples. The normalized read counts were used to determine differentially expressed genes.

Before performing differential transcriptomic analysis between the adaxial and abaxial samples, overall similarity among samples were assessed to exclude

the presence of replicates not representative of their group. Biological replicates of both adaxial and abaxial side show shorter distance within groups than between groups, confirming that every biological replicate can be considered representative of their group (Fig. 2.3 B).

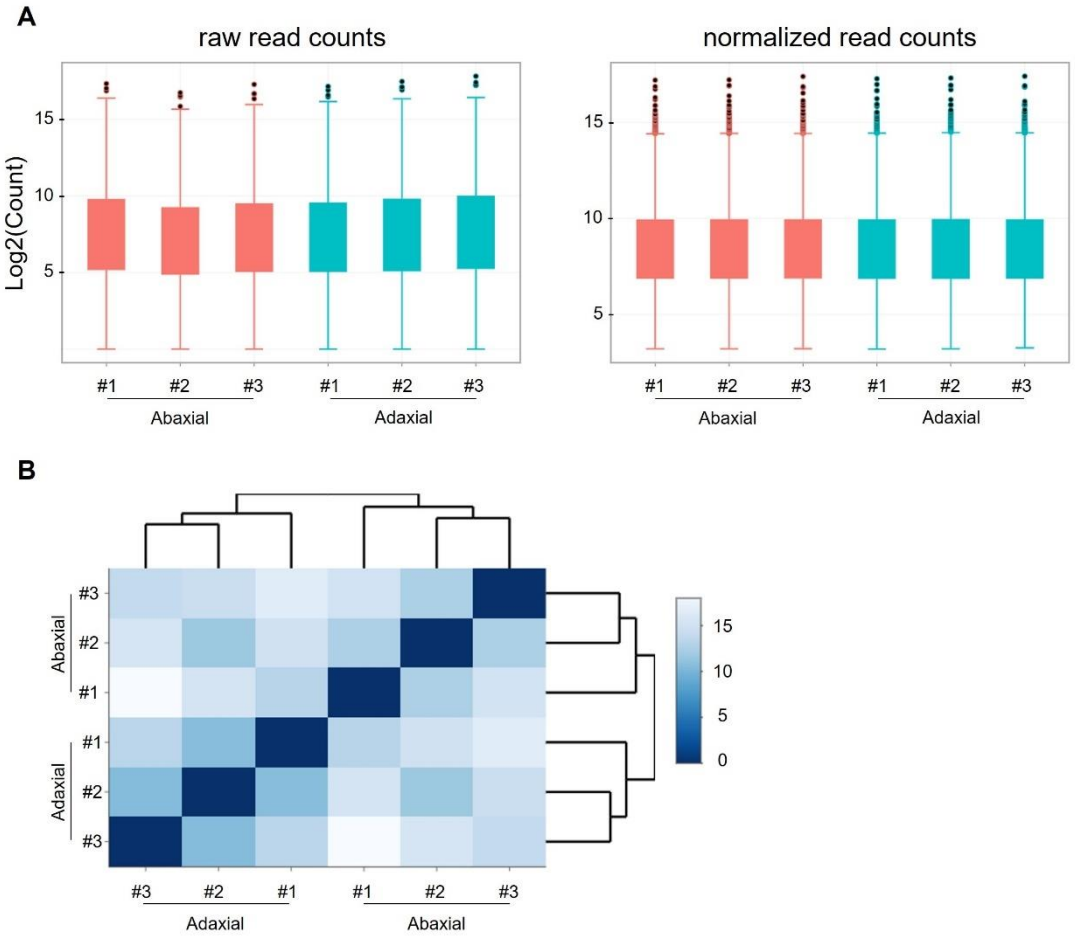

Figure 2.3: RNASeq data quality control

A) Box plot of distribution of non-normalized and normalized (by sequencing yield) read counts. Box boundaries indicate the interquartile range (IQR). Black dots indicate outliers. Box whiskers represent data points 1.5x from the IQR. Read counts were transformed on to a $\log_2$ scale. # indicates the number of replicate. B) Heat-map of sample-to-sample distance. In the colour-code scale, shorter distances are represented by low numbers. The shorter is the distance between samples the more closely related the samples are.

DESeq2 was used to perform a comparison of gene expression between abaxial and adaxial samples. The Wald test was used to generate p-values and $\log_2$ fold changes. Genes with adjusted p-value < 0.05 and absolute $\log_2$ fold change > 1 were called as differentially expressed genes. Gene ontology was performed using Fisher exact test (GeneSCF v1.1-p2).

2.4 EMS mutagenesis

2.4.1 Mutagenesis

Around 20,000 *rcn1-1* seeds were soaked in 100 mM phosphate buffer at 4°C overnight. Seeds were then incubated with 33 mM of ethyl methanesulfonate (EMS) inside an atmos bag (Sigma-Aldrich) under a fume hood, and left at room temperature for 16 hours. The EMS solution was decanted into a beaker and neutralised with 1 M NaOH. Seeds were washed twice with a solution of 100 mM Sodium Thiosulphate for 15 minutes. The same washing procedure was repeated with water. Seeds were then left dry overnight in a fume hood on filter paper. To test the germination rate of the mutagenized seeds, 100 seeds were surface sterilised with chlorine gas, plated on petri dishes containing ATS media, stratified for two days at 4°C, and then incubated in a growth room under long day photoperiod (16h day) at 20-22 °C. Germination rate was measured 5 days after germination (~ 80%).

2.4.2 Screening of mutagenized plants

Mutagenized seeds (M_1) were divided in 80 pools, sown and left self to produce M_2 seeds. Chlorophyll mutation frequency was estimated by counting the seedlings showing phenotypes with impaired leaf pigmentation among the ~ 20,000 mutated seedlings (< 1%). M_2 seeds were plated and left grow for 12-14 days, before being screened. Seedlings that shown the desired phenotype were transferred to soil, left grown and self to produce M_3 seeds. M_3 seeds were plated and screened again. Seedlings maintaining the desired phenotype were transferred to soil and left grow.

2.4.3 Whole genome sequencing preparation

M_3 plants were backcrossed to *rcn1-1* and the following F_1 generation was plated and, after 12 days, the lateral root GSA phenotype was analysed. Based on the segregation of the GSA phenotype, suppressor mutations were classified in recessive or dominant, then F_1 seedlings were transferred in soil and left self. The same GSA analysis was performed for F_2 seedlings. For each mutated line seedlings were dived in “phenotype”, showing the suppressor phenotype, and “non phenotype” showing *rcn1-1* phenotype. For mutated lines classified as recessive, leaf segments of 50 “phenotype” seedlings and 200 “non phenotype” seedlings were collected. The “non phenotype” seedlings were then transferred to soil and left self. The F_3 generation was screened for GSA phenotypes and the lines that did not show segregation of the *rcn1-1* phenotype were selected as homozygous for the absence of the suppressor mutation, while the segregating lines showing both

rcn1-1 phenotype and the suppressor phenotype were labelled as heterozygous for the suppressor mutations and the leaf collected from the F_2 parent lines was discarded. The process was repeated for mutated lines classified as dominant with the difference of collecting 50 leaf segments from "non phenotype" seedlings and 200 from "phenotype" seedlings, the latter were then transplanted to soil, left generate F_3 seeds that were similarly screened and divided into homozygous and heterozygous for the suppressor mutation. At the end of this screening process for each suppressor line selected, the 50 "phenotype" leaf segment were pooled together, and genomic DNA was extracted using DNeasy Plant kit from Qiagen. The same was repeated for the 50 "non phenotype" leaf segments. Genomic DNA was sequenced by Novogene (UK) using Illumina NovaSeq 6000 platform, at 20x sequencing depth, producing long reads sequencing with paired ends.

2.4.4 Whole genome sequencing analysis

Data produced by Illumina sequencing was returned in FASTQ format. FASTQ files were analysed using the bioinformatic tools ArtMap (Javorka *et al.*, 2019) and DiscoSNP++ (Uricaru *et al.*, 2015; Gauthier *et al.*, 2020). ArtMap was run on a Windows system with recommended settings (quality controls and PCR duplicates removal ON, depth filter 10-100) and frequency threshold at 60%. DiscoSNP++ was run on a Linux system using the following command line:

./run_discoSnp++.sh -r file/fof.txt -T -G file/reference_genome.fa

TAIR10 genome was used as reference genome to map the sequenced reads. Variant call format (VCF) files produced by the analysis were compared and, for each suppressor line sequenced, a list of the most interesting SNPs was compiled.

2.5 Phenotypical analysis

2.5.1 Lateral root and shoot gravitropic setpoint angle analysis

For lateral root gravitropic setpoint angle (GSA) analysis, seeds plated on ATS in square petri dishes were grown vertically in a growth room for 12 days. After that, plates were scanned using an Epson Perfection V370 or V800 photo scanner at 600 dpi. Stage III lateral root (~1 mm) tip angle was measured using FIJI/ImageJ. For lateral shoot GSA analysis, 21-28 days old plants were photographed using a RICOH GR II camera. Lateral shoot profile was then divided into 0.5 cm long segments and the angles of each segment was measured using FIJI/ImageJ software.

2.5.2 Lateral shoot growth kinetics

Plants were grown in growth room or glasshouses for 21-28 days. Once bolted, plants were photographed using a RICOH GR II camera every 24 hours following lateral shoot development until mature stage was reached.

2.5.3 Analysis of lateral root gravikinetics

Seeds plated in square petri dishes were grown vertically in a growth room for 12 days. Plates were then kept in the dark for 1 hour before being reoriented by 30°. With a 920 nm infra-red LED backlight positioned behind the plates and a SONY alpha 7R camera with an infra-red adjusted FE 2.8/50 MACRO lens, images were taken in the dark every 30 minutes from the reorientation for 6 hours, using SONY Imaging Edge Desktop software with Remote function's manual mode, 1/13 shutter speed, F4 aperture and ISO 64 settings. Images were then analysed using FIJI/ImageJ software.

2.5.4 Lateral shoot GSA reorientation and gravicompetence assays

For both assays plants were grown in soil in a growth room. For GSA reorientation assay plants with lateral shoots at different developmental stages, were photographed and then tilted 45° from the vertical, moving lateral shoots to lower angles with respect to their previous growing angle (as shown in Fig. 4.2 A). Tilted plants were then photographed again after 6 hours. For gravicompetence assay (perpendicular assay), plants with stage III lateral shoots were photographed and then laid down flat, moving lateral shoots perpendicularly to the gravity vector (as shown in Fig. 4.3 A). As for the previous assay, reoriented plants were photographed again after 6 hours. This was repeated in the dark, with plants kept in the dark 1 hour prior reorientation. To stop the primary shoot gravitropic response from affecting lateral branch inclination, all assays were performed with the primary shoot secured to a thin wooden stick inserted in the pots. Photographs were taken using either a SONY alpha 7R camera with an infra-red adjusted FE 2.8/50 MACRO lens or a RICOH GR II camera.

2.5.5 Shoot clinorotation assay

Plants at rosette stage (~ 2-3 weeks old) growing in a growth room were taped on 1-D Mikrops Electric Clinostats (Flatters & Garnett, Manchester, UK). The clinostats were then positioned horizontally, with the rotation axis perpendicular to the gravity vector (parallel to the ground) and clinorotation at

4 rph (rotations per hour) was started. Clinostats with control plants were left clinorotating vertically, with the rotation axis parallel to the gravity vector. Plants were left clinorotating up to 2 weeks and photographed with a SONY alpha 7R camera every hour after bolting, following the lateral shoot development.

2.5.6 Toluidine blue staining

Transverse sections of lateral shoot stems were obtain by hand-sectioning. The sections were incubated in 0.02% w/v of Toluidine blue dissolved in distilled water, and left in solution for 5 minutes at room temperature as described in (Pradhan Mitra and Loqué, 2014). After that, sections were washed 3 to 5 times with water and mounted on microscope slides. Sections were imaged using a Zeiss Scope.A1 microscope.

2.6 Microscopy

2.6.1 DIC microscopy

Differential Interference Contrast (DIC) microscopy was used to observe statolith presence in lateral roots of EMS mutants and in young lateral shoots. Both lateral roots and shoots were stained using Lugol solution (Sigma) for 3-5 minutes and cleared with a wash of chloral hydrate solution (8:3:1 mixture of chloralhydrate: water: glycerol), before being mounted on slides. A Zeiss Scope.A1 microscope (10x and 40x magnification) with an Axiocam 305 colour camera was used to image the mounted slides.

2.6.2 Preparing lateral shoot for confocal microscopy

For PIN3/4/7-GFP analysis, lateral shoots were hand-sectioned with the help of a stereoscope immediately before being imaged. For imagining lateral shoot epidermal and cortical cells, sections of primary inflorescence containing a SII/SIII lateral shoots were kept in tubes maintaining the natural branch orientation while getting fixed under vacuum with 4% Paraformaldehyde (PFA) dissolved in Phosphate-buffered saline (PBS) solution 1X at pH 6.9 for 2 hours. Afterwards samples were washed twice in 1X PBS and lateral shoots sectioned with the help of a stereoscope, dividing the adaxial side from the abaxial side of the branch. To stain the cell wall, sections were then either incubated with calcofluor white (0.25 μg/ml) dissolved in 1X PBS and left shaking overnight or with calcofluor white (0.1 % w/v) dissolved in clearsee solution (10% w/v xylitol (Sigma), 15% w/v sodium

deoxycholate (Sigma), 25% w/v urea (Sigma))(Kurihara *et al.*, 2015; Ursache *et al.*, 2018) and left shaking for 1 hour. After that, samples were washed for 30 minutes in 1X PBS before being imaged.

2.6.3 Confocal microscopy and image analysis

After mounting section of lateral shoots with water on slides, a Zeiss LSM880 upright confocal microscope with a 488 nm (for GFP excitation) or 405 nm (for calcofluor white) laser at a 10x to 40x magnification was used to take Z-stack and Tile-scan images of lateral shoot sections. Images were then analysed using FIJI/ImageJ software. For cell length and number quantification, images of whole sections were divided by a 10-15k μm^2 grid and cell length and number were measured in ~1k µm of total length.

2.7 Statistical methods

Data visualization and statistical analyses were performed in R, using RStudio software. ggplot2, plyr and dplyr packages (Tidyverse) were used to build box plots and bar charts for data visualization. Statistical analysis was performed using the following R functions: aov() – one-way ANOVA, TukeyHSD() – Tukey's HSD post-hoc test, t.test() – independent t-test, wilcox.test() – Mann-Whitney-Wilcoxon test, pairwise.wilcox.test() – pairwise Wilcox test with Benjamini-Hochberg correction.

Chapter 3. Identification of new regulators of Arabidopsis lateral root GSA

Introduction

During development, lateral roots can be classified in stages based on their length and age. In Arabidopsis, lateral roots emerge at an angle of approximately 90° (stage I) and, following the development of a differentiated columella and elongation zone, undergo a brief period of downward growth (stage II), before transitioning to increasingly vertical GSAs (Stage III-V). At these later stages, lateral roots have acquired full gravicompetence and ability to robustly maintain GSAs (Guyomarc'h *et al.*, 2012). Differently from primary roots, where PIN3, PIN4 and PIN7 are expressed at the same time in the columella, in lateral roots PIN proteins shows differential spatio-temporal expression (Guyomarc'h *et al.*, 2012; Roychoudhry *et al.*, 2013). From emergence until stage III, PIN3 is the only PIN detectable in the lateral root columella. At stage III, PIN7 starts to become visible. Following the transition towards stage IV, PIN3 begins to decline while PIN7 expression increases. Finally, as lateral roots enter stage IV, PIN3 expression is no longer detectable and PIN4 expression is turned on (Guyomarc'h *et al.*, 2012). Due to this differential expression of PIN proteins, it has been suggested that the non-vertical growth in lateral roots could be the result of impaired gravitropism linked to a weaker transport of auxin by the columella cells (Rosquete *et al.*, 2013; Waidmann *et al.*, 2019). However, this model cannot account for the robust maintenance of GSA showed by lateral roots and, more importantly, their unique capacity to bend upwards (against the direction of gravity) when reoriented to angles lower than their GSAs. Furthermore, it has been shown that the spatial expression of PIN3 and PIN7 in the columella of stage III lateral roots correlates with their role in maintaining non-vertical GSAs, with PIN7 localization biased towards the upper side of columella cells accounting for the antigravitropic auxin flux (Roychoudhry *et al.*, 2019). Conversely, PIN3 polarization is slightly biased toward the lower side, contributing to the angle-dependent gravitropic auxin flux (Roychoudhry *et al.*, 2019). Upon reorientation, both PIN proteins are involved in the asymmetric redistribution of auxin that generate the root anisotropic growth (Roychoudhry *et al.*, 2019). Furthermore, similarly to what has been shown in primary roots (Grones *et al.*, 2018), the phosphorylation and dephosphorylation of serine residues S316, S317 and S321, located in PIN3 cytoplasmic loop, influence the targeting of

PIN3 respectively to the upper and lower side of columella cells (Roychoudhry *et al.*, 2019). PIN3 dephosphorylation is regulated by PP2A/RCN1 phosphatase (Roychoudhry *et al.*, 2019). Consistent with this, loss-of-function of RCN1 determines a shift of PIN3 localization to the upper side of the columella cells, leading to an increased AGO and shallow lateral root phenotype (Roychoudhry *et al.*, 2019). Conversely, overexpression of *RCN1* in the columella determine PIN3 to predominantly localise to the lower side of the columella cells determining more vertical lateral root GSAs (Roychoudhry *et al.*, 2019). Auxin treatment of lateral roots positively regulates RCN1 protein stability and induces a shift to more vertical GSAs, while *rcn1* fails to respond to exogenous application of auxin, maintaining shallow lateral roots (Rosquete *et al.*, 2013; Roychoudhry *et al.*, 2019). Taken together this evidence strongly suggests that non-vertical GSAs are controlled entirely by PIN-mediated auxin distribution at the root tip and that auxin regulation of lateral root GSAs is dependent on RCN1 activity in the columella.

The recent evidence of the role of RCN1 and LZY proteins in the control of non-vertical GSA has highly contributed to our understanding of the gravitropic-dependent auxin redistribution in lateral roots (Roychoudhry *et al.*, 2019; Furutani *et al.*, 2020). Among the AGCVIII kinase family, WAG2 is expressed in lateral root tips and could, therefore, contribute to lateral root GSA regulation (Roychoudhry *et al.*, 2019). Consistent with this, lateral roots of the double loss-of-function mutant *wag1wag2* maintain a more vertical GSA compared to wt plants (Roychoudhry *et al.*, 2019). However, PIN3 subcellular localization is not altered in the absence of WAG2 and the expression of WAG2 in *wag1wag2* columella cells fails to rescue the altered GSA phenotype, suggesting the presence of other kinases involved in PIN3 phosphorylation in the columella of lateral roots (Roychoudhry *et al.*, 2019). To identify possible kinases involved in PIN3 phosphorylation, and new GSA regulators working in antagonism to RCN1, an EMS mutagenesis was carried out on RCN1 loss-of-function mutant *rcn1-1.* Around 7500 M_1 (mutated) seeds were screened and 115 M_2 lines that showed suppression of the *rcn1* phenotype were selected. Among these, 27 lines conserved the suppressor phenotype in M_3. Four of the 27 lines, which showed no additional phenotypes in the root system and no growth and seed production impairments compared to wt, were selected to further studies and were named *suppressor of rcn1* (*sor*) *1, 2, 3* and *4*.

Results

3.1 Phenotypical characterization of *rcn1sor* mutants

The identified *suppressor of rcn1 1* (*sor1*), *sor2, sor3* and *sor4* displayed different degrees of phenotypic recovery of the shallow lateral root phenotype of *rcn1-1* (Fig 3.1 A and B). *sor1, 2* and *3* mutations restore *rcn1* lateral root GSA to wt levels (Wassilewskija ecotype - Ws), while *sor4* induces a more vertical lateral root GSA compared to both *rcn1* and wt (Fig 3.1 A and B).

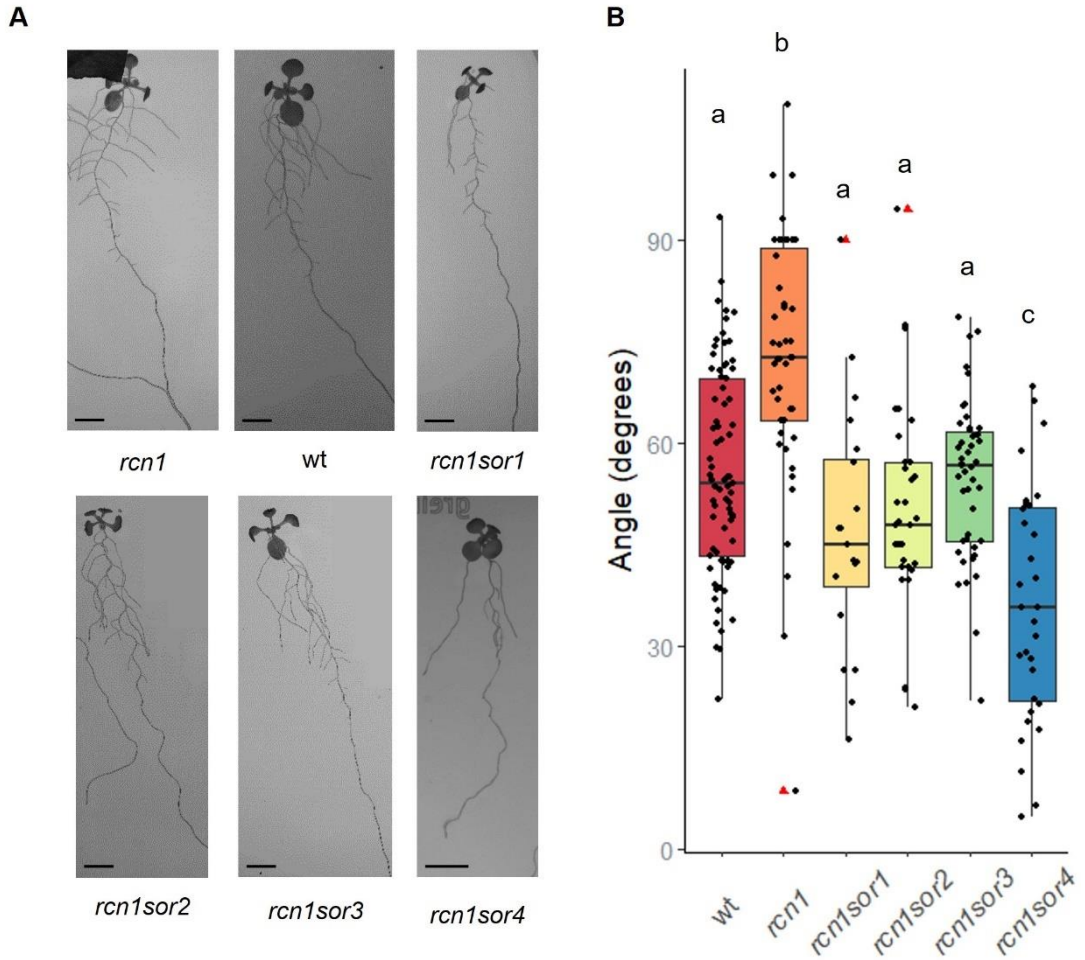

Figure 3.1: *sor* mutations rescue *rcn1* lateral root phenotype

A) Representative images of *rcn1-1*, wt (Ws) and *rcn1sor* double mutants, 12-14 days after germination. Scale bar = 0.5 cm B) Box plot of quantitative analysis of stage III lateral root GSA of wt, *rcn1* and *rcn1sor* mutants. Box boundaries indicate the interquartile range (IQR), with central line representing the median. Red triangles indicate outliers. Box whiskers represent data points 1.5x from the IQR. Statistical analysis was performed using one-way ANOVA with Tukey's HSD post-hoc test. Different letters indicate significant difference with $p < 0.0005$. A minimum of 20 lateral roots per line were measured.

Although *rcn1* does not display any abnormal lateral shoot GSA phenotype (Fig. 3.2 A and B), the mechanisms mediating GSA control is similar in lateral shoots and roots (Roychoudhry *et al.*, 2013). For this reason, lateral shoot development of the *rcn1*-suppressing mutants was also analysed, to assess whether additional phenotypes could be detected. Shoots of *rcn1sor2*, *rcn1sor3* and *rcn1sor4* develop normally, with *sor2* and *sor3* mutations not altering the lateral shoot phenotype, and *sor4* inducing more vertical lateral shoot GSAs, similarly to lateral roots (Fig. 3.2 C). *rcn1sor1* mutant developed a small rosette and short primary and secondary inflorescences, displaying a dwarf-like phenotype (Fig. 3.2 C). Interestingly, this shoot phenotype segregates independently from the *rcn1*-suppressing phenotype in lateral roots, indicating the presence of other mutations in one or more genes most likely involved in the *rcn1sor1* shoot phenotype but not in the root one.

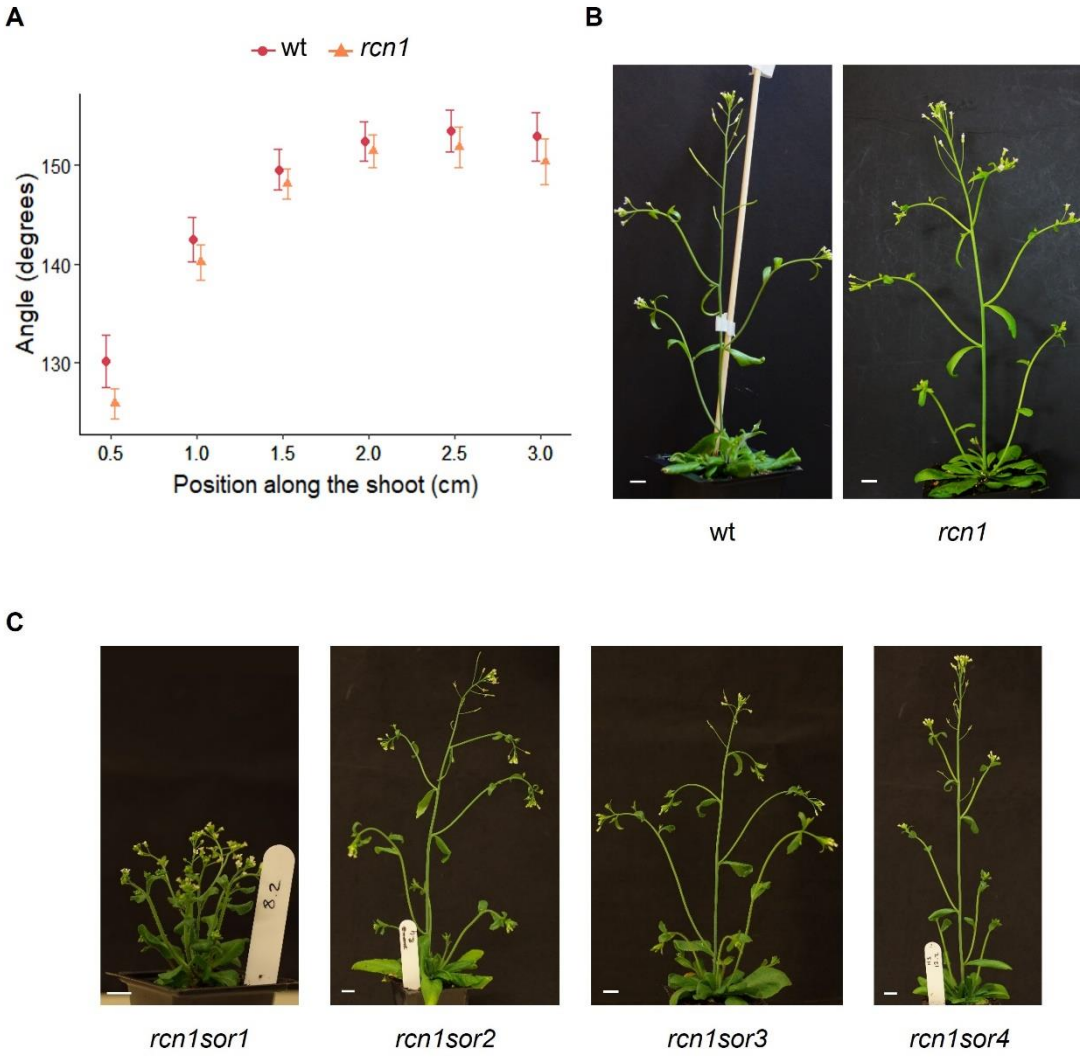

Figure 3.2: Phenotypical analysis of *rcn1sor* shoots

A) Quantitative analysis of lateral shoot GSA of wt (Ws) and *rcn1-1*. Error bars show 95% confidence interval. Number of lateral shoots measured was 35 for wt and 34 for *rcn1*. B) Representative images of 21-28 days old wt and *rcn1* plants. C) Representative images of 21-28 days old *rcn1sor* mutants. Scale bars = 1 cm.

Due to statolith role in gravity perception, alterations in starch accumulation during statolith development can lead to impairments in root gravitropism and GSA maintenance (Kiss, Hertel and Sack, 1989). To check if any of the *sor* mutations determine alterations in statolith formation, statolith morphology was analysed using Lugol staining. In all four *rcn1sor* lines, statoliths appear normal with morphology comparable to wt and *rcn1* (Fig. 3.3).

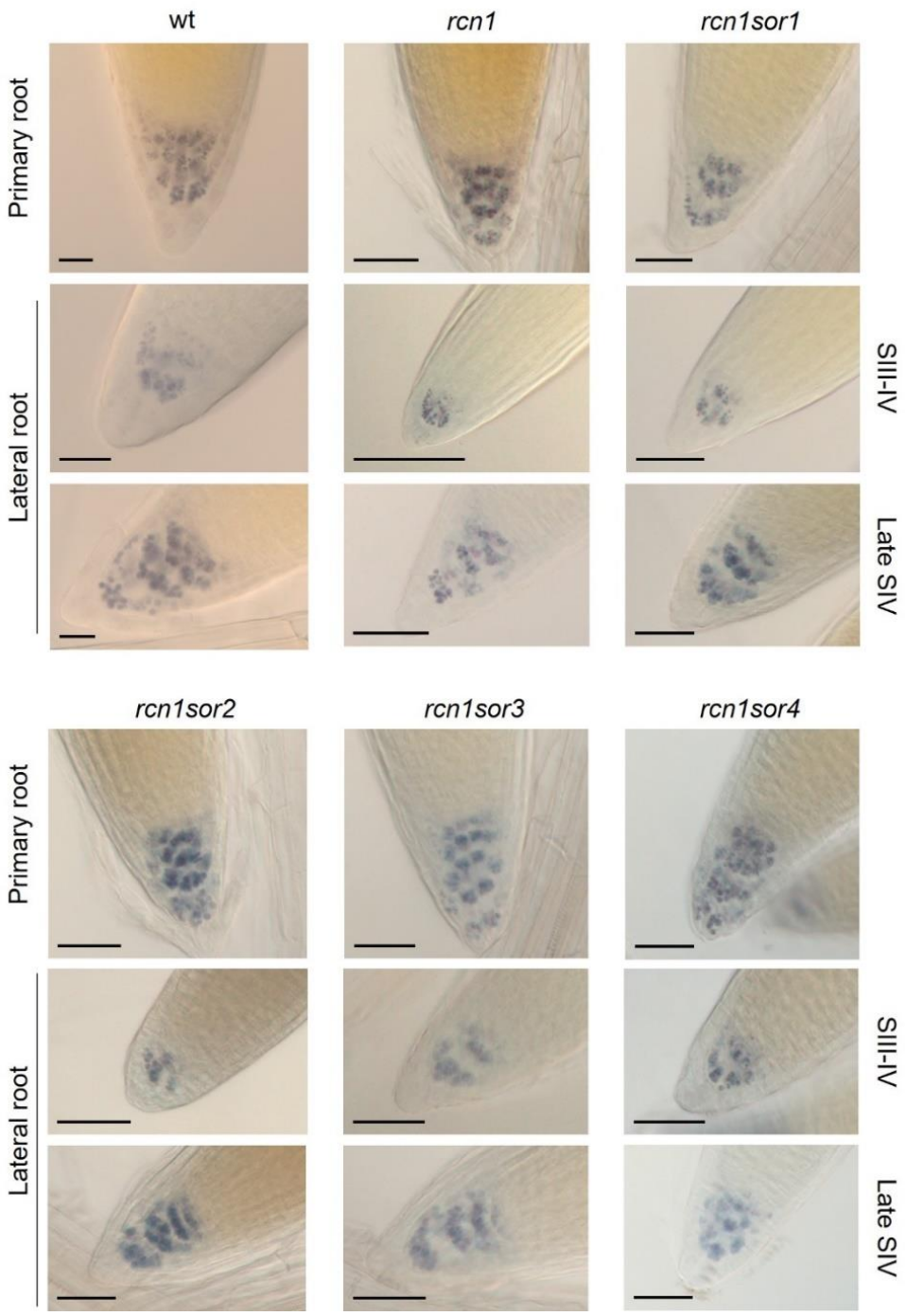

Figure 3.3: Statoliths of *rcn1sor* mutants are comparable to wt

Representative images of primary and lateral root tips stained with Lugol's solution of wt, *rcn1* and *rcn1sor* mutants. Root statoliths were checked in five seedlings per line. Scale bars = 150 μm.

3.2 *sor* mutations restore *rcn1* gravitropic response in lateral roots

As previously described, the lack of PP2A/RCN1 activity determines a delay in lateral root gravitropic response (Roychoudhry *et al.*, 2019). Such delay can be explained by RCN1 control of PIN3 phosphorylation status in the columella of lateral roots, and the consequent variation in PIN3 subcellular localization (Roychoudhry *et al.*, 2019). Upon reorientation, lateral roots normally restore their GSA after around two hours, with downward bending lateral roots responding slightly slower than upward bending ones (Fig. 3.4 A). In comparison, *rcn1* lateral roots take double the time to grow back to their GSA. Downward bending roots are the most affected, needing more than four hours to grow towards their previous GSA (Fig. 3.4 B). All the *rcn1sor* double mutants rescue in different degrees *rcn1* slow gravitropic response (Fig. 3.4 and 3.5). *sor1* and *sor3* mutations rescues *rcn1* slow gravitropism with lateral roots bending both upward and downward slightly faster than wt (Fig. 3.4 C and 3.5 B). Similarly, *sor4* mutation rescues *rcn1* gravitropism showing lateral root restoring their GSAs slightly faster than wt (Fig. 3.5 C). *rcn1sor2* downward bending lateral roots, instead, rescue *rcn1* gravikinetic impairments but restore their GSA slightly slower than wt (Fig. 3.5 A).

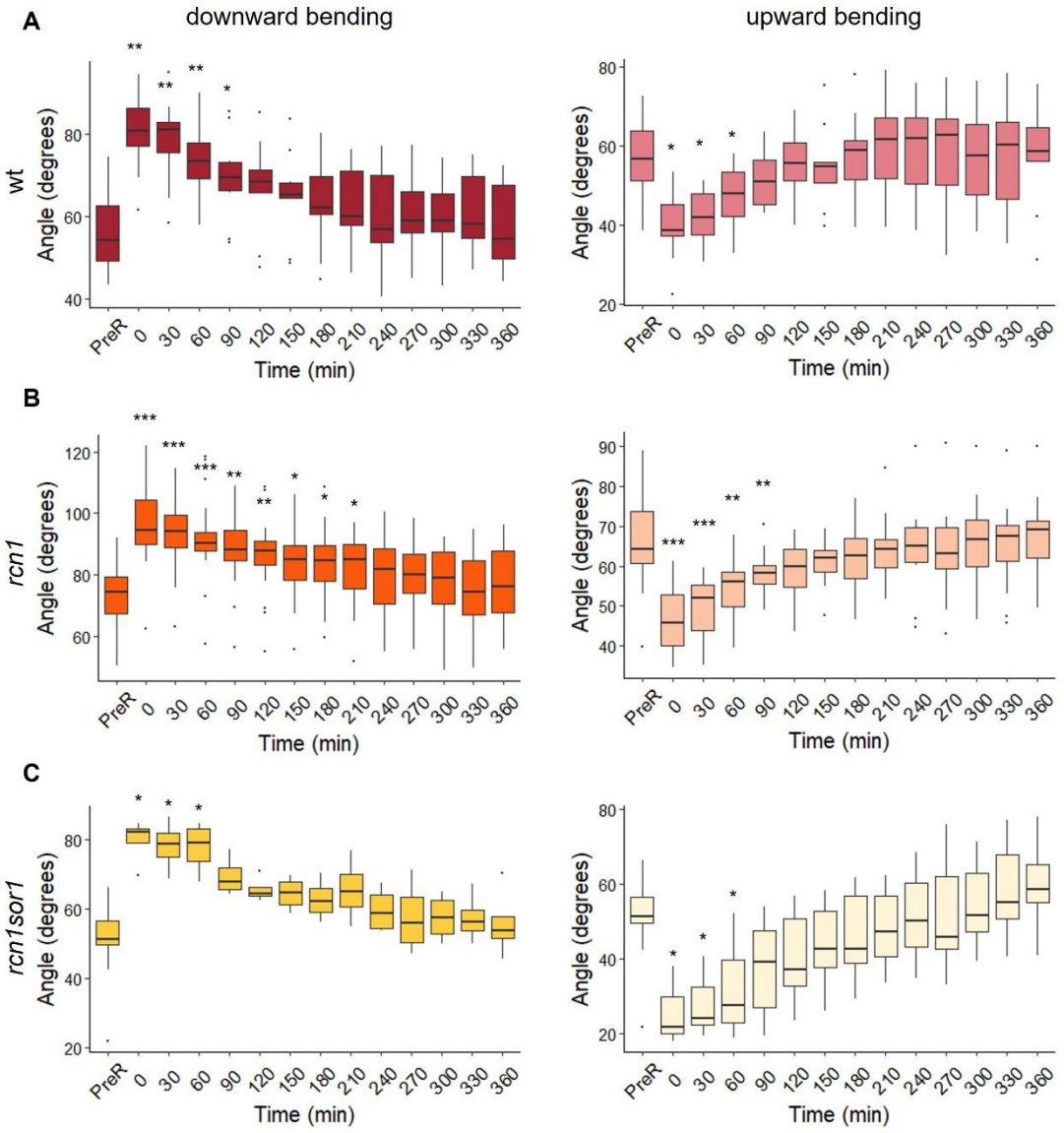

Figure 3.4: *sor1* mutation rescue *rcn1* slow gravitropic response

Box plots showing quantitative analysis of stage III lateral root gravitropic response upon 30 degrees reorientation of wt (Ws) (A), *rcn1* (B) and *rcn1sor1* (C). Box boundaries indicate the interquartile range (IQR), with central line representing the median. Black dots indicate outliers. Box whiskers represent data points 1.5x from the IQR. Statistical analysis was performed using pairwise Wilcox test with Benjamini-Hochberg correction. *** = $p < 0.0005$, ** = $p < 0.005$, * = $p < 0.05$. Number of lateral roots measured was between 13 and 26. PreR indicates angle measurements taken before reorientation, time 0 indicates angle measurements taken immediately after reorientation. Subsequent measurements were taken every 30 minutes from reorientation.

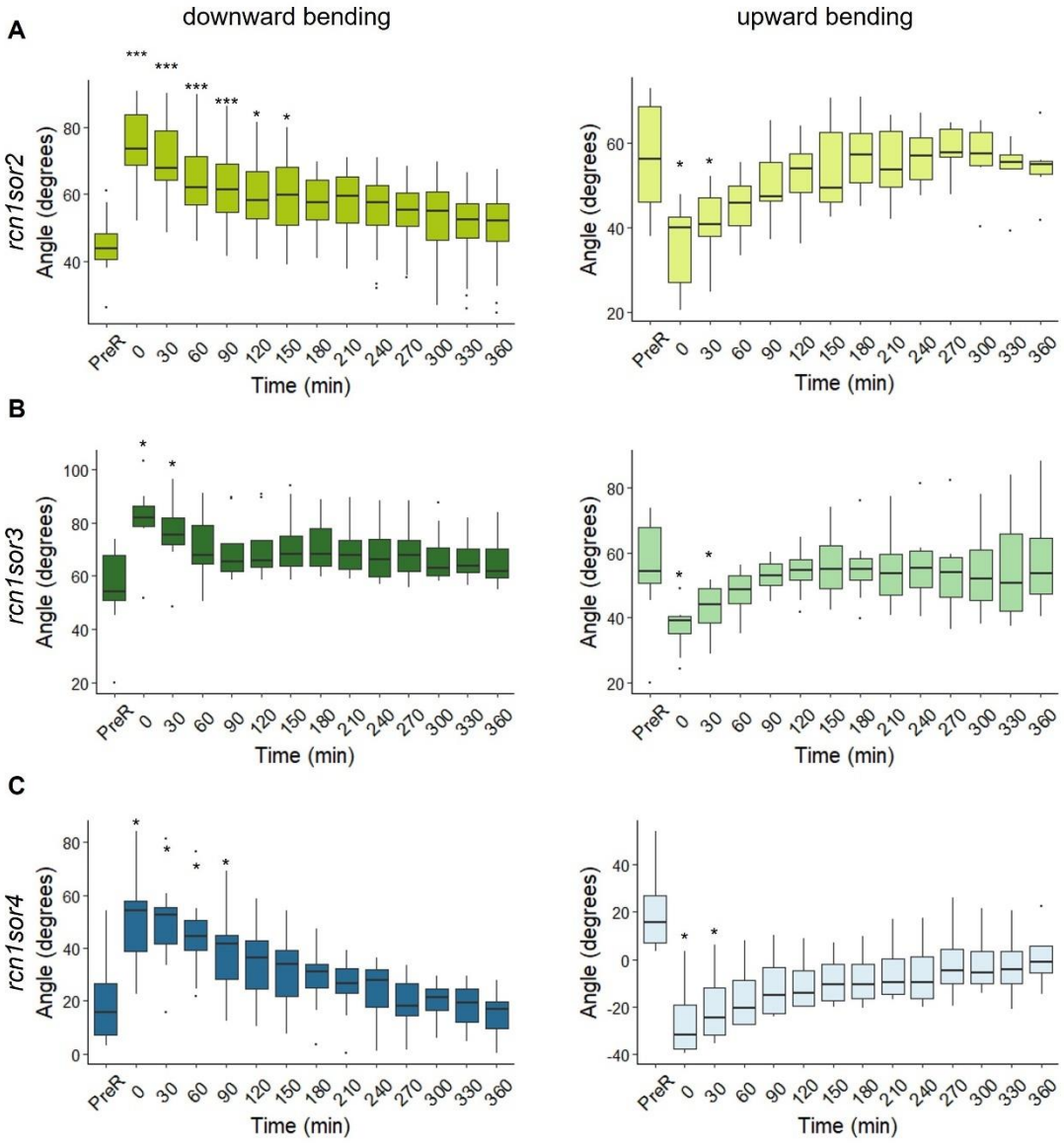

Figure 3.5: *sor2, sor3* and *sor4* rescue *rcn1* slow gravitropism

Box plots showing quantitative analysis of stage III lateral root gravitropic response upon 30 degrees reorientation of *rcn1sor2* (A), *rcn1sor3* (B) and *rcn1sor4* (C). Box boundaries indicate the interquartile range (IQR), with central line representing the median. Black dots indicate outliers. Box whiskers represent data points 1.5x from the IQR. Statistical analysis was performed using pairwise Wilcox test with Benjamini-Hochberg correction. *** = $p < 0.0005$, ** = $p < 0.005$, * = $p < 0.05$. Number of lateral roots measured was between 16 and 12. PreR indicates angle measurements taken before reorientation, time 0 indicates angle measurements taken immediately after reorientation. Subsequent measurements were taken every 30 minutes from reorientation.

3.3 *sor* mutations do not alter *rcn1* response to auxin

As previously described, exogenous auxin application determines lateral roots to shift to more vertical GSAs (Ruiz Rosquete, Barbez and Kleine-Vehn, 2012). This shift is caused by the auxin-dependent positive regulation of RCN1 stability, which in turn leads to PIN3 relocalization to the lower side of the columella cells determining an increase of the auxin efflux to the lower side of the lateral root (Roychoudhry *et al.*, 2013, 2019). The RCN1 role in mediating lateral root response to auxin is further proven by the lack of change in GSA to a steeper orientation in *rcn1* lateral roots after exogenous application of indole 3-acetic acid (IAA) (Fig. 3.6) (Roychoudhry *et al.*, 2019) Similarly to the single *rcn1* mutant, all four *rcn1sor* mutants are insensitive to IAA applications, showing that none of the mutations in the *SOR* genes is able to restore the RCN1-dependent response to auxin of lateral roots.

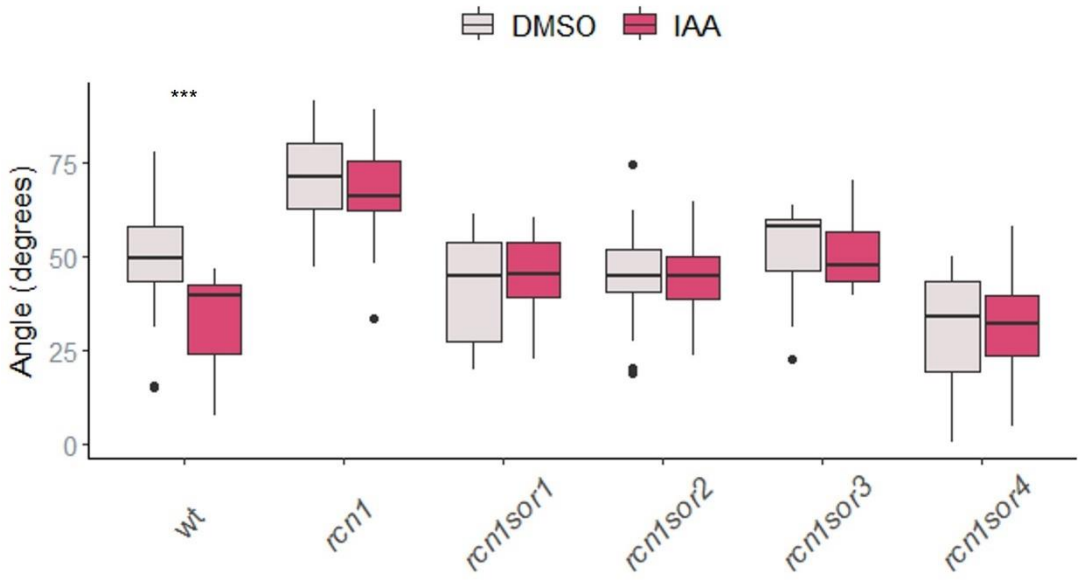

Figure 3.6: *rcn1* lack of auxin responsiveness is maintained in *rcn1sor* mutants

Box plot of quantitative analysis of stage III lateral roots growing in control media (DMSO) or supplied with 50 nM IAA. Box boundaries indicate the interquartile range (IQR), with central line representing the median. Black dots indicate outliers. Box whiskers represent data points 1.5x from the IQR. Statistical analysis was performed using Mann-Whitney test. *** = $p < 0.0005$. A minimum of 10 lateral roots per line per treatment were measured.

3.4 Identification of *SOR* genes

To identify the causative mutations of *rcn1sor* suppressing phenotypes, *rcn1sor* mutants were backcrossed to *rcn1-1* and the segregating F_2 populations were used to perform whole genome sequencing (WGS) and analysis. In addition, the nature of the *sor1, sor2, sor3* and *sor4* mutant alleles was determined by analysing the lateral root phenotype displayed by *rcn1*$^{-/-}$*sor*$^{+/-}$ lines. Lateral roots of all the *rcn1*$^{-/-}$*sor*$^{+/-}$ lines showed the *rcn1* lateral root shallow phenotype, indicating that all the selected *sor* mutations were recessive (Fig. 3.7).

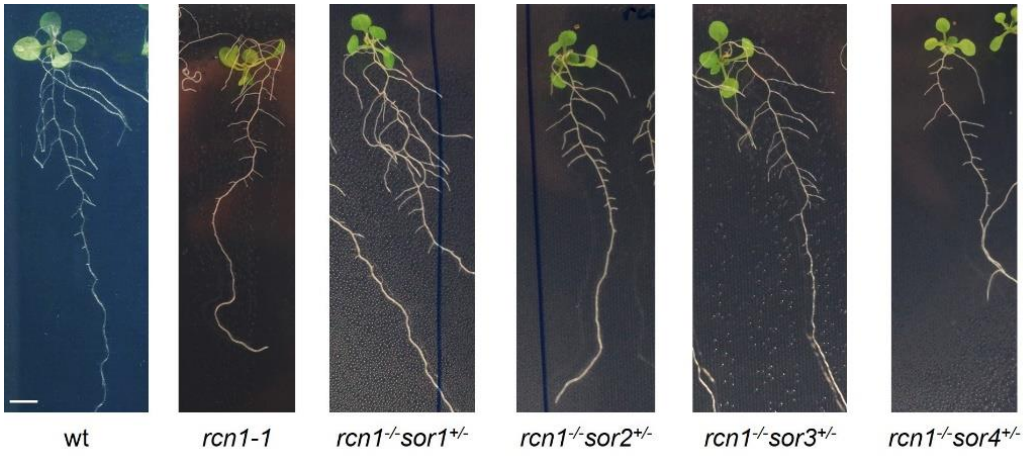

Figure 3.7: *sor* mutations are recessive

Representative images of ~12 days old *rcn1-/-sor*+/- F_1 seedlings. Scale bar = 0.5 cm.

Using the bioinformatic tools ArtMap and DiscoSNP^{++} (Javorka *et al.*, 2019; Gauthier *et al.*, 2020) raw data from Next Generation Sequencing (NGS) was mapped to Arabidopsis TAR10 genome and single nucleotide polymorphisms (SNPs), unique to the *rcn1sor* mutant lines, were isolated and classified in "high", "moderate" and "low" impact. SNPs marked as "high" impact determined coding sequences to either gain a premature stop codon, lose the start codon or change the gene transcript structure through the alteration of splice acceptor and donor sites. SNPs inducing single amino acid substitutions, also known as missense mutations, together with mutations in promoters, 3' and 5'-UTRs were classified as "moderate" impact. All the other SNPs, including mutations in intronic sites not involved in RNA splicing and exon mutations not altering the amino acid sequence (also known as synonymous mutations), were ranked as "low" impact. For each mutant line,

both already characterised and uncharacterised genes containing “high” and “moderate” impact SNPs were selected as putative *sor* mutant candidates (listed in Table 7.1). Using publicly available microarray data (Voß *et al.*, 2015) the expression of putative gene candidates in the root was checked. Characterised candidates regulating processes that could influence lateral root GSA, such as membrane trafficking, and uncharacterised genes which *in silico* analysis pointed out similar putative functions containing SNPs directly altering the coding sequence were shortlisted and knock-out mutants were obtained for further analysis (Table 3.1).

Table 3.1: List of candidate genes containing SNPs in *rcn1sor* mutants

sor1

Gene ID	Type of mutation	aa change	Other names
AT1G19880	missense	Ser473Asn	PLASTICITY OF ROSETTE TO NITROGEN 1 (PROTON1)
AT1G24764	missense	Arg194Gln	MICROTUBULE-ASSOCIATED PROTEINS 70-2 (MAP70-2)

sor2

Gene ID	Type of mutation	aa change	Other names
AT1G63420	missense	Arg305Lys	O-GLUCOSYLTRANSFERASE-LIKE PROTEIN (O-GT)
AT5G41070	missense	Gly305Arg	DSRNA-BINDING PROTEIN 5 (DRB5)

sor3

Gene ID	Type of mutation	aa change	Other names
AT1G60370	stop codon	Trp37*	KURZ UND KLEIN (KUK) F-box domain protein
AT2G02780	stop codon	Trp726*	LEUCINE-RICH REPEAT PROTEIN KINASE (LRR-K)
AT1G52290	splice accept var	/	PROLINE-RICH EXTENSIN-LIKE RECEPTOR KINASE 15 (PERK15)
AT1G34340	missense	Pro67Ser	ALPHA/BETA-HYDROLASE PROTEIN (ABHY)

AT1G38131	missense	Ala341Thr	O-FUCOSYLTRANSFERASE PROTEIN (O-FT)
AT1G09720	missense	Ala791Thr	NETWORKED 2B (NET2B)
AT1G50120	missense	Ala160Thr	LOSS OF TRANS-GOLGI NETWORK (LOT)
AT3G06030	missense	Pro596Leu	NPK1-RELATED PROTEIN KINASE 3 (ANP3)
AT4G13750	missense	Ala994Thr	NO VEIN (NOV)
AT4G15090	missense	Thr465Met	FAR-RED IMPAIRED RESPONSE 1 (FAR1)
AT4G16100	missense	Ser322Asn	Putative heat shock protein (PHS)

sor4

Gene ID	Type of mutation	aa change	Other names
AT3G25160	stop codon	Arg.18*	Putative ER lumen protein retaining receptor (ERRP)
AT3G18370	splice donor var	/	C2 domain-containing protein (C2DP)
AT1G28440	missense	Ser778Asn	HAESA-LIKE 1 (HSL1)

3.4.1 *SOR1* candidate genes

Among the possible *SOR1* candidate genes, *PLASTICITY OF ROSETTE TO NITROGEN 1* (*PROTON1*) was chosen for its role as regulator of nitrogen-induced growth responses in Arabidopsis (Duarte *et al.*, 2021). Nitrate is the main source of nitrogen absorbed by plants in soil and its availability highly impacts root system architecture, with limiting concentrations negatively regulating root growth and inducing a shift to more horizontal lateral root GSAs (Guan *et al.*, 2017; Roychoudhry *et al.*, 2017). PROTON1 belongs to the regulator of chromosome condensation (RCC1) family proteins. It is mainly expressed in roots and young leaves and its expression increases under limiting nitrate availability, negatively regulating genes involved in nitrate transport and signalling (Duarte *et al.*, 2021). As nitrate is an environmental regulator of root architecture, PROTON1 might be involved in GSA regulation.

MICROTUBULE-ASSOCIETED PROTEIN 70-2 (MAP70-2) belongs to a plant-specific family of microtubules associated proteins formed by other four members (Korolev *et al.*, 2005). Microtubule dynamics have long been associated with root growth and tropism for their role in regulating both the orientation of cellulose microfibrils during cell growth and vesicle trafficking (Lehman, Smertenko and Sanguinet, 2017). Furthermore, microtubules associated proteins have been linked to PIN2 polarity and recycling control (Kleine-Vehn, Łangowski, *et al.*, 2008; Ambrose *et al.*, 2013). For this reason, *MAP70-2* was chosen as a possible candidate gene for *SOR1*.

Both *PROTON1* and *MAP70-2* in *rcn1sor1* contain a missense mutation in their amino acid sequence that could alter their conformation and consequently their activity. To understand if these mutations in either PROTON1 or MAP70-2 are involved in the suppression of *rcn1* GSA phenotype, knock-out T-DNA insertional mutants of *proton1* (SALK_117261) and *map70-2* (SALK_060997) were crossed to *rcn1*-6 (SALK_059903 – Columbia ecotype) and lateral root GSA was analysed. Both *proton1* and *map70-2* single mutants show no differences in lateral root GSA compared to wt (Fig. 3.8 A). Analysis of *rcn1map70-2* homozygous lines shows a rescue of *rcn1* shallow lateral roots (Fig. 3.8 A and B), suggesting that the SNP found in *MAP70*-2 might be the causative mutation in *rcn1sor1*. Homozygous lines for *rcn1proton1* are still being isolated and their lateral root phenotype is still to be analysed.

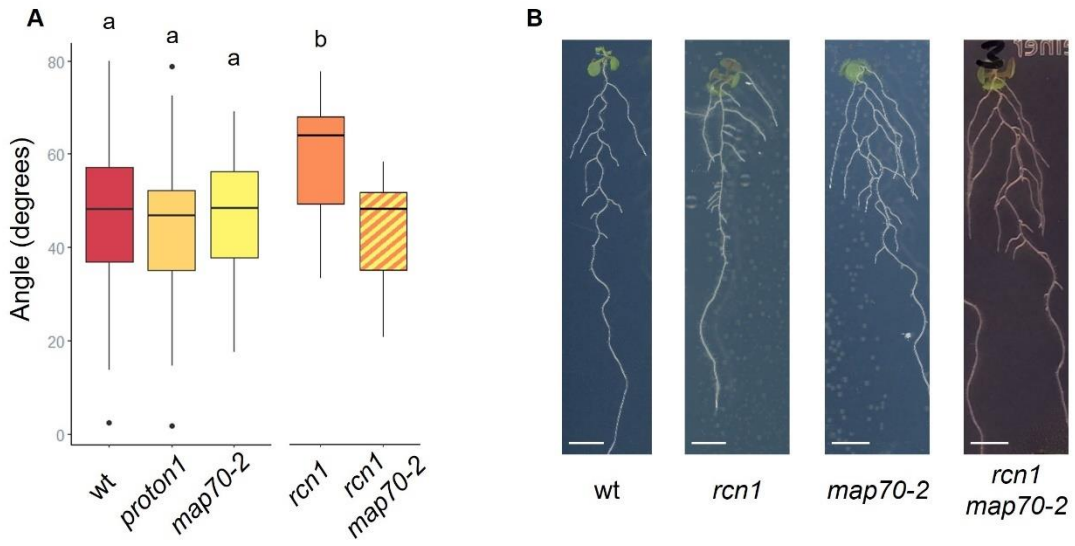

Figure 3.8: Analysis of *SOR1* candidates

A) Box plot showing quantitative analysis of lateral root GSA of knock-out *SOR1* candidate single loss-of-function mutants and *rcn1map70-2* F_2 homozygous line compared to wt (Col) and *rcn1-6*. Box boundaries indicate the interquartile range (IQR), with central line representing the median. Black dots indicate outliers. Box whiskers represent data points 1.5x from the IQR. A minimum of 58 lateral roots were measured for wt, *proton1*, *map70-2* and *rcn1*, while for *rcn1map70-2* only 15 roots at stage III were available to measure. To compare measurements from wt, *proton1, map70-1* and *rcn1* statistical analysis was performed using one-way ANOVA with Tukey's HSD post-hoc test. Different letters indicate significant difference with $p < 0.0005$. B) Representative images of *map70-2* single mutant and *rcn1map70-2* F_2 homozygous line compared with wt and *rcn1-6*. Scale bar = 0.5 cm.

3.4.2 *SOR2* candidate genes

AT1G63420 encodes an O-glucosyltransferase-like protein of unknown function, here referred as O-GT. Protein glycosylation is a post-translational modification that can alter stability, functionality and localization of proteins (Strasser *et al.*, 2021). For example, glycosylation of CLAVATA3 peptide contributes to the final conformation of the peptide and its interaction with CLAVATA1 receptor (Ohyama *et al.*, 2009; Shinohara and Matsubayashi, 2013). *O-GT* mRNA has also been found to be mobile, moving through the phloem from shoot to roots (Thieme *et al.*, 2015). Due to its possible role in regulating protein activity and/or stability, *O-GT* was chosen as a putative *SOR2* candidate.

DSRNA-BINDING PROTEIN 5 (DRB5) is a double-stranded RNA binding protein and is believed to function, together with four other DRBs, in RNA silencing (Eamens *et al.*, 2012). Research around the five DRBs has been focused on the shoot and GUS staining analysis of *DRB5* promoter and have pointed to *DRB5* expression being restricted to the shoot apical meristem (Eamens *et al.*, 2012). However, analysis of publicly available microarray dataset in primary roots (Voß *et al.*, 2015) suggests that *DRB5* mRNA is also present in the root meristematic zone. Because RNA silencing machinery producing miRNA has essential roles both in development and growth responses to environmental stimuli (Guo *et al.*, 2005; Vidal *et al.*, 2010), *DRB5* was selected as possible *SOR2* candidate.

As mutations found in the *rcn1sor1* line, WGS analysis found missense mutations in both *O-GT* and *DRB5* that could alter their activity. To understand if O-GT and DRB5 are involved in the GSA regulation, knock-out T-DNA insertional mutants *o-gt* (SALK_083047) and *drb5* (SALK_031307) were crossed to *rcn1-6,* and their lateral root GSA was analysed. Both *o-gt* and *drb5* single mutants do not show significant differences in lateral root GSA compared to wt (Fig. 3.9 A), while lateral roots of homozygous lines of *rcn1drb5* display similar phenotype of *rcn1* (Fig. 3.9 A). This demonstrates that loss-of-function mutations in *DRB5* does not alter *rcn1* shallow roots. Homozygous lines for *rcn1o-gt* are still being isolated and their lateral root phenotype is still to be analysed.

3.4.3 *SOR3* candidate genes

WGS analysis of *rcn1sor3* revealed a higher number of genes containing SNPs compared to the other *rcn1sor* mutant lines (Table 7.1). A selection

based on the role of the gene and the availability of knock-out mutants led to the selection of 11 candidates.

KURZ UND KLEIN (KUK) is a F-box protein involved in regulating cell proliferation and differentiation in root transition and elongation zones (Meijón *et al.*, 2014). Although not expressed in the columella and not apparently related to GSA control, *KUK* gene was taken into consideration due to the highly disruptive SNP present in *rcn1sor3* mutant, determining a premature stop codon early in the coding sequence of the gene (Table 3.1).

AT2G02780 encodes an uncharacterised Leucine-rich repeat (LRR) kinase, here mentions as LRR-K. LRR kinases, as other transmembrane receptor-like kinases (RLKs), are formed by an extracellular receptor domain, which binds specific ligands, a transmembrane domain, and a cytoplasmatic kinase domain. Once the ligand interacts with the receptor domain, the activated LRR kinase phosphorylates its cellular substrates transducing the signal inside the cell (Jose, Ghantasala and Roy Choudhury, 2020). RLKs occupy an important role in organ development and plant response to environmental stimuli. *LRR-K* was therefore taken into consideration as a possible *SOR3* candidate. The SNP found in *LRR-K* determines that the protein to lack its final 16 amino acids, due to a premature stop codon (Table 3.1). Although outside of its catalytic domain the absence of the C-Terminal domain could alter LRR-K interactions with its substrates.

PROLINE-RICH EXTENSIN-LIKE RECEPTOR KINASE 15 (*PERK15*) also encodes an uncharacterised RLK protein. The PERK protein family encompasses 15 members. Only few of them have been characterised and are associated to the regulation of developmental and growth processes in roots and root hairs (Invernizzi *et al.*, 2022). The mutation found in *PERK15* determines a variation in a splice acceptor site in proximity of the fifth exon, that is part of the cytoplasmic kinase domain (Table 3.1). Such mutation could alter the splicing of *PERK15* RNA and determine exon deletions or intron insertions, impairing the functionality of the protein. For this reason and its potential role in integrating extracellular signals inside the cell, *PERK15* was selected as a *SOR3* candidate.

AT1G34340 encodes an uncharacterised protein containing an alpha/beta hydrolase (ABH) domain, here named ABHY. Enzymes containing ABH domains can perform different catalytic activities such as peptidase and lipase activities and be involved in hormone signalling (Mindrebo *et al.*, 2016). To

obtain more information about ABHY, the protein sequence was analysed using Uniprot (https://www.uniprot.org/) and Interpro (https://www.ebi.ac.uk/interpro/) webtools. Such analysis predicted the presence of a transmembrane domain both at the C and N-Terminal ends of the protein, and a putative short-chain carboxylesterase activity. Furthermore, the analysis predicted a putative involvement of ABHY in cellular lipid metabolism. Due to the importance lipid composition of membranes can play in PIN endo and exocytosis at the plasma membrane, and the uncharacterised role of ABHY proteins, *ABHY* was taken into consideration as possible *SOR3* candidate.

AT1G38131 encodes an O-fucosyltransferase protein of unknown function, here named as O-FT. O-fucosyltransferases catalyse the glycosylation of proteins adding fucose to specific serine and threonine residues. As described above, glycosylation can drastically alter protein activity. For example, the O-fucosyltransferase SPINDLY is able to glycosylate DELLA gibberellin signalling repressors, enhancing their activity (Zentella *et al.*, 2017). To gather more information about O-FT, Uniprot and Interpro *in silico* analysis was performed. Such analysis predicted the presence of a transmembrane domain at N-Terminus of the protein. For its possible role in regulating the stability and/or the activity of proteins, *O-FT* was chosen a possible *SOR3* candidate.

NET2B is a member of NETWORKED (NET) actin binding proteins. A closely related member of the family, NET2A, has been shown to be associated with the actin cytoskeleton during pollen germination, and to facilitate the establishment of contact points between the actin filaments and the plasma membrane (Duckney *et al.*, 2021). Actin cytoskeleton is important during PIN vesicle trafficking and statolith sedimentation (Blancaflor, 2013). NET2B could play in the root a similar role played by NET2A in pollen formation. *NET2B* was therefore selected as a putative *SOR3* candidate.

LOSS OF TRANS-GOLGI NETWORK (LOT) has been identified as a novel Ras-related GTPases (Rab) guanine nucleotide exchange factor (GEF) associated with the *trans*-Golgi network (TGN) (Jia *et al.*, 2018). Similarly to ARG-GEFs, Rab-GEFs are important components of membrane trafficking in the cell and are required for vesicle generation and vesicle fusion between membranes. LOT is involved in TGN biogenesis and has been shown to participate in intracellular trafficking of PIN2 in the root meristematic zone (Jia *et al.*, 2019). Loss-of-function of *LOT* is male sterile, showing defects in pollen tube growth (Jia *et al.*, 2018). For this reason, to assess the potential function

of *LOT* mutation in suppressing *rcn1* shallow roots phenotype, a knock-down *LOT* mutant was analysed (SALK_130228) here named *lot-2.*

NPK1-RELATED PROTEIN KINASE 3 (ANP3) is a member of the mitogen-activated protein kinase kinase kinase (MAPKKK). It is associated with multiple developmental and growth responses, among which cell division, growth and responses to oxidative stress (Krysan *et al.*, 2002; Marti *et al.*, 2021). Interesting, ANP3 protein shows multiple subcellular localizations, being able to translocate from the cytosol to the nucleus, mitochondria and plastids (Marti *et al.*, 2021). Although the ability of ANP3 to translocate to multiple subcellular localizations seems determined in response to stress signals (Marti *et al.*, 2021), it is worth investigating a possible interaction between ANP3-related signalling response and GSA control in lateral roots. For this reason, *ANP3* was selected as possible *SOR3* candidate.

NO VEIN (NOV) is a nuclear factor involved in the regulation of leaf vasculature formation and root patterning (Tsugeki *et al.*, 2009, 2010). Although just lowly expressed in the QC, NOV has been shown to influence *PIN3, PIN4* and *PIN7* expression in the columella, and PIN2 polarity in root cortex (Tsugeki *et al.*, 2009). Several *NOV* loss-of-function alleles have been linked to impairment of root patterning, showing alteration in cellular organization of the root (Tsugeki *et al.*, 2009), a phenotype that is not present in *rcn1sor3* mutant, suggesting that if NOV is involved in GSA lateral root regulation, the SNP presents in *rcn1sor3* most likely does not strongly impair NOV activity. However, NOV is a particularly interesting candidate to investigate.

As the name suggests, FAR-RED IMPAIRED RESPONSE 1 (FAR1) is a transcription factor involved in plant responses to far red light mediated by the phytochrome A (phyA) (Wang and Wang, 2015). Together with its homolog FAR-RED ELONGATED HYPOCOTYLS3 (FHY3), FAR1 is also involved in regulating the circadian clock, flowering time and strigolactone-mediated shoot branching (Wang and Wang, 2015). FAR1 and FHY3 have also been shown to interact with ELONGATED HYPOCOTYL5 (HY5), antagonistically regulating downstream targets of phyA signalling (Li *et al.*, 2010). Furthermore, HY5 has been recently proposed to work as a shoot-to-root signal regulating lateral root development in response to light stimuli perceived in the shoot (Chen *et al.*, 2016; van Gelderen *et al.*, 2018). For the possible involvement of FAR1, together with HY5, in lateral root regulation mediated by light, this gene was selected as possible *SOR3* candidate.

AT4G16100 encodes a protein of unknown function, classified as putative heat shock protein, here named PHS. *In silico* analysis of PHS protein sequence does not point out to any known catalytic domain or known functional motif. To gather more information about PHS, protein structure prediction was performed using AlphaFold (https://alphafold.ebi.ac.uk/). The predicted protein structure showed a central globular organised domain, surrounded by disordered regions modelled with very low confidence loops (Fig. 3.10 A). Although these predictions do not explain much about the function of this protein, as other uncharacterised proteins in this screening, analysis of publicly available microarray dataset shows *PHS* expression in the meristematic zone of primary roots (Voß *et al.*, 2015). In addition, heat shock proteins have been linked not only to the control of protein folding under stress condition, but also to modulation of auxin transport and responses (Voß *et al.*, 2015; Li *et al.*, 2018). For these reasons, PHS was selected as a potential uncharacterised factor participating to the GSA regulation of lateral roots.

To determine if any of the selected genes are involved in lateral root GSA regulation, knock-off/down T-DNA insertional mutants of *kuk* (SALK_019083), *lrr-k* (SALK_006948), *perk15* (SALK_020345), *abhy* (SALK_057422), *o-ft* (SALK_152459), *net2b* (SAIL_2_F03C1), *lot-2* (SALK_130228), *anp3* (SALK_081990), *nov* (SALK_053496), *far1* (SALK_031652), and *phs* (SALK_034519) were crossed to *rcn1-6* and their lateral root GSA was analysed. Lateral root GSAs of all the single mutants are comparable to wt (Fig. 3.9 B). Interestingly *o-ft* shows a phenotype in floral development, with flowers lacking petals and showing variable impairments such as fused carpels and stamens with defective morphology (Fig. 3.10 B). Among the double mutants generated *rcn1lrr-k*, *rcn1perk15*, *rcn1abhy*, *rcn1o-ft*, *rcn1net2b*, *rcn1lot-2*, *rcn1anp3* and *rcn1far1* show all lateral root GSA comparable with *rcn1* (Fig. 3.9 C), suggesting that the loss-of-function or knock-down mutations of these genes are not involved in the suppression of *rcn1* phenotype in lateral roots of *rcn1sor3*. Homozygous lines for *rcn1kuk*, *rcn1nov* and *rcn1phs* are still being isolated and their lateral root phenotype is still to be analysed.

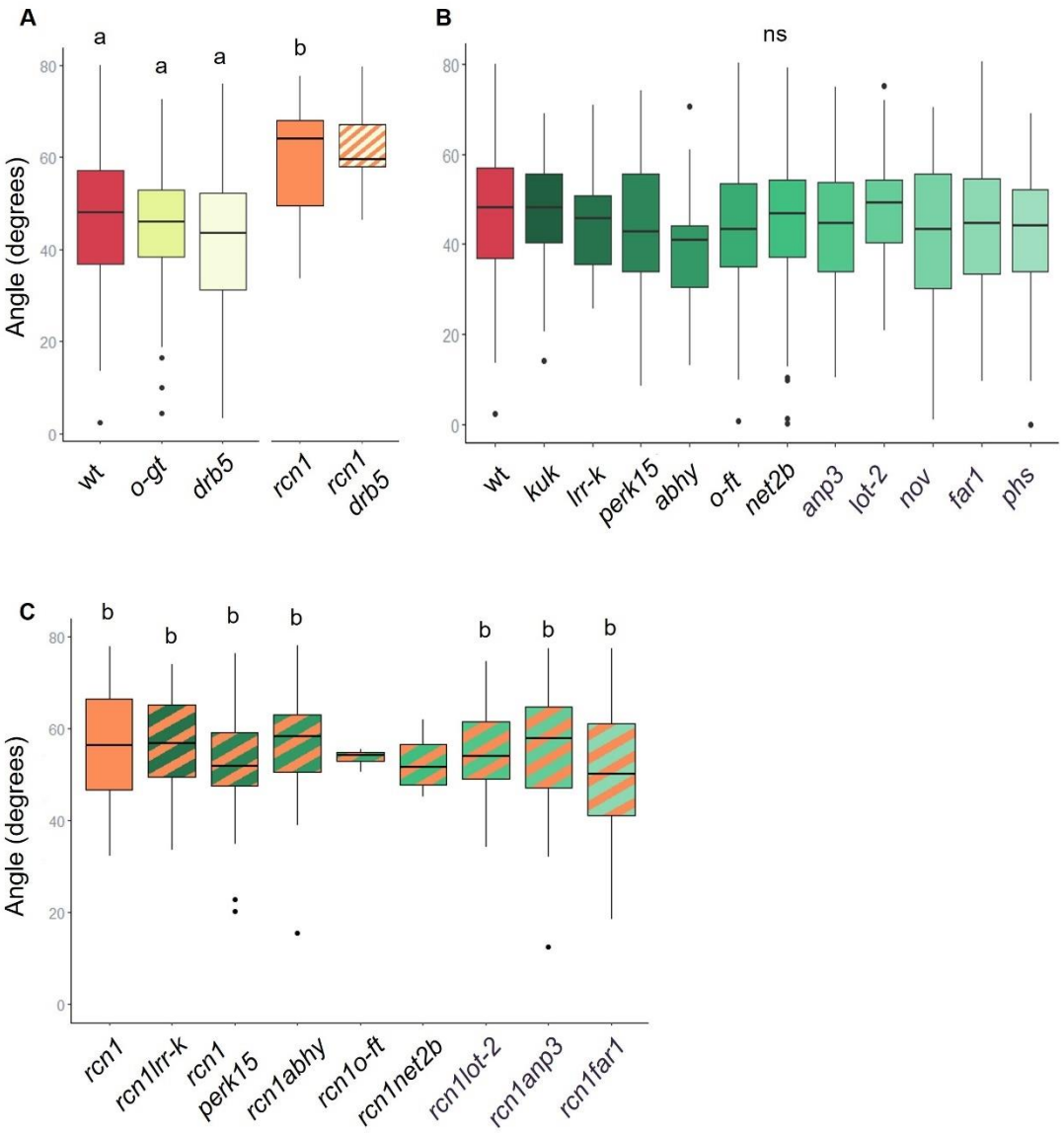

Figure 3.9: Analysis of *SOR2* and *SOR3* candidates

A-C) Box plots of quantitative analysis of lateral root GSA of knock-out *SOR2* candidate mutants and *rcn1drb5* F_2 homozygous line, compared to wt and *rcn1-6* (A), knock-out/down *SOR3* candidate mutants compared to wt (B) and candidate *SOR3* mutants crossed to *rcn1* (C). Box boundaries indicate the interquartile range (IQR), with central line representing the median. Black dots indicate outliers. Box whiskers represent data points 1.5x from the IQR. A minimum of 50 lateral roots were measured for all the lines (wt and F_3 homozygous lines) except for *rcn1drb5* (n = 6), *rcn1o-ft* (n = 4) and *rcn1net2b* (n = 10) which are F_2 homozygous lines. For wt and F_3 lines statistical analysis was performed using one-way ANOVA with Tukey's HSD post-hoc test. Different letters indicate significant difference with $p < 0.0005$, ns = non-significant.

3.4.4 *SOR4* candidates

AT3G25160 encodes an uncharacterised protein with putative function as an endoplasmic reticulum (ER) lumen retaining receptor, here named ERRP. ER lumen retaining receptors play an important role in maintaining ER functions by capturing ER proteins cycling between ER and Golgi (Gerondopoulos *et al.*, 2021). *In silico* analysis of ERRP shows the presence of multiple transmembrane domains (4 to 8) with a C-Terminal tail predicted to be cytoplasmic. The presence of a premature stop codon very early on in *ERRP* sequence (Table 3.1) suggests a possible loss-of-function mutation of this gene. Due to this highly destructive mutation, *ERRP* was selected as possible *SOR4* candidate.

AT3G18370 encodes an uncharacterised C2 domain-containing protein, here referred as C2DP. C2 domains mediate calcium-dependent binding of target molecules, such as phospholipids and proteins (Rizo and Südhof, 1998). C2 domain-containing proteins have been shown to be involved in signal transduction and membrane traffic (Rizo and Südhof, 1998). *In silico* analysis of C2DP showed the presence of three C2 domains and a Synaptotagmin-like mitochondrial-lipid-binding (SPM) domain at the N-Terminus of the protein. SPM domains have been shown to mediate lipid transfer between adjacent membranes (Reinisch and de Camilli, 2016), suggesting a role of C2DP in membrane fusion during trafficking. Due to the importance of endosome trafficking in PIN protein dynamics, *C2DP* was selected as possible *SOR4* candidate.

HAESA-LIKE 1 (HSL1) is a LRR kinase reported involved in the regulation of seed longevity and CLE9/10-dependent stomatal development (Qian *et al.*, 2018; D. Chen *et al.*, 2022). *HSL1* is expressed in the whole root, suggesting a possible role in signal transduction in the root system (Qian *et al.*, 2018; D. Chen *et al.*, 2022). As discussed above, due to the role LRR receptor can have in integrating extracellular signals into the cell, *HSL1* was selected as possible *SOR4* candidate.

To understand if any of the selected genes are involved in the suppression of *rcn1* shallow root phenotype in *rcn1sor4*, loss-of-function mutants *errp* (SALK_208480), *c2dp* (SALK_200658) and *hsl1* (SALK_141756) were crossed with *rcn1-6* and their lateral root GSA was analysed. Lateral roots of *errp* and *hsl1* show no differences in GSA compared to wt (Fig. 3.10 C). Interestingly, lateral roots of *c2dp* have significantly more vertical GSA than

wt (Fig. 3.10 C and D), suggesting a possible role for this uncharacterised C2 domain-containing protein in the regulation of lateral root GSAs. Analysis of F_2 homozygous lines of *rcn1errp* showed no differences in lateral root GSA compared to *rcn1* (Fig. 3.10 C), demonstrating that loss-of-function of *ERRP* does not alter *rcn1* shallow root phenotype. On the other hand, *rcn1c2dp* lateral roots have wt-like phenotype, with GSAs significantly more vertical than *rcn1* (Fig. 3.10 C and D). This demonstrates that loss-of-function of *C2DP* alters lateral root phenotype of *rcn1* and suggests a role for this uncharacterised protein in GSA regulation. Homozygous lines for *rcn1hsl1* are still being isolated and their lateral root phenotype is still to be analysed.

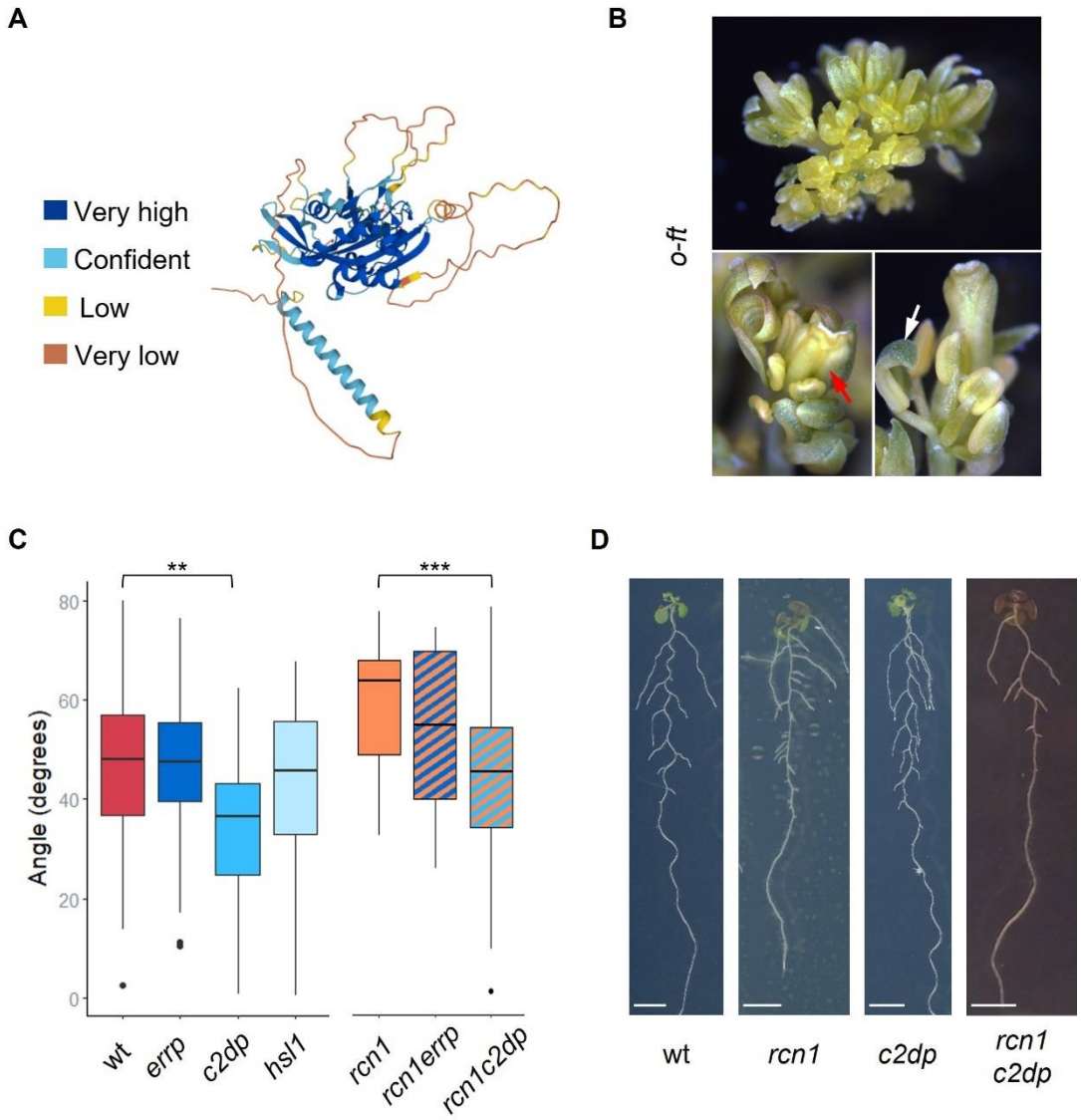

Figure 3.10: Analysis of *SOR4* candidates

A) Predicted 3D structure of PHS (AlphaFold). Colour scheme represents model confidence. B) Representative images of *o-ft* floral organs. Red arrow indicates fused carpels, white arrow indicates a stamen with defective morphology. C) Box plot of quantitative analysis of lateral root GSA of knock-out *SOR4* candidate mutants. Box boundaries indicate the interquartile range (IQR), with central line representing the median. Black dots indicate outliers. Box whiskers represent data points 1.5x from the IQR. A minimum of 52 lateral roots were measured for all the lines (wt and F_3 homozygous lines) except for *rcn1errp* (n = 8) which is a F_2 homozygous line. For wt and F_3 lines statistical analysis was performed using one-way ANOVA with Tukey's HSD post-hoc test. *** = $p < 0.0005$, ** = $p < 0.005$. D) Representative images of 12 days old wt, *rcn1*, *c2dp* and *rcn1c2dp* seedlings. Scale bars = 0.5 cm.

Discussion

Although time consuming, forward genetic screening methods such as EMS mutagenesis still provide a powerful tool for discovering novel regulators of plant development. Point mutations introduced with this method can not only lead to loss-of-function mutations, generated for example by SNPs causing premature stop codons, but also more complex alterations like gain-of-function mutations, mutations that can alter protein-protein/protein-substrate interactions, or mutations that alter stability or expression of a protein. For this reason, this type of analysis offers a plethora of possibilities and, in the long run, might give the chance of acquiring important information on the structure and function of unknown proteins. At the same time, though, forward genetic screenings can also be a double-edged weapon due to their complexity. Thanks to bioinformatic tools like Artmap (Javorka *et al.*, 2019), the long list of SNPs that can be generated during an EMS mutagenesis is automatically scored by the software, but the operator can still be left to navigate a huge number of alterations found in the genome with very little evidence of their real significance in altering the correspondent protein activity.

Here I have presented the analysis I performed on four different *rcn1* suppressor mutants, selected for their ability to stably rescue the shallow root phenotype caused by the *RCN1* loss-of-function. Phenotypical analysis of statolith morphology suggested that none of the suppressors have altered starch accumulation and amyloplast formation in the columella cells of both primary and lateral roots. Consistent with this, all the suppressors showed gravitropic response comparable with wt and rescued the previously described *rcn1* slow gravitropism (Roychoudhry *et al.*, 2019). Finally, in all the suppressors, lateral root GSAs are insensitive to exogenous applications of auxin in a similar way to *rcn1*. This result adds evidence on the current auxin mode of action in regulating lateral root GSAs (Roychoudhry *et al.*, 2019). In the model, auxin mediates a shift to more vertical GSAs through the regulation of RCN1 stability. Increase in RCN1 leads to higher PIN3 dephosphorylation in the columella of lateral roots. Dephosphorylated PIN3 is then targeted to the lower side of the columella cells, prompting an increase in auxin efflux to the lower side of the root. This shift in auxin distribution changes the balance of cell expansion in the root expansion and differentiation zone, leading to more vertical GSAs. This framework could also explain the shift to more vertical GSAs as lateral roots age (Rosquete *et al.*, 2013; Roychoudhry *et al.*, 2017). It has been shown that as lateral roots age, levels of auxin increase in

the root tip, this could result in the activation of the variation in RCN1 regulation and PIN3 localization, as just described (Roychoudhry *et al.*, 2017). The fact that the suppressor mutations do not rescue the *rcn1* lack of sensitivity to auxin confirms the central role of RCN1 in mediating the auxin response in lateral roots.

Among the SNP-containing genes identified by WGS across the four *rcn1sor* lines, 18 were selected as potential *sor* candidates. The selection was guided by the severity and effect of mutations, but both characterized and uncharacterized genes were considered. In two cases, the T-DNA insertional mutation of the selected gene was able to suppress *rcn1* phenotype, suggesting that the identified allele was responsible for the *sor* mutation. With their possible interaction with RCN1, these genes represent new tools for the identification of novel lateral root GSA regulatory pathways.

MAP70-2 and C2DP are possible novel regulators of lateral root GSA

MAP70-2 was selected, among the SNP containing genes in *rcn1sor1*, for its putative association with the microtubules and its possible role in vesicle trafficking. Although the single loss-of-function of *MAP70-2* does not alter lateral root GSA phenotype, the knock-out mutation is able to rescue lateral root phenotype of *rcn1* to wt GSAs. Due to its possible role in vesicle trafficking, MAP70-2 could participate in PIN protein endocytosis and recycling, and influence PIN polarization in the columella. While RCN1 has been shown to regulate PIN3 localization, it is currently unknown what controls PIN7 polarity in the columella of lateral roots, as changes in RCN1 expression do not alter the localization of PIN7 (Roychoudhry *et al.*, 2019). Furthermore, PIN7 localization shows a bias for the upper side of the columella cells, consistent with the gravitropic response of *pin7* loss-of-function, with lateral roots showing slower upward bending kinetics (Roychoudhry *et al.*, 2019). The gravitropic response of *rcn1sor1* shows a downward bending response similar to wt, while the upward bending is delayed by 30 minutes. This might depend on an impairment in the regulation of PIN7 at the upper membrane of *rcn1sor1.* If MAP70-2 is involved directly or indirectly in the endocytosis and/or recycling of PIN7 at the upper membrane of lateral root columella cells, the presence of a functional mechanism regulating PIN3, including RCN1, could attenuate the imbalance of auxin export at the upper side of the columella cells and explain why lateral roots lacking MAP70-2 function maintain a wt-like GSA phenotype. On the other hand, in the absence of RCN1, PIN3 localization is

impaired and an increase of phosphorylated PIN3 at the upper side might be counteracted by a decrease of PIN7 due to the lack of a functional MAP70-2, resulting in a suppression of *rcn1* phenotype. In this hypothesis, MAP70-2 and RCN1 regulate lateral root GSA working in independent pathways controlling auxin export from the columella. Furthermore, this would suggest that the MAP70-2 missense mutation present in *rcn1sor1* probably compromises the protein functionality. Nevertheless, the absence of a phenotype in *map70-2* single mutant does not exclude a possible regulation of MAP70-2 of PIN3, or of other membrane trafficking regulators. Due to the lack of information about MAP70-2 in the literature it is currently not possible to bring forward a sound hypothesis on its involvement in lateral root GSA in relationship with RCN1. Visualization of PIN3:GFP and PIN7:GFP expression and localization in *rcn1sor1* and in both *map70-2* and *rcn1map70-2* would clarify the possible role of this protein in PIN trafficking.

Among the genes containing SNPs in *rcn1sor4, C2DP* encodes an uncharacterised protein predicted to be involved in membrane trafficking, containing a SPM domain involved in membranes fusion. What makes C2DP particularly interesting is the presence of calcium-binding C2 domains, that can mediate a calcium-dependent activity of the protein. Differently from MAP70-2, *C2DP* loss-of-function not only rescues *rcn1* phenotype, but the single knock-out mutant has lateral roots significantly more vertical than wt. Due to its possible role in membrane trafficking, as MAP70-2, C2DP could function in regulating PIN cycling at the upper side of the columella cells. Consistent with this *rcn1sor4* lateral root gravitropic response is slower for upward bending roots compared to wt, suggesting that PIN repolarization at the upper side of the columella cells might be impaired. Differently from *rcn1c2dp*, lateral roots of *rcn1sor4* have GSAs more vertical than wt, suggesting that if indeed *C2DP* is *SOR4*, the mutation in the suppressor mutant might not result in a loss-of-function of the protein, but the splice donor variant present in *C2DP* might determine an alternative version of the protein that could result in an altered function. Otherwise, a second mutation not yet characterised in *rcn1sor4* could be responsible for the more vertical GSA phenotype. In addition to this, *rcn1sor4* shows a more vertical GSA phenotype also in lateral shoots, a phenotype not present in neither *c2dp* nor *rcn1c2dp*, suggesting again that either *sor4* allele is not a loss of function or that a second mutation determines this additional phenotype in *rcn1sor4*. Analysis of *C2DP* transcript in *rcn1sor4* will provide evidence on the possible status of C2DP

protein in *rcn1sor4*. Similarly to *rcn1sor1*, analysis of PIN3:GFP and PIN7:GFP expression and localization in *rcn1sor4*, *c2dp* and *rcn1c2dp* will shed some light on the possible involvement of C2DP in PIN trafficking. In addition, analysis of the activity of C2DP in relationship to calcium signalling, will provide evidence on a possible calcium-dependent regulation of the protein.

Together with a better characterization of MAP70-2 and C2DP in relationship to RCN1 and the visualization of PIN localization and membrane trafficking, complementation analyses of *rcn1sor1* and *rcn1sor4* will need to be carried out to confirm the identity of *SOR1* and *SOR4*. Furthermore, due to their shared potential regulation of membrane trafficking it would be interesting to determine if these two novel regulators work in the same pathway or not.

Searching for genes suppressing rcn1 phenotype in *rcn1sor2* and *rcn1sor3*

The mutations behind the suppression of *rcn1* phenotype in *rcn1sor2* and *rcn1sor3* remain to be uncovered. For these two suppressors, analysis of knock-out/down mutants in selected genes did not show alteration in lateral root GSA in both single mutants, in which the GSA was comparable to wt, and double mutants, which failed to suppress *rcn1* phenotype. Analysis of *rcn1o-gt*, *rcn1kuk*, *rcn1nov* and *rcn1phs* lateral roots still need to be performed. This will determine if loss-of-function of any of these putative suppressors can rescue *rcn1* phenotype. Lateral root GSAs of *o-gt*, *kuk*, *nov* and *phs* are comparable with wt, suggesting that the absence of any of these genes does not alter the normal maintenance of the GSA. However, as in the case of MAP70-2, this does not exclude a possible interaction with the *rcn1* mutation. If *o-gt*, *kuk*, *nov* and *phs* failed to rescue *rcn1* phenotype, the list of putative genes could be re-evaluated, starting with the selected genes already presented. The majority of these genes contain SNPs that result in missense mutations in the amino acid sequence of the corresponding proteins. This could alter the function of the protein in ways not reproducible with a loss-of-function mutation. For example, changes in regions important for protein-protein interaction could alter the specificity of the protein, leading to diminished or off-target interactions. In addition to the re-evaluation of the previously selected genes, a second screening of genes discarded from the first analysis could be carried out. Few potentially interesting genes were discarded due to the unavailability of loss-of-function mutants. For example, among *rcn1sor3* putative genes, *ATPI4αK* encodes a phosphatidylinositol 4-

kinase which has been shown to be recruited to the plasma membrane in specific domains, and possibly influence endocytosis (Noack *et al.*, 2022). Furthermore, a closer analysis of SNPs classified as “moderate” impact, residing in promoter regions and UTRs could reveal new interesting candidates. Since these types of SNPs do not alter the coding sequence but influence the expression pattern of a gene, a first analysis on the levels of the transcripts selected in the suppressors compared to wt could give indications on their possible role in rescuing *rcn1* phenotype.

Chapter 4. Arabidopsis lateral shoots display two distinct developmental phases

Introduction

In Arabidopsis, lateral shoots originate from axillary meristems (AMs), which are initiated from a population of undifferentiated cells in the leaf axil expressing the meristematic marker *SHOOT MERISTEMLESS* (*STM*) (Wang and Jiao, 2018). Up-regulation of *STM* determine the AM initiation through the activation of cell division (Shi *et al.*, 2016). This is followed by *de novo* expression of *WUSCHEL* (*WUS*) and the establishment of a new organization centre with the same potential as the shoot apical meristem (Wang *et al.*, 2017; Xin *et al.*, 2017). Low levels of auxin are required in the leaf axil to maintain the meristematic competence of AM precursors and allowed *STM* up-regulation, while cytokinin (CK) signalling activates *WUS* expression and contributes to maintain the stem-cell niche organised (Wang *et al.*, 2014). After its initiation, the AM can either remain dormant or outgrow into a lateral shoot, depending on both endogenous and exogenous factors, such as hormones, light and nutrients (Wang *et al.*, 2019). After bud outgrowth, lateral shoots set and maintain non-vertical GSAs similarly to lateral roots, thanks to the balanced action of the gravitropic response and the AGO (Roychoudhry *et al.*, 2013). The molecular mechanisms behind shoot gravitropic response have been mainly studied in hypocotyls, where in the endodermis PIN3 is the main carrier responsible for the redistribution of auxin to the lower side of the organ upon gravistimulation (Rakusová *et al.*, 2011, 2016). Here, PIN3 polarity is controlled by phosphorylation and a trafficking system involving GNOM (Rakusová *et al.*, 2011). Due to the similarities between PIN3 regulation in roots and hypocotyls, it is reasonable to hypothesise that the same mechanism controls the gravitropic response in stems of primary and lateral shoots. In primary shoots, PIN3, PIN4 and PIN7 have been shown to be broadly expressed in the stem and to mediate lateral auxin fluxes in and out the vasculature (Bennett *et al.*, 2016). Analysis of *PIN3*, *PIN4* and *PIN7* loss-of-function double and triple mutants shows a progressive decrease of lateral shoot GSAs, suggesting that these PIN proteins are probably expressed in lateral shoots similarly to primary shoots and participate to the GSA maintenance (Bennett *et al.*, 2016). In addition, LZY proteins might control PIN3 polarity in lateral shoots similar to lateral roots. Three members of the LZY family, *LZY1*, *LZY2* and *LZY3,* are redundantly expressed in shoot

endodermis and their loss of function determines impairments in the GSA maintenance caused by a reduction in the gravitropic response (Yoshihara, Spalding and Iino, 2013; Taniguchi *et al.*, 2017; Kawamoto *et al.*, 2020).

Studies on lateral shoot development have focused on axillary bud formation/activation and mature branch regulation, leaving the early development of growth angle unexamined. To fill this gap in our knowledge, the different stages of lateral shoot development were classified and phenotypically characterised.

Result

4.1 Lateral shoot early developmental stages are gravicompetent

After bud outgrowth, newly formed Arabidopsis lateral shoots elongate, growing away from the primary shoot and assuming a downward/rootward trajectory (Fig. 4.1 A and B). This first period of growth lasts 5 to 7 days and precedes the setting of the GSA, indicating the existence of a new phase of lateral shoot development that has not yet been described. To characterise this early phase in more detail, lateral shoot development was divided into four stages, based on the changes in growth angle shown by the branch (Fig. 4.1 A). During stage I (SI) lateral shoots elongate vertically, maintaining proximity with the primary stem. This stage is followed by a downward/rootward growth that was marked as stage II (SII). SII downward growth ends after 2 to 3 days, with lateral shoots reaching a nearly horizontal growth angle in stage III (SIII). After that, lateral shoots grow bending upward/shootward and setting their given GSA in stage IV (SIV), that will be actively maintained for the rest of the plant life (Fig. 4.1 B) (Roychoudhry *et al.*, 2013). To understand the nature of SII-SIII downward bending and the role played by gravity in these early developmental stages, gravicompetence of young lateral shoots was assessed. In the endodermis of SII and SIII lateral shoots, starch-filled plastids are already present (Fig. 4.1 C), suggesting that young lateral shoots can already perceive gravity.

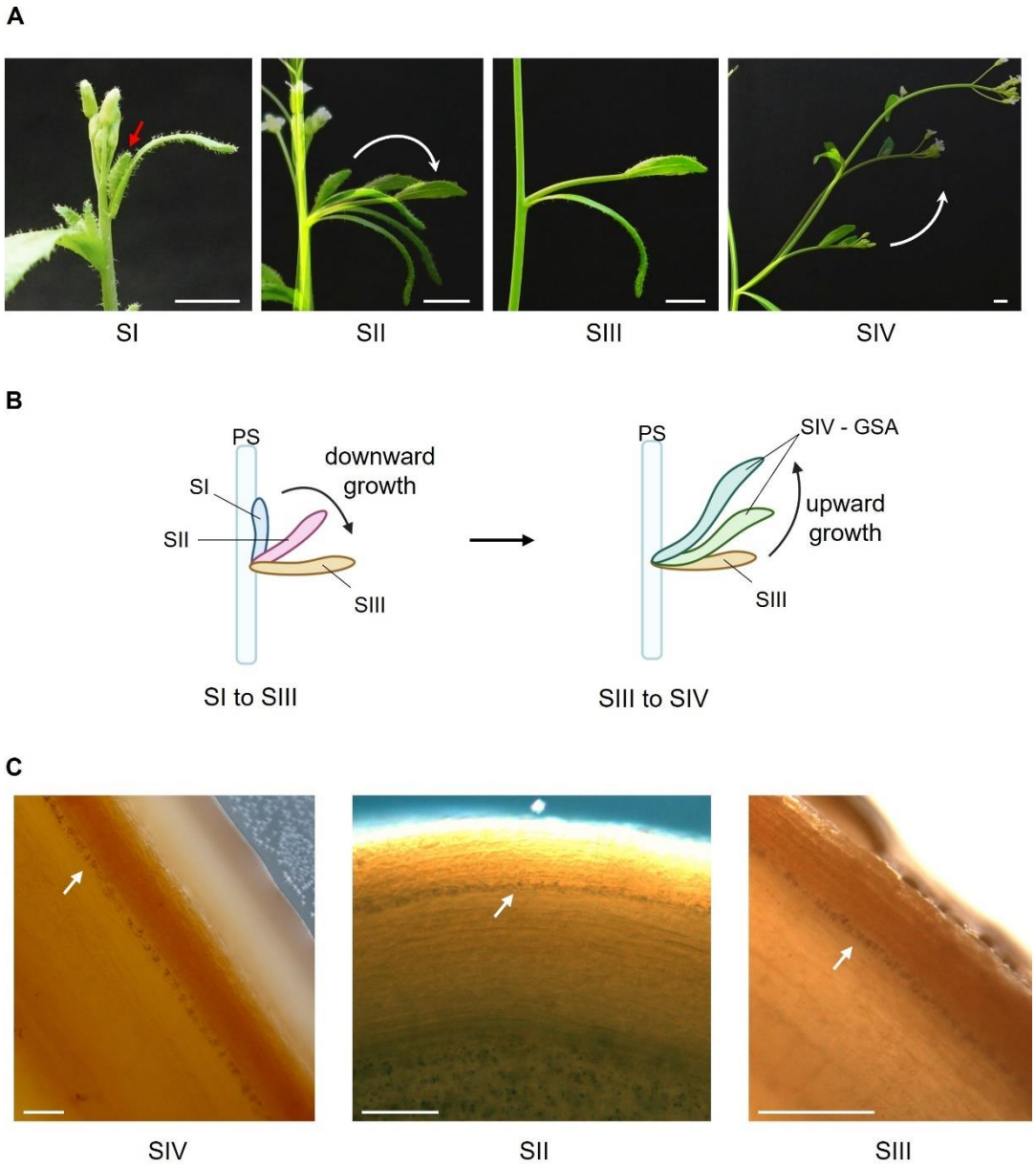

Figure 4.1: Characterization of early lateral shoot development

A) Representative images of the four developmental stages of Arabidopsis lateral shoots. SII and SIV images are obtained overlaying three pictures taken 24 hours from each other. Red arrow indicates the SI lateral shoot, white arrows indicate the direction of lateral shoot growth. Scale bars = 0.5 cm. B) Schematic representation of lateral shoot early (SI to SIII) and late (SIII to SIV) development. Black arrows indicate the direction of growth. PS = primary shoot. Lateral shoot stages are represented in different colours. C) Representative images of Lugol staining of SIV, SII and SIII lateral shoots. White arrows indicate the statolith-containing endodermis layer. Scale bars = 100 μm.

Two different reorientation assays were performed to discriminate the GSA maintenance from a more general gravicompetence in early developmental stages (Fig. 4.2 A and 4.3 A). Firstly, the capacity of young lateral shoots to maintain GSAs was tested. Plants were tilted 45° from the vertical, so that branches were reoriented to lower angles compared to their previous angles of growth (Fig. 4.2 A). As previously demonstrated, within 6 hours from the reorientation SIV lateral shoots restore their GSA bending upwards (Fig. 4.2 B and D) (Roychoudhry *et al.*, 2013). SII-III lateral shoots, instead, do not respond to this gravistimulation and do not alter their growth in response to the new position they are placed in (Fig. 4.2 C and D). A second type of reorientation assay was devised to test if, although not responding to the 45° tilting assay, young lateral shoots still show gravicompetence. Plants were laid horizontally, and lateral shoots reoriented perpendicular to the gravity vector (Fig. 4.3 A). For this reason, this assay was named “perpendicular assay”. After 6 hours from the perpendicular reorientation, both SII and SIII lateral shoots bend upwards, showing gravitropic response (Fig. 4.3 B). This behaviour was observed both in the light and in the dark (Fig. 4.3 B), confirming that, although not maintaining GSAs, lateral shoots have the capacity to sense and respond to gravity. Further, any contribution from phototropism to the bending response can be excluded.

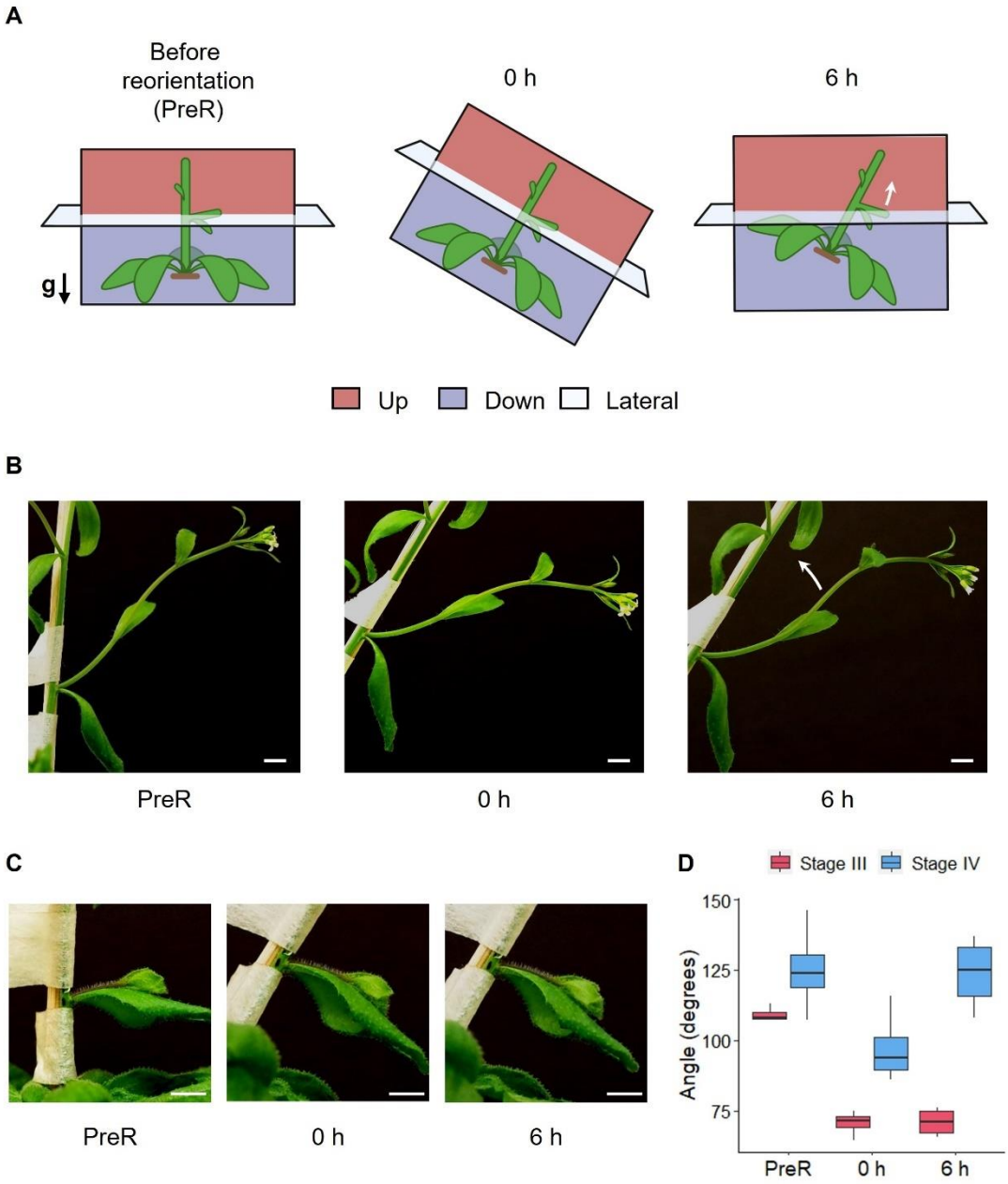

Figure 4.2: Young lateral shoots do not maintain GSAs

A) Schematic representation of the 45° tilting assay. Up, down and lateral indicate the polarity of the plant with respect to gravity. The black arrow indicates the direction of gravity, g = gravity. B) Representative images of SIV lateral shoots during tilting assay. White arrows indicate the direction of the bending. C) Representative images of SIII lateral shoots during tilting assay. Scale bars = 0.5 cm. D) Box plot of quantitative analysis of 45° tilting assay of SIII and SIV lateral shoots. Box boundaries indicate the interquartile range (IQR), with central line representing the median. Box whiskers represent data points 1.5x from the IQR. Four stage III and four SIV lateral shoots were measured. PreR = before reorientation, 0 h = 0 hours after reorientation, 6 h = 6 hours after reorientation.

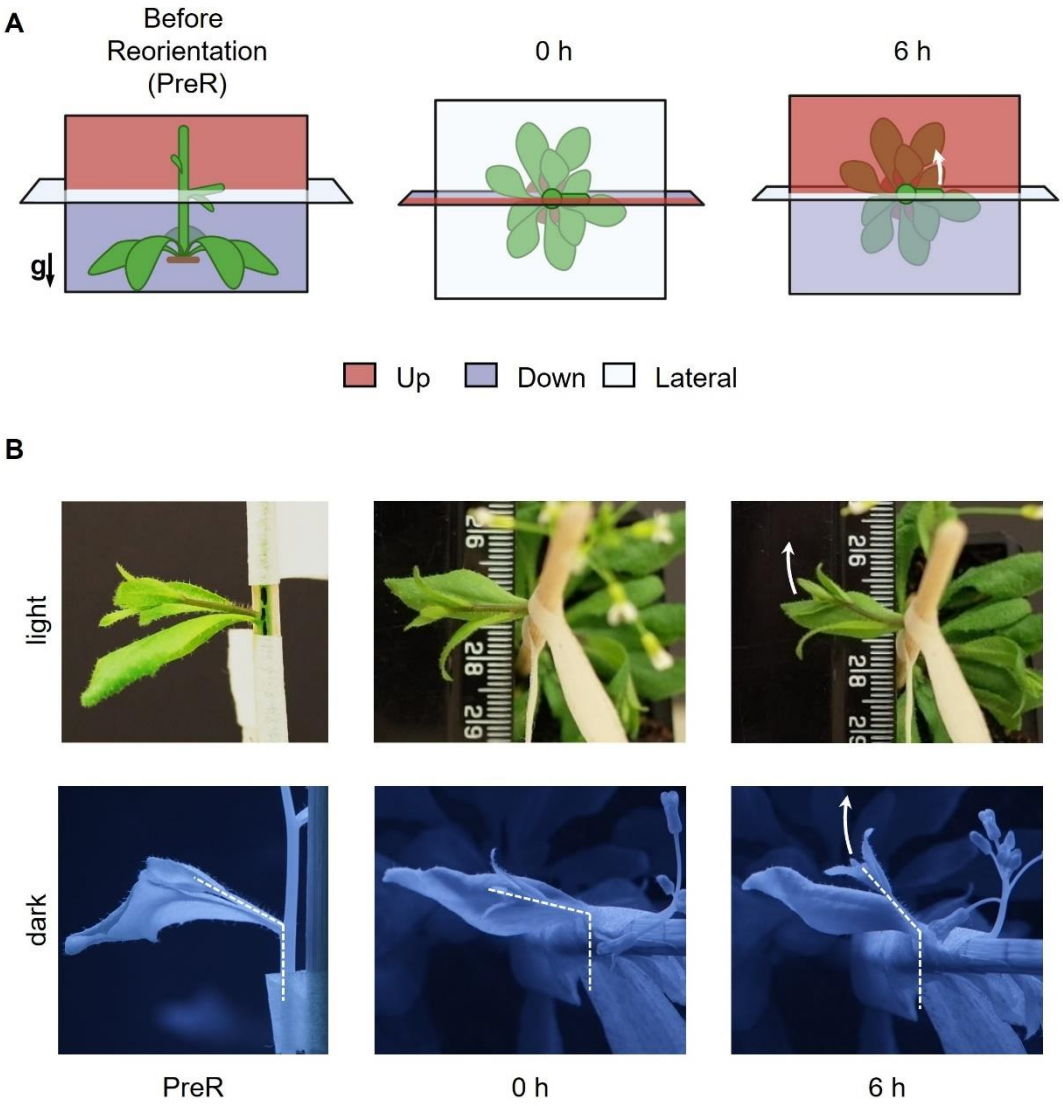

Figure 4.3: Young lateral shoots are gravicompetent

A) Schematic representation of the perpendicular assay. Up, down and lateral indicate the polarity of the plant with respect to gravity. The black arrow indicates the direction of gravity, g = gravity. B) Representative images of perpendicular assay of SII-SIII lateral shoots performed in the light or in the dark. White arrows indicate the direction of the bending, dashed lines indicate the angle of lateral shoot during the reorientation with respect to gravity. Four plants with SII-SIII lateral shoots were reoriented in the light and four in the dark. PreR = before reorientation, 0 h = 0 hours after reorientation, 6 h = 6 hours after reorientation.

4.2 Young lateral shoots develop independently from gravity

Since young lateral shoots can perceive and respond to gravity, clinorotation was used to understand the contribution of gravity during early stages of development (Fig. 4.4 A). Plants were mounted on a clinostat before bolting and subjected to clinorotation for the entire duration of development of the primary and lateral shoots, meaning that lateral shoots had never experienced a stable, polarising gravity reference. Under no stable reference to gravity, lateral shoot development progresses from stage I to stage II similarly to non-clinorotating plants (Fig. 4.4 B). After that, lateral shoots continue to grow rootward without setting SIII and SIV, while in non-clinorotated plants lateral shoots stop bending in SIII and set SIV GSA normally (Fig. 4.4 C-E). To check if clinorotation determines any impairments in the organization of lateral shoot stem tissues, transverse sections of stems stained with toluidine blue were obtained. Toluidine blue is a polychromatic staining able to dye different compounds of the cell wall with different colours, facilitating the observations of possible defects in cell morphology and cell wall composition (O'Brien, Feder and McCully, 1964). No differences in tissue organization were observed between clinorotated and control plants (Fig. 4.4 F), suggesting that stem tissues differentiate correctly under no stable reference to gravity. The phenotypes showed by lateral shoots developing under clinorotation suggest the existence of two distinct phases in lateral shoot development: an early gravity-independent phase consisting of SI and SII, and a following gravity-dependent phase that start with the arrest of lateral shoot rootward growth in SIII and terminates setting the GSA in SIV.

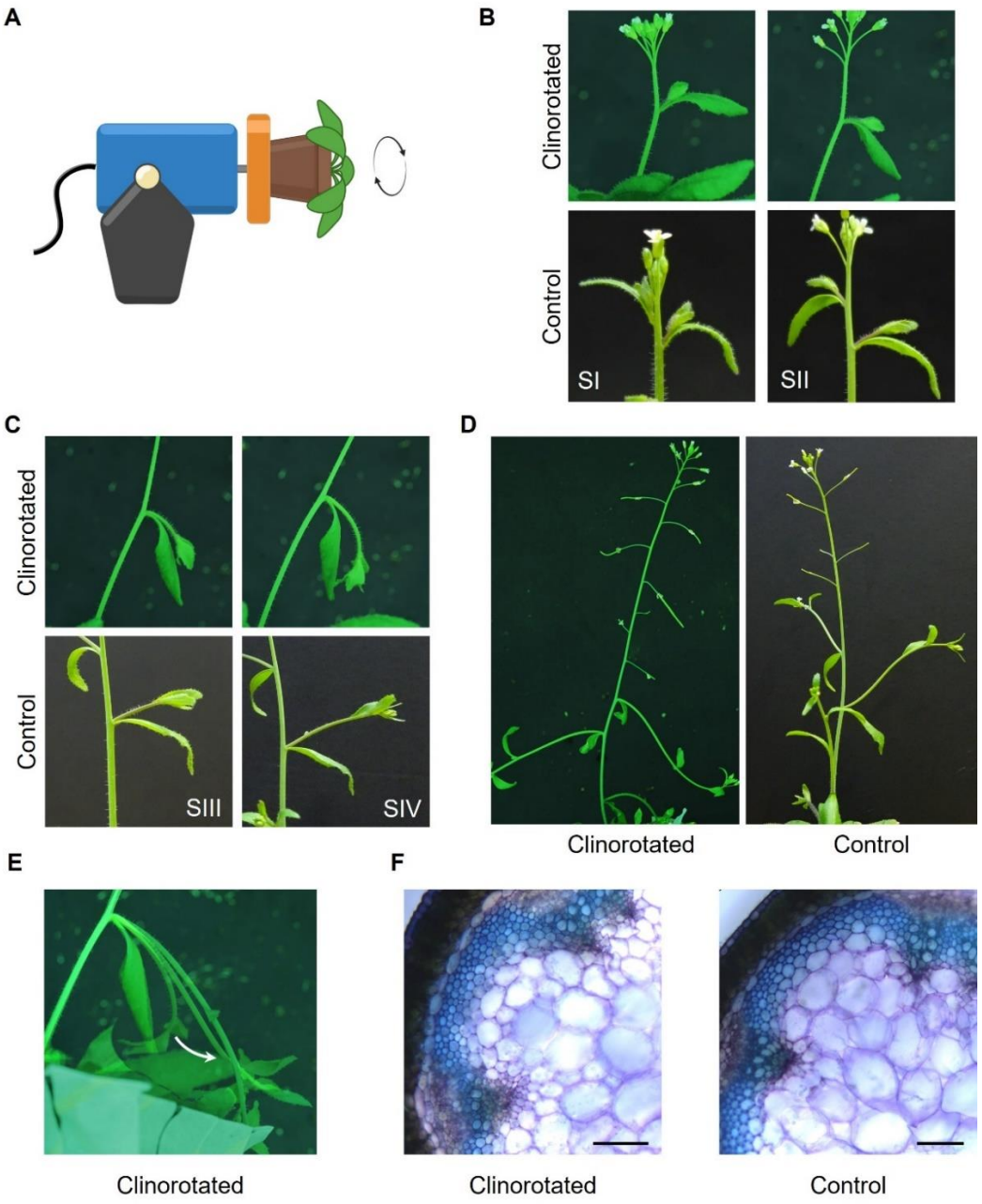

Figure 4.4: Lateral shoot development consists in a gravity-independent and a gravity-dependent phase

A) Schematic representation of clinorotation. Black arrows indicate the rotation of the clinostat. B) Representative images of early developmental stages (SI-SII) of lateral shoots of clinorotated and non-clinorotated (control) plants. C-E) Representative images of late developmental stages (SIII-SIV) of lateral shoots during clinorotation and in control plants. Figure (E) is obtained overlayed three images of taken 24 hours from each other. White arrow indicates the direction of growth. Six plants were used for clinorotation and three were grown as control. All the plants used showed same development under clinorotation. F) Representative images of transverse sections of clinorotated and control lateral shoot stems stained with toluidine blue. Scale bars = 100 μm.

4.3 Lateral shoot early developmental phase is independent from the GSA setting

To gather more evidence around the gravity-independence of early stages of lateral shoot development, loss-of-function mutants of *PHOSPHOGLUCOMUTASE* (*PGM*) and *SCARECROW* (*SCR*) genes, involved in gravity perception, were analysed. PGM is a plastid enzyme involved in starch synthesis, while SCR is a transcription factor required for endodermis specification (Caspar and Pickard 1989, Fukaki 1998). For this reason, loss-of-function mutants *pgm1* and *scr-3* lack, respectively, starch-filled statoliths and the endodermis layer in the whole plant (Caspar and Pickard 1989, Fukaki 1998). Lateral shoots of both mutants show SI to SIII early development comparable to wt (Fig. 4.5 A), while as expected SIV lateral shoots are impaired in GSA setting and maintenance (Fig. 4.5 B). This, together with the clinorotation results presented in the previous section, demonstrates that lateral shoot early development does not require gravity and therefore the gravity-sensing machinery. In addition, to understand if alteration of GSA regulators can influence lateral shoot early phase, loss-of-function mutants of *LAZY1* (*LZY1*) and *TILLER ANGLE CONTROL 1* (*TAC1*) genes were analysed. Both genes belong to the *IGT* family and regulate lateral shoot orientation antagonistically, with LZY1 promoting upward orientation and TAC1 inducing downward growth (Hollender *et al.*, 2020). In addition, it has been shown that TAC1 regulates lateral shoot GSA in response to light (Yu *et al.*, 2007; Dardick *et al.*, 2013; Waite and Dardick, 2018). Due to the opposite phenotypes displayed by *lzy1* and *tac1*, it has been proposed an antagonistic function of the two regulators (Hollender *et al.*, 2020). Lateral shoots of *tac1* and *lzy1* show normal SI-SII development (Fig. 4.5 A). Interestingly, the magnitude of the rootward growth ending in SIII shows opposite phenotypes in the two mutants. In *lzy1* the young lateral shoot displays a more pronounced rootward bending compared to *tac1*, where the rootward growth appears slightly reduced (Fig. 4.5 A). After that, both mutants set their altered GSA in SIV, with *lzy1* lateral shoots growing horizontally due to its weak gravitropic response, and *tac1* setting a more vertical GSA compared to wt (Dardick *et al.*, 2013; Yoshihara and Spalding, 2017).

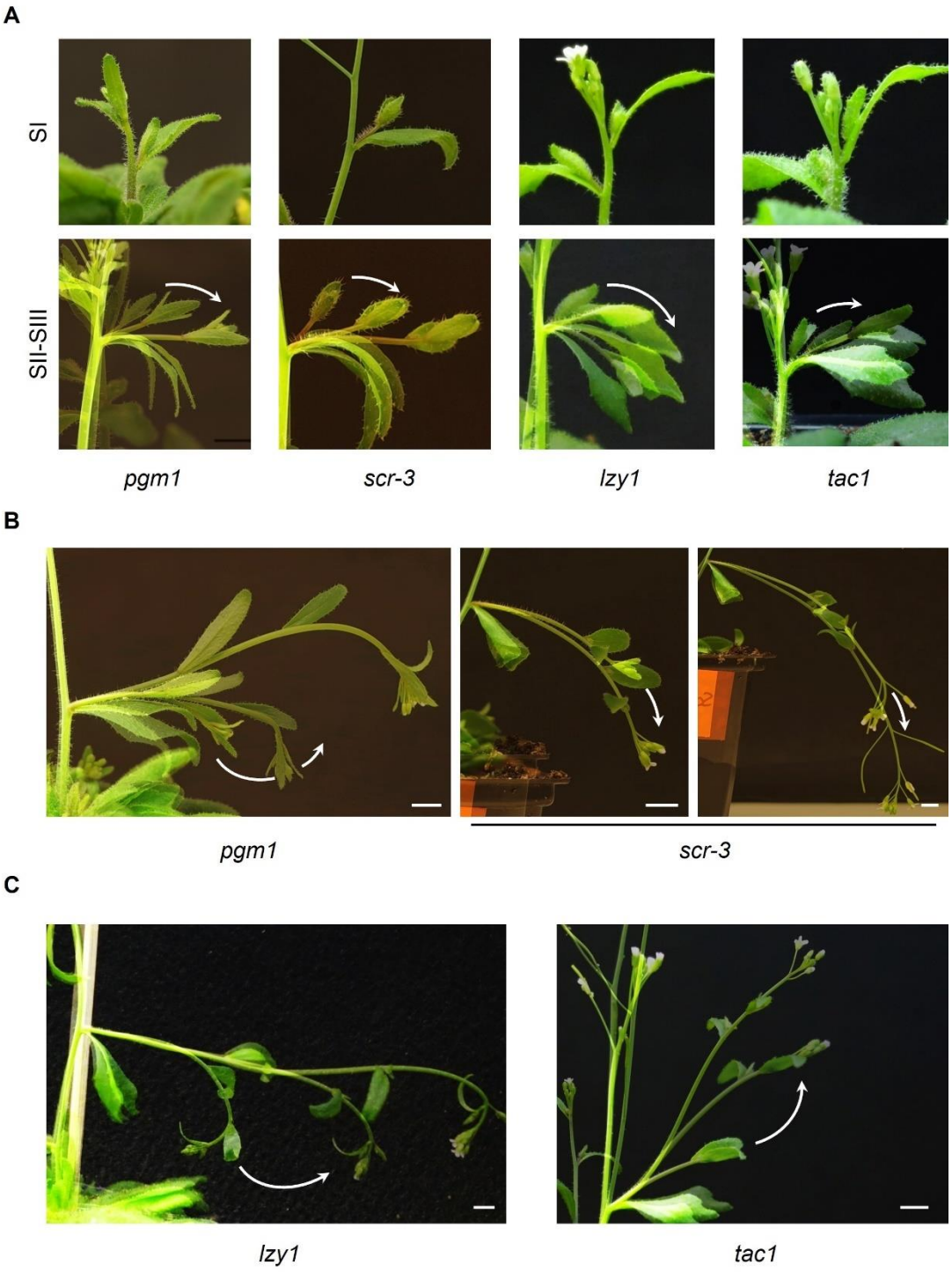

Figure 4.5: Lateral shoot early development is independent from late GSA setting

A) Representative images of early lateral shoot development of *pgm1, scr-3, lzy1* and *tac1*. SII-SIII images are obtained overlaying three pictures taken 24 hours from each other. B-C) Representative images of SIV lateral shoots of *pgm1*, *scr-3*, *lzy1* and *tac1*. Images were obtained overlaying three pictures taken 24 hours from each other. White arrows indicate the direction of growth. Scale bars = 0.5 cm.

The possible function of PIN3, PIN4 and PIN7 in early development was also analysed. Firstly, the expression of the three PIN proteins in lateral shoot endodermis was confirmed using GFP marker lines (Blilou *et al.*, 2005; Žádníková *et al.*, 2010). Both PIN3:GFP and PIN7:GFP are strongly expressed in the endodermis layer, showing a non-polar distribution in the cell, while PIN4:GFP expression is weaker and appears mainly polarised on the upper and/or lower side of the endodermis cells (Fig 4.6 A and B). After confirming that PIN3, PIN4 and PIN7 are indeed expressed in lateral shoot endodermis and most likely function in maintaining lateral shoot GSAs, early development of *pin3pin4pin7* (*pin347*) triple mutant was analysed. Similarly to *lzy1*, lateral shoots of *pin347* display normal SI and SII, with a slightly increase in the magnitude of the rootward growth ending in SIII (Fig 4.6 C). As already reported, SIV lateral shoots maintain more horizontal GSAs than wt due to gravitropic impairments in the absence of the three PIN proteins (Fig. 4.6 C) (Bennett *et al.*, 2016). Taken together these observations demonstrate that the early phase of lateral shoot development is independent from the late GSA setting, and alterations of regulators of the latter do not influence the former.

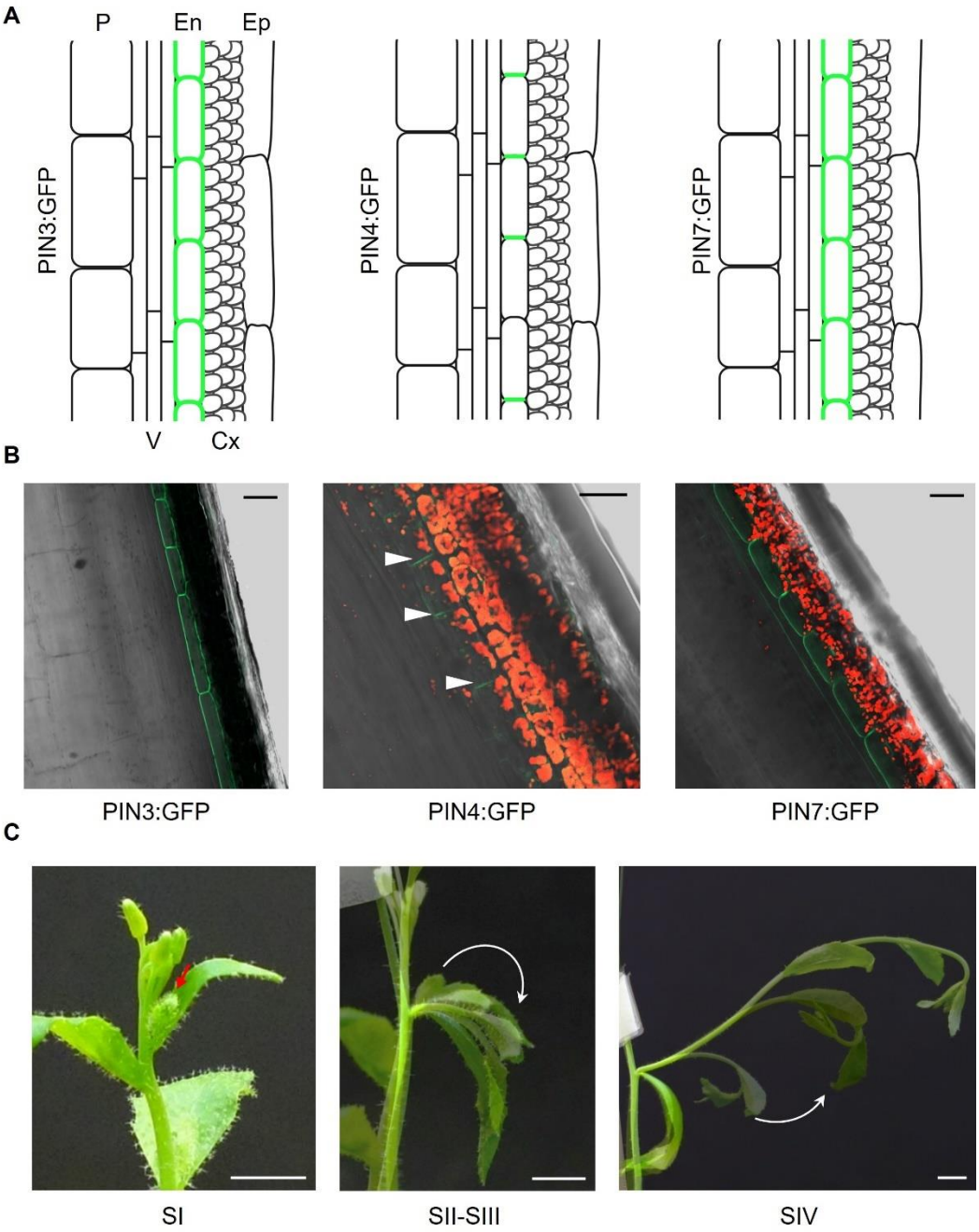

Figure 4.6: PIN3, PIN4 and PIN7 function in lateral shoot development

A) Schematic representation of longitudinal sections of lateral shoot stem expressing PIN3/4/7:GFP. The GFP signal is indicated in green. Ep = epidermis, Cx = cortex, En = endodermis, V = vasculature, P = pith. B) Representative images of PIN3/4/7:GFP expression in lateral shoot longitudinal sections. 10 lateral shoots were analysed per line. White arrows indicate PIN4 expression. GFP signal is in green, chlorophyll autofluorescence is in red. Scale bars = 50 μm. C) Representative images of *pin347* lateral shoot development. Red arrow indicates SI lateral shoot, white arrows indicate the direction of bending. SII-III and SIV images are obtained overlaying three pictures taken 24 hours from each other. Scale bars = 0.5 cm.

Discussion

Branching is a fundamental trait of shoot architecture and contributes to plant fitness and productivity. The manipulation of lateral shoot growth habits, through classic plant breeding programs, has been critical for the domestication and improvements of both herbaceous and woody species, and today continues to be an important trait targeted for crop improvement (Hill and Hollender, 2019). Although multiple works have been focused on understanding the molecular and environmental regulation of shoot branching, studying both the formation and activation of AM and the control of the final lateral shoot orientation with respect to environmental cues, the developmental events between these two processes have remained uncharacterised (Roychoudhry *et al.*, 2013; Wang and Jiao, 2018; Hollender *et al.*, 2020). Here, I presented my work aimed to fill the gap in our understanding of lateral shoot development using Arabidopsis. To better characterise the first phase of lateral shoot outgrowth I proposed a simple classification in stages describing the growth angle displayed by the branch, starting with a first vertical elongation of the branch in SI and ending with the GSA setting of mature lateral shoots in SIV.

Lateral shoot development consists of two distinct phases

Based on the classification proposed here, lateral shoot development can be divided into an early phase, consisting of SI and SII, and a late phase, corresponding to the GSA maintenance in SIV, with SIII marking the boundary between the two phases. The evidence obtained using reorientation and clinorotation assays, and following the branch development in gravity-sensing and GSA impaired mutants, demonstrates that the early phase is independent from both gravity and the GSA. This is particularly interesting because, at this early stage of development, the presence of starch-filled plastids in the endodermis, and the gravitropic response elicited by the perpendicular assay show that lateral shoots already possessed the mechanisms to perceive and respond to gravity but the gravitropic response, acting at the lower side of the lateral shoot, is prevented to affect the branch growth. In addition, based on the strength of the branch response to the perpendicular assay, the magnitude of the gravitropic response can be assumed to be the same in SII-SIII and SIV lateral shoots. Consequently, the differences in lateral shoot growth during development are most likely due to changes in the activity of forces working in opposition to the gravitropic response. Based on these observations, here

I propose a model in which the existence of a new gravity-independent growth component drives the downward/rootward growth during the early phase of lateral shoot development, in contraposition to the gravitropic response at the lower side of the branch (Fig. 4.7 A). This force, referred as SII-growth from here on, is independent from both gravity and the GSA. Previous observations and the data presented here suggest that the SII-growth is substantially different from the AGO that counteracts the gravitropic response in SIV lateral shoots (Roychoudhry *et al.*, 2013). The AGO, similarly to the gravitropic response, can be reset in the branch with respect to gravity. For example, when plants are reoriented upside down, lateral shoots re-establish their GSA switching the AGO and the gravitropic polarity in accordance with statolith sedimentation (Roychoudhry *et al.*, 2019; Kawamoto *et al.*, 2020). This shows that the AGO is dependent on gravity, a property not shared by the SII-growth. In addition, although the early phase is extended by lack of stable reference to gravity or impairment in gravitropism, it eventually ceases to lead the SII downward/rootward growth. This suggests that, as the lateral shoot tissues age, the branch ability to maintain the downward/rootward growth in the early phase decreases and, in the presence of gravity, it is replaced by the GSA control (Fig. 4.7 B). Although at this stage it is not possible to determine when the AGO is precisely set during the branch development, it can be hypothesised that, as the early phase terminates, the AGO is set and, counteracting the gravitropic response, determines the maintenance of non-vertical GSAs (Fig. 4.7 C).

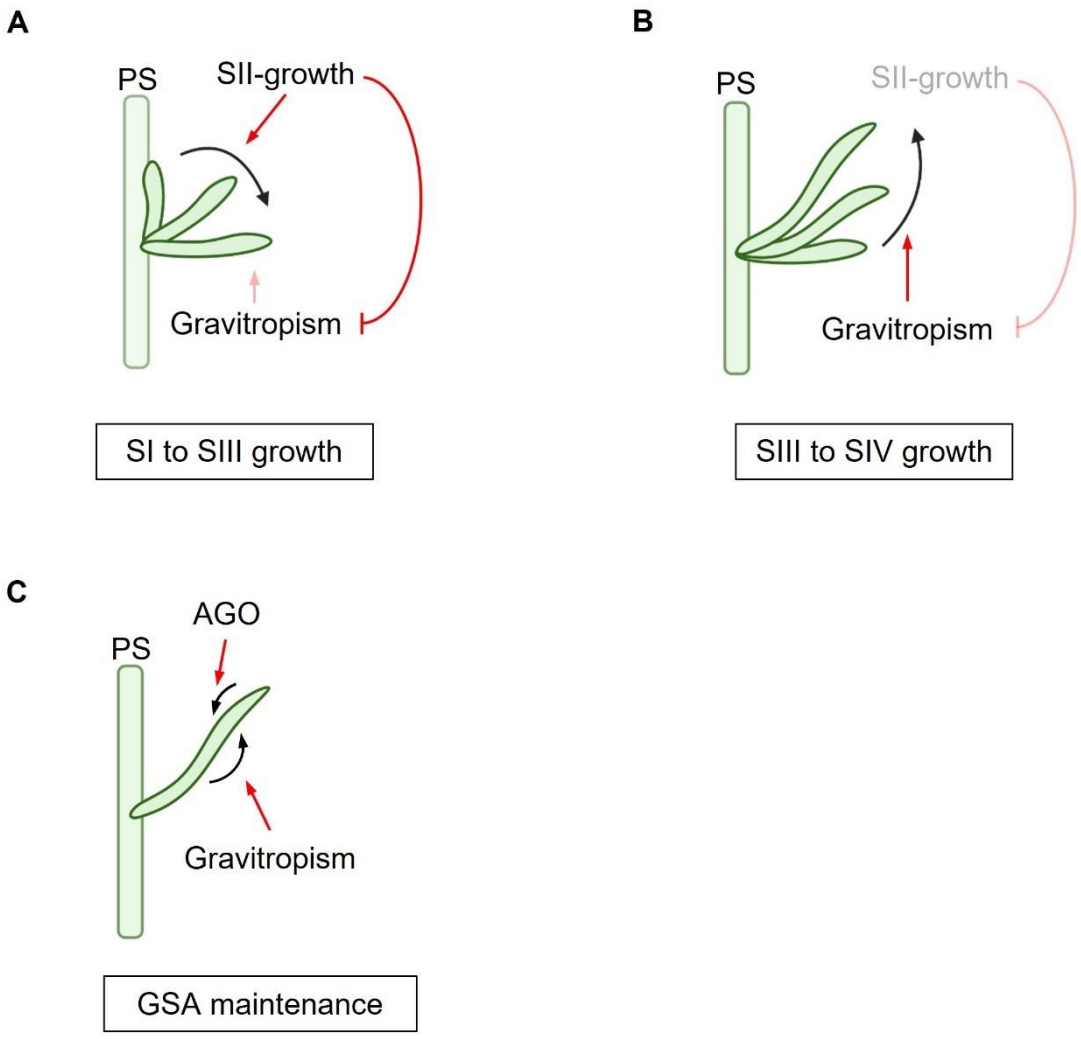

Figure 4.7: Lateral shoot development

Schematic representation of early (A) and late (B-C) lateral shoot development. During early development (A) SII-growth, in opposition to gravitropism, determines the young lateral shoot to bend downward and progress from SI to SII and SIII. Once the branch has reached SIII (B), SII-growth ceases, and gravitropism determines the lateral shoot to bend upward and establish the GSA (C). The balance between AGO and gravitropism, working respectively at the upper and lower side of the lateral shoot, determine the maintenance of the GSA.

This model can also explain why during the tilting assay, young lateral shoots do not respond to gravistimulation, while the perpendicular assay elicits the gravitropic response. In the first case, although the reorientation determines statoliths sedimentation, the planes of growth of the plant with respect to gravity remain largely unchanged (Fig. 4.2 A). In other words, the lower side of the lateral shoot with respect to gravity before the reorientation remain substantially the same when the plant is tilted, maintaining its lower polarity that coincides with the abaxial side of the branch. For this reason, the SII-growth, driving the downward/rootward growth at the adaxial side of the branch, prevents any action from the gravitropic response at the lower side of the lateral shoot. Conversely during the perpendicular assay, laying down the plant determines a change in the gravity-dependent polarity of the branch, which leads to the establishment of a new upper and lower sides (Fig. 4.3 A). This determines a separation between the upper-lower polarity and the ad-abaxial polarity, which is developmentally set and independent from the orientation of the branch with respect to gravity (Fig. 4.3 A). This allows the gravitropic response, not opposed anymore by the SII-growth that lead the rootward growth at the unchanged adaxial side, to be triggered at the new lower side of the branch and induce the lateral shoot to bend upwards. With the progression from SII to SIII and SIV, lateral shoots switch from a growth dominated by the SII-growth to a gravity-dependent elongation based on the GSA control. The development shown by lateral shoots during clinorotation demonstrates that this transition is not developmentally fixed, but rather is determined by gravity. In addition, lateral shoot development of *pgm1*, *scr-3, lzy1* and *pin347* demonstrate that the duration of SII rootward growth is determined by the gravicompetence of the branch.

Building a global understanding of lateral shoot growth angle control

In addition to the characterization of the early developmental phase of lateral shoot development, the analyses presented here offer the opportunity to gather more information on other aspects of growth angle control in shoot branches. The presence of PIN3, PIN4 and PIN7 in the endodermis of lateral shoots provides more evidence for their role in mediating auxin distribution in the gravity-sensing layer during GSA regulation. However, although impaired, the setting of the GSA in SIV following SIII in *pin347* still takes place, suggesting the existence of other redundantly expressed auxin transporters in the endodermis participating to the process, and/or the presence of ectopic

activity of the remaining PINs to partially balance the absence of PIN3, PIN4 and PIN7, a mechanism already described in roots (Blilou *et al.*, 2005). Similarly, the growth behaviour shown by *pgm1*, in which the lateral shoot still presents a upward/shootward growth marking the passage from SII-SIII to SIV, suggests the presence of a residual sensitivity to gravity and/or another gravity-dependent mechanism determining the straightening of the branch to horizontal growth angles. In either case, lateral shoot development of *scr-3* suggests that the presence of the endodermis is necessary to mediate this process. A straightening of the branch is also present in clinorotating plants, following the termination of the downward/rootward growth as the stem ages (Fig. 4.4 E). This could be led by the stem proprioception, a mechanism by which the plant controls its posture, allowing a steady growth in response to fluctuations in plant shape, both during development and as a consequence of tropic growth in response to environmental stimuli (Moulia, Douady and Hamant, 2021). In gravistimulated shoots, proprioception is responsible for counteracting the stem curvature triggered by the gravitropic response, preventing the stem to overbend thanks to the actin-myosin cytoskeleton that, in the cortical cells, forms long filaments proposed to sense the organ posture and respond to its changes (Okamoto *et al.*, 2015).

After the transition to SIV, the stable maintenance of the GSA in the older region of the stem, and the continuous growth led by the meristematic activity at the tip of the branch determine the lateral shoot to acquire a sigmoid shape. The position assumed by this young part at the tip of the branch is particularly interesting and, similarly to SII-SIII stems, as the newly-formed stem develops away from the meristem it bends upward, aligning with the rest of the stem and maintaining the GSA. During reorientation of SIV lateral shoots, the middle region of the stem strongly responds to gravistimulation, triggering the gravitropic response that restores the GSA, while the tip of the branch does not seem to participate to this tropic response. Assuming that equally to SII-SIII lateral shoots the branch tip is gravicompetent, a similar mechanism to the one proposed to regulate young lateral shoots might be in place to counteract the gravitropic response at the lower side of the tip. Together with gravity, light quality influences lateral shoot GSA, with low red/far-red (R/FR) light ratios, typical of a shaded environment, leading lateral shoots to shift to more vertical GSAs (Roychoudhry *et al.*, 2017). This phototropic response, also known as shade avoidance, is mediated by auxin biosynthesis and distribution across the branch (de Wit, Galvão and Fankhauser, 2016;

Roychoudhry *et al.*, 2017). In lateral shoots, TAC1 has been proposed as a downstream target of the phototropic signal, negatively regulating the shift of lateral shoots to vertical GSAs (Waite and Dardick, 2018). The phenotype shown by SIV lateral shoots of *tac1*, in which both the GSA and the growth angle of the branch tip are more vertical than wt, suggests that light might be another factor regulating the tip orientation in SIV lateral shoots. Furthermore, *tac1* shows a reduced downward growth in SII suggesting that light might also be involved in the regulation of SII-SIII duration during lateral shoot development.

These observations, together with previous analyses, reveal that the growth angle of lateral shoots is spatio-temporally regulated, and the final shape of the branch is determined by the integration of developmentally set identities, such as the ad-abaxial polarity, endogenous stimuli, like the proprioceptive response, and tropic growth elicited by environmental cues. More work is needed to better characterise the early phase of lateral shoot development with respect to other environmental factors, such as light. In addition, although the molecular basis of SIV GSA control is assumed to be similar to lateral roots, a deeper study of the mechanism is needed to confirm the proposed molecular regulators involved in the process and identify the uncharacterised ones.

Chapter 5. Uncovering the biophysical and molecular basis of ab-adaxial polarity in lateral shoots

Introduction

Axial polarity establishment is a process essential for the plant spatial development and is determined by the organization of organs along the body axes. Lateral shoots develop along two main axes: the proximal-distal axis with respect of the primary shoot, and the radial axis in which the branch cellular layers organise around the vasculature. The data presented in the previous chapter show the existence of another important axial polarity along which the lateral shoot organises: the adaxial-abaxial polarity. The adaxial and abaxial sides of an organ can be defined as the surfaces of the organ facing respectively upward and downward with respect to the main axis. The establishment of the ad-abaxial polarity has been vastly studied in leaves, representing a good example of polarity regulation and maintenance during organ development. The coordination of cell proliferation, expansion and differentiation across the leaf is fundamental to determine its final shape (Gonzalez, Vanhaeren and Inzé, 2012). Firstly, different cell growth rates along the ad-abaxial axis determine the leaf to grow away from the SAM, than cell differentiation establishes the morphological identity of the adaxial and abaxial side (Manuela and Xu, 2020). The regulation of the time needed to complete the mitotic cell cycle is important to control the cellular growth rate during the first phase of leaf development. Mitotic cell cycle consists of four phases, the G1 phase, the S phase in which DNA is duplicated, the G2 phase and the M phase in which mitosis happens. Progression from one phase to the next is controlled by phase-specific cyclin-dependent kinases (CDKs) and their cyclin activators (CYCs) (Komaki and Sugimoto, 2012). It has been shown that in leaves, the anaphase-promoting complex/cyclosome 10 (APC10) regulates cell cycle progression through the degradation of CYCB1;1 (Eloy *et al.*, 2011). CDK-CYCB complexes determine the progression from G2 to M phase (Komaki and Sugimoto, 2012). Degradation of this complex induces the exit from the M phase and allows the cell to begin a new cycle. Similarly, CDK-CYCD complexes are responsible for the transition from G1 to S phase, inducing cells to enter the cell cycle (Komaki and Sugimoto, 2012). During leaf development, CYCD3 is involved in the regulation of cell proliferation, and has been shown to mediate CK control of cell division during shoot development (Riou-Khamlichi *et al.*, 1999; Dewitte *et al.*, 2007). As the

leaf develops, cell differentiation along the ad-abaxial axis is secured by a network of differentially expressed regulators. Among these regulators, class III HD-ZIP transcription factors are responsible for the specification of the adaxial side, while KANADI (KAN) and YABBY (YAB) family proteins are involved in conferring the abaxial identity (Eshed *et al.*, 2001; Kerstetter *et al.*, 2001; Emery *et al.*, 2003; Prigge *et al.*, 2005). Together with the specification of their respective domains, adaxial and abaxial factors repress each other expression both directly and indirectly, building a complex network responsible for maintaining the leaf polarity (Yamaguchi, Nukazuka and Tsukaya, 2012). In addition, both KAN and REVOLUTA (REV), a class III HD-ZIP factor expressed in leaf adaxial side, have been shown to antagonistically regulate genes involved in auxin biosynthesis, transport and signalling during the early phase of development (Huang *et al.*, 2014; Ram *et al.*, 2020). Two auxin responsive factors, ETT/ARF3 and ARF4, have also been shown to participate to the specification of the leaf abaxial side, with ETT physically interacting with KAN (Pekker, Alvarez and Eshed, 2005; Kelley *et al.*, 2012). Differently to leaves, lateral shoots do not seem to differ morphologically along the ad-adaxial axis, but as demonstrated in the previous chapter, adaxial and abaxial identity are defined in the early phase of development. To identify the biophysical and molecular basis of the ad-abaxial polarity, SII-SIII lateral shoot cell morphology and transcriptome along this axis were analysed.

Results

5.1 Lateral shoot adaxial and abaxial side differ for number of cells

The rapid change in growth angle displayed during SII downward growth, leading to the nearly horizontal growth angle in SIII, implies the existence of differences in cell number and/or length between the adaxial and abaxial side of the branch. To determine which mechanism lies behind the downward growth, epidermal and cortical cells of SIII lateral shoots were analysed. As expected across the lateral shoot, epidermis cells show a proximal-distal polarity with respect to the primary shoot (Fig 5.1 A). Distal cells, closer to the lateral floral meristem, show a meristematic morphology and have very small size (~ 10-15 μm) with stomatal cells not yet differentiated (Fig. 5.1 B). Progressing to the proximal region of the branch, cells start to show the anisotropic growth that will result in their final elongated shape, together with differentiating and fully formed stomata (Fig. 5.1 B). Similarly, the underlying cortex show changes in cell size on the proximal-distal axis (Fig. 5.1 B). Due to the meristematic morphology of distal cells, analyses of cell length and number were performed on the proximal region of the branch. No significant differences were found in cell length between the adaxial and abaxial side of the epidermis, while in the same area the adaxial side contained around 21% (± 5%) more cells per 0.1 per mm^2 (Fig 5.1 C). To confirm these differences, the first layer of cortex immediately under the epidermis was also analysed. Similarly to the epidermis, cortical adaxial side contains around 17% more cells per mm compared to the adaxial side (Fig. 5.1 C). These results suggest that the downward growth shown in young lateral shoots is based on differences in cell proliferation along the ad-abaxial axis.

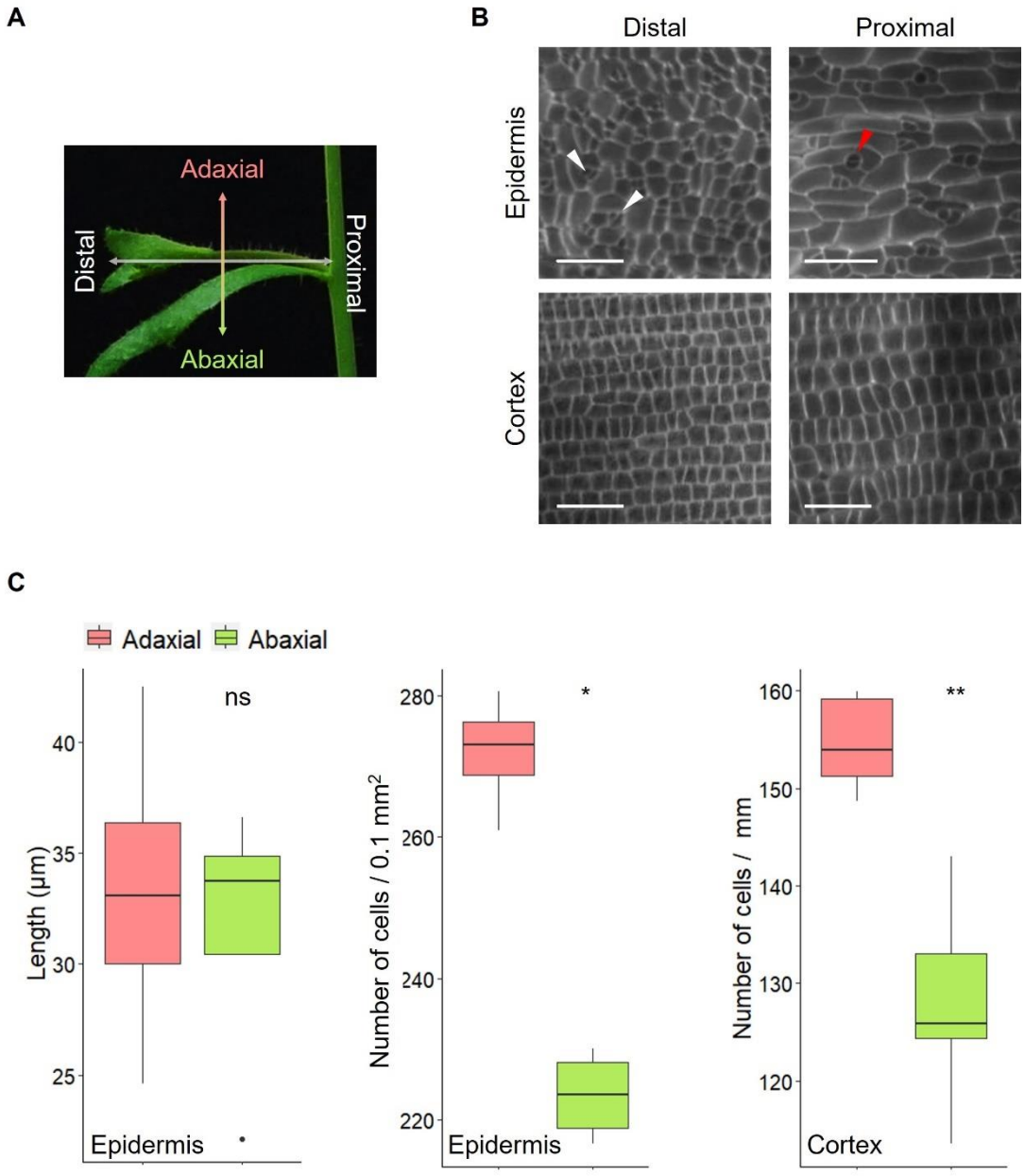

Figure 5.1: Adaxial and abaxial side of young lateral shoots differ in cell number

A) Schematic representation of proximal-distal and adaxial-abaxial axes in a SIII lateral shoot. B) Representative images of distal and proximal regions of epidermal and cortical cells in SIII lateral shoots. White arrows indicate stomatal cells asymmetrically dividing, red arrow indicates differentiated stomata. Scale bar = 50 µm C) Box plot showing quantitative analysis of cell length and number of epidermis and cortex in the proximal region of SIII lateral shoots. Box boundaries indicate the interquartile range (IQR), with central line representing the median. Black dots indicate outliers. Box whiskers represent data points 1.5x from the IQR. Three biological replicates were used per plot. Statistical analysis was performed using pairwise Wilcox test with Benjamini-Hochberg correction. ** = $p < 0.005$, * = $p < 0.05$. ns = non-significant.

5.2 B- and D-Type cyclins regulate cell cycle during early development

Cell size and morphology observed along lateral shoot proximal-distal axis demonstrate that during SII and SIII cells are not yet fully differentiated. Although epidermal cells in the proximal region of the branch are starting to elongate, the tissue appears heterogeneous with neighbour cells showing different degrees of growth (Fig. 5.1 B). To determine at which stage lateral shoot cells stop dividing the expression of *CYCB1;1* and *CYCD3* were analysed using GUS reporter lines. *CYCB1;1* is strongly expressed across the branch during SII, while in SIII the expression is turned down and active in a reduced number of cells, in line with cell differentiation starting at this later stage of development (Fig. 5.2 A). Arabidopsis CYCD3 is encoded by three genes, *CYCD3;1*, *CYCD3;2* and *CYCD3;3*, with overlapping expression (Dewitte *et al.*, 2007). No GUS activity was detected for *CYCD3;1::GUS* line in any of the developmental stages of lateral shoots, while *CYCD3;2* and *CYCD3;3* are both expressed in SI and SII (Fig. 5.2 B). *CYCD3;3* expression is turned off during SIII and SIV, while *CYCD3;2* continues to be expressed both in SIII and in the distal region of SIV lateral shoots (Fig. 5.2 B and C). These results confirm that cell division strongly contributes to lateral shoot growth during SII and SIII and in the younger region of SIV branches. Interestingly, both *CYCD3;2* and *CYCD3;3* show a pattern of expression along the apical-basal axis with respect to the primary shoot, with branches nearer the primary shoot apex having a lower expression compared to branches at the basal end (Fig. 5.2 E).

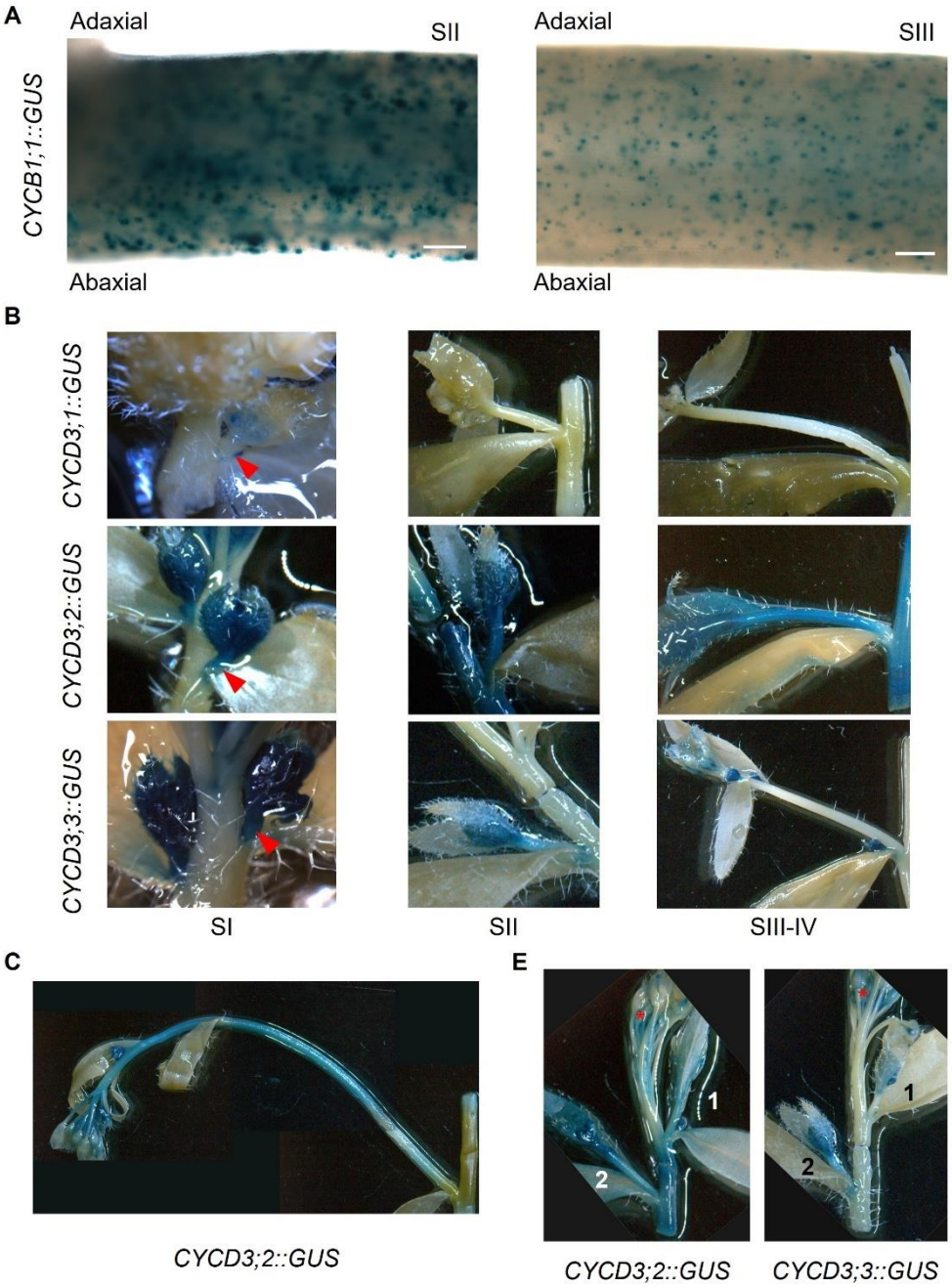

Figure 5.2: *CYCB1* and *CYCD3* expression in lateral shoot development

A) Representative images of longitudinal sections of SII and SIII lateral shoots expressing *CYCB1;1::GUS*. Scale bars = 100 μm. B) Representative images of lateral shoots expressing *CYCD3;1-3::GUS* at different stages of development. Red arrows indicate the SI lateral shoot. C) Representative images of a SIV lateral shoot expressing *CYCD3;2::GUS*. E) Representative images of primary inflorescence segments containing two lateral shoots of lines expressing *CYCD3;2::GUS* and *CYCD3;3::GUS*. Red stars indicate the primary shoot apex, lateral shoots are numbered based on the distance from the primary apex. 1 = apical branch, 2 = basal branch. Blue stain = GUS signal.

5.3 Cytokinins role in lateral shoot early development

In the shoot, sugar availability and CK are positive regulators of cell proliferation via the induction of *CYCD3* expression (Riou-Khamlichi *et al.*, 2000; Dewitte *et al.*, 2007). To understand if CK pathway is involved in regulating cell proliferation through the expression of CYCD3 in lateral shoots, branch development of mutants impaired in CK biosynthesis and signalling was analysed. ISOPENTENYLTRANSFERASES (IPT) are a family of enzymes catalysing the initial steps of CK biosynthesis (Takei, Sakakibara and Sugiyama, 2001). The triple loss of function mutant *ipt3ipt5ipt7* (*ipt357*) contains reduced levels of CK, which cause the development of short and thin shoots (Miyawaki *et al.*, 2006). Lateral shoot development of this mutant shows a reduced downward growth in SII and set a more vertical GSA compared to wt (Fig. 5.3 A and C). Loss of function mutants of the CK receptors ARABIDOPSIS HISTIDINE KINASES (AHKs) *ahk2ahk3*, *ahk2ahk4* and *ahk3ahk4* (Higuchi *et al.*, 2004), instead, do not show significant differences both during early development and GSA setting (Fig. 5.3 B and C). Similarly, the constitutively active gain-of-function variants of the AHK2 and AHK3 *repressor of cytokinin deficiency 2* (*rock2*) and *rock3* (Bartrina *et al.*, 2017) show a normal lateral shoot development, with SIV GSA slightly more horizontal than the wt (Fig. 5.3 B and C). Analysis of cortical cell number of *ipt357* young lateral shoots reveals reduced differences between the adaxial and abaxial side, which explain the diminished downward growth observed in the early phase of branch development (Fig. 5.3 D). These observations demonstrate that CK are needed to generate the cell proliferation differences that drives the SII rootward growth during early lateral shoot development.

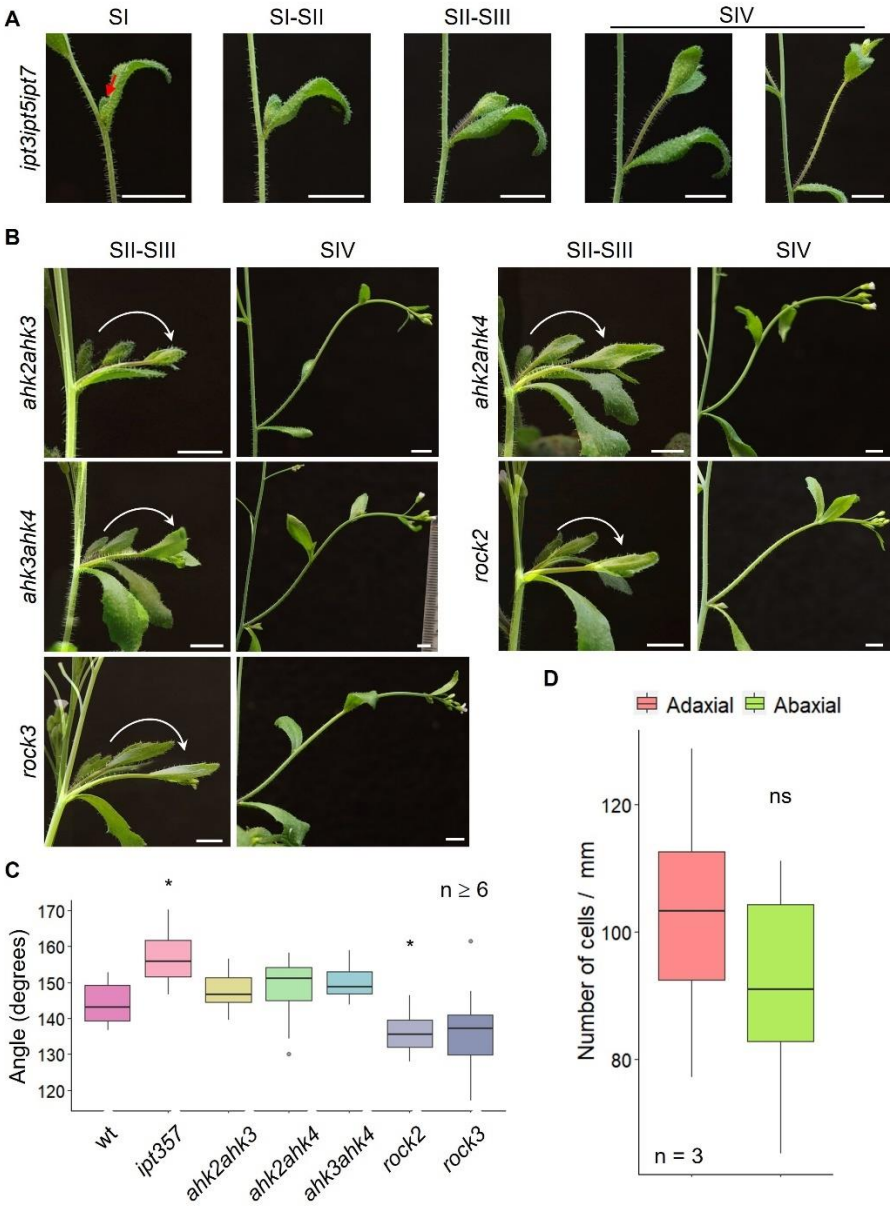

Figure 5.3: Cytokinins are involved in driving cell proliferation during early development

A-B) Representative images of lateral shoot development of *ipt3ipt5ipt7*, *ahk2ahk3*, *ahk2ahk4*, *ahk3ahk4*, *rock2* and *rock3* mutants. Red arrow indicates the SI lateral shoot. SII-SIII images in (B) are obtained by overlaying three pictures taken 24 hours from each other. White arrows indicate the direction of growth. Scale bars = 0.5 cm. C-D) Box plot of quantitative analysis of lateral shoot GSA (C) and cortical cell number in *ipt3ipt5ipt7* (D). Box boundaries indicate the interquartile range (IQR), with central line representing the median. Black dots indicate outliers. Box whiskers represent data points 1.5x from the IQR. Statistical analysis was performed using one-way ANOVA with Tukey's HSD post-hoc test for (C) and Wilcoxon test with Benjamini-Hochberg correction for (D). * = $p < 0.05$, ns = non-significant, n = number of biological replicates.

5.4 ARF4 and ETT are involved in shoot ad-abaxial polarity

Among the factors controlling plant polarity, the auxin responsive factors ETT/ARF3 and ARF4 are redundantly involved in the specification of the abaxial polarity in leaves (Pekker, Alvarez and Eshed, 2005). To determine if these two ARFs also participate in lateral shoot development, branch outgrowth of loss-of-function single and double mutants were analysed. Both *arf4* and *ett-3* single mutants show normal lateral shoot development and GSA setting (Fig. 5.4 A). As previously reported, *arf4ett-3* double mutant develops leaves with impaired abaxial identity, and floral organs with altered morphology leading to plant sterility (Pekker, Alvarez and Eshed, 2005). In addition to this, lateral shoot early development of *arf4ett-3* is altered (Fig. 5.4 B). Newly formed lateral shoots start their elongation normally, growing in proximity of the primary shoot and quickly bending rootward reaching a horizontal growth angle, in what can be consider a fast progression to SII-SIII (Fig. 5.4 B). After that, branches continue to grow bending rootward for a couple of days, until transitioning to SIV GSA setting (Fig. 5.4 C). Interestingly, once lateral shoots have progressed out of the early phase their development proceeds as normal, and the GSA is set similarly to wt plants (Fig. 5.4 D). This demonstrates, again, that the early phase of development and the GSA setting are two separate and distinct events in lateral shoot development, regulated by different molecular factors. Furthermore, the phenotype shown by *arf4ett-3* demonstrates that ETT and ARF4 are redundantly involved in early development.

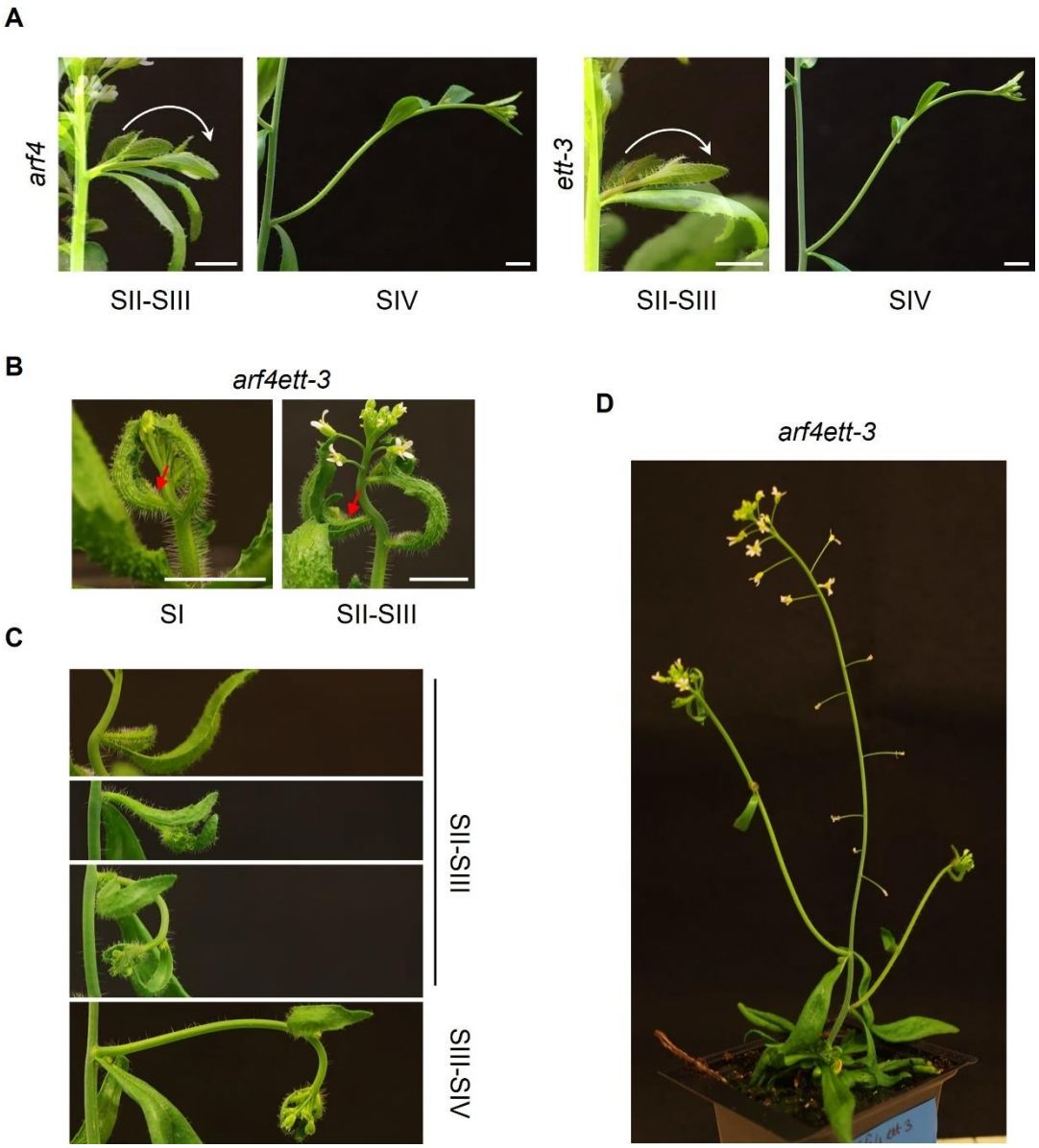

Figure 5.4: ETT and ARF4 are redundantly involved in lateral shoot development

A) Representative images of SII-SIII and SIV lateral shoots of *arf4* and *ett-3*. SII-SIII images are obtained overlaying three pictures taken 24 hours from each other. White arrows indicate the direction of growth. B-C) Representative images of early development and SIII-SIV transition of *arf4ett-3* lateral shoots. Red arrows indicate the lateral shoot. D) Representative image of ~28 days old *arf4ett-3* plant maintaining normal lateral shoot GSAs. Scale bars = 0.5 cm.

5.5 Transcriptomic analysis reveals differentially expressed genes between the adaxial and abaxial side of young lateral shoots

To identify novel factors involved in the specification of the ad-abaxial polarity, transcriptomic analysis of young lateral shoots was performed. Nine SII lateral shoot stems growing from independent plants were hand-sectioned dividing the adaxial from the abaxial side. Three adaxial sides were then pooled together as one biological replicate. The same was done for the abaxial sections. Total RNA from the three biological replicates was then extracted and sent to Azenta/GENEWIZ for sequencing and analysis. Using DESeq2 function with Wald test, lateral shoot adaxial and abaxial transcriptomic data was compared and p-values and $\log_2$ fold change were generated. From this comparative analysis, genes with a $\log_2$ fold change > 1 and an adjusted p-value < 0.05 were considered differentially expressed between the adaxial and abaxial side of lateral shoots. Sixty-three genes were found differentially expressed, with the majority of them showing higher expression on the adaxial side (Table 7.2). To determine which biological processes were linked to the differentially expressed genes (DEGs), gene ontology (GO) analysis was performed using Fisher exact test. Most of the adaxially expressed genes were clustered under biological processes linked to responses to light and production of photoprotective compounds, reflecting the greater exposure to light of the adaxial side compared to the abaxial one (Fig. 5.5). In addition, differentially expressed genes from both the adaxial and abaxial side clustered under “cell differentiation” and “floral development”, suggesting that cell differentiation is happening during SII on the two sides and that factors previously linked to floral development are also involved in stem growth (Fig. 5.5).

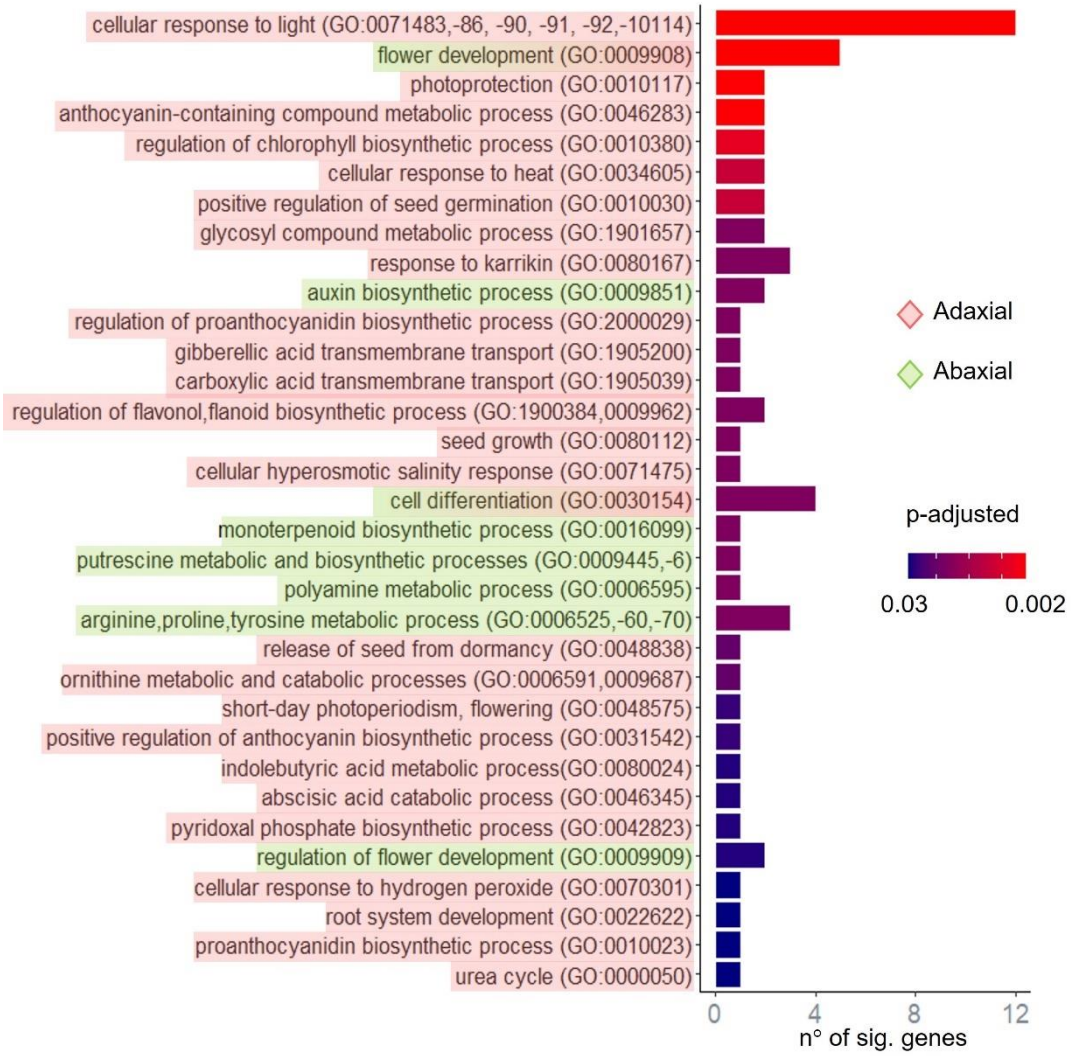

Figure 5.5: Gene ontology analysis

Gene ontology analysis of significant DEGs between the adaxial and abaxial side of SII lateral shoot stems. The number of significant genes for each category is plotted on the x-axis, the adjusted p-value (p-adjusted), indicating the significance of each category, is colour-coded.

To visualise the differences of expression along the ad-abaxial axis, the normalised counts of the top-half most significant DEGs were plotted in a heatmap (Fig. 5.6 A). Among the genes showing the stronger differences in expression between the adaxial and abaxial side, the transcription factors AGAMOUS-LIKE 71/FOREVER YOUNG FLOWER-LIKE 1 (AGL71/FYL1), AGL72/FYL2 and TEOSINTE BRANCHED1, CYCLOIDEA and PCF 1 (TCP1) were the most significant (Fig. 5.6 B). *TCP1* is mainly expressed on the adaxial side, while *AGL71* and *72* are expressed on the abaxial side (Fig. 5.6 A and B). All three genes cluster under “floral development” in GO analysis, with *AGL71* and *72* also appearing in “cell differentiation”. TCP1 have been linked to regulation of both cell proliferation and cell elongation in flowers and leaves respectively (Busch and Zachgo, 2007; Koyama, Sato and Ohme-Takagi, 2010; Busch, Horn and Zachgo, 2014). In addition, it has been shown that TCP1 positively regulates brassinosteroid (BR) biosynthesis in leaves, through the induction of the biosynthetic BR gene *DWARF4* (*DWF4*) (Guo *et al.*, 2010; Gao, Zhang and Li, 2015). AGL71 and AGL72 are two MADS-box transcription factors related to SUPPRESSOR OF OVEREXPRESSION OF CO 1 (SOC1)/AGL20. It has been shown that together with SOC1, AGL71 and AGL72 are redundantly involved in floral transition in both primary and lateral inflorescences (Dorca-Fornell *et al.*, 2011). Furthermore, a role for these two AGLs has been suggested in regulating gibberellin acid (GA) biosynthesis during flowering, flower senescence and flower abscission together with FOREVER YOUNG FLOWER (FYF)/AGL42 transcription factor (Dorca-Fornell *et al.*, 2011; W.-H. Chen *et al.*, 2022). Due to *TCP1*, *AGL71* and *AGL72* differential expression along the ad-abaxial axis of SII branches, their role as transcription factors and their potential involvement with cell proliferation and differentiation, these three genes were selected as potential regulators of lateral shoot development.

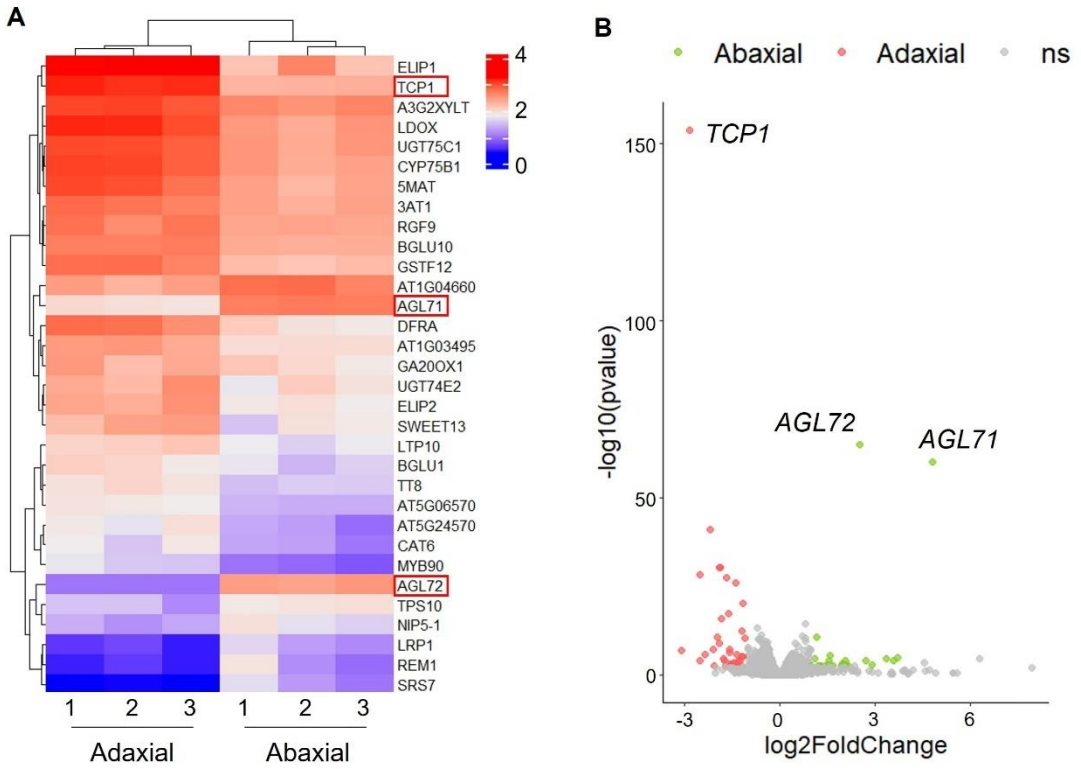

Figure 5.6: Transcriptomic analysis of SII lateral shoots

A) Heatmap of the top-half most significant DEGs. Plotted using a red-white-blue colour scale is the $\log_{10}$ of the normalised counts of each gene obtained per sample sequenced. Numbers indicate biological replicates. Red boxes indicate the three most significant genes. B) Volcano plot showing the fold change and the statistical significance of DEGs found between the adaxial and abaxial side of SII lateral shoot stems. Pink dots indicate adaxially expressed genes, green dots indicate abaxially expressed genes and grey dots indicate non-significant genes expressed across the branch. *TCP1, AGL71* and *AGL72* represents the top three most significantly DEGs in the data set.

5.6 *TCP1*, *AGL71* and *AGL72* are possible regulators of ad-abaxial polarity

To confirm the transcriptomic data obtained from SII lateral shoots, *TCP1*, *AGL71* and *AGL72* expression was analysed in both SII and SIII branches using RT-qPCR. The expression of these three transcription factors during early development confirms the transcriptomic data of adaxially expressed *TCP1* and abaxially expressed *AGL71* and *AGL72* (Fig. 5.7 A). Similarly to early stages, expression of *TCP1* and *AGL71* is maintained polarised in SIV, while *AGL72* is variable on both the abaxial and the adaxial side (Fig. 5.7 B). As demonstrated above, ARF4 and ETT are redundantly involved in lateral shoot early development, with *arf4ett-3* mutant showing altered SII-SIII growth. To understand if ARF4 and ETT are involved in *TCP1*, *AGL71* and *AGL72* transcription along the ad-abaxial axis, *TCP1*, *AGL71* and *AGL72* expression in *arf4ett-3* was analysed. In SII *arf4ett-3* branches, *TCP1* expression is maintained at the adaxial side similarly to wt, while *AGL71* and *ALG72* show very variable expression among samples in both the adaxial and abaxial side, suggesting a misregulation of their transcription (Fig. 5.7 C). This indicates a possible role of ARF4 and ETT in regulating the abaxial expression of *AGL71* and *AGL72*.

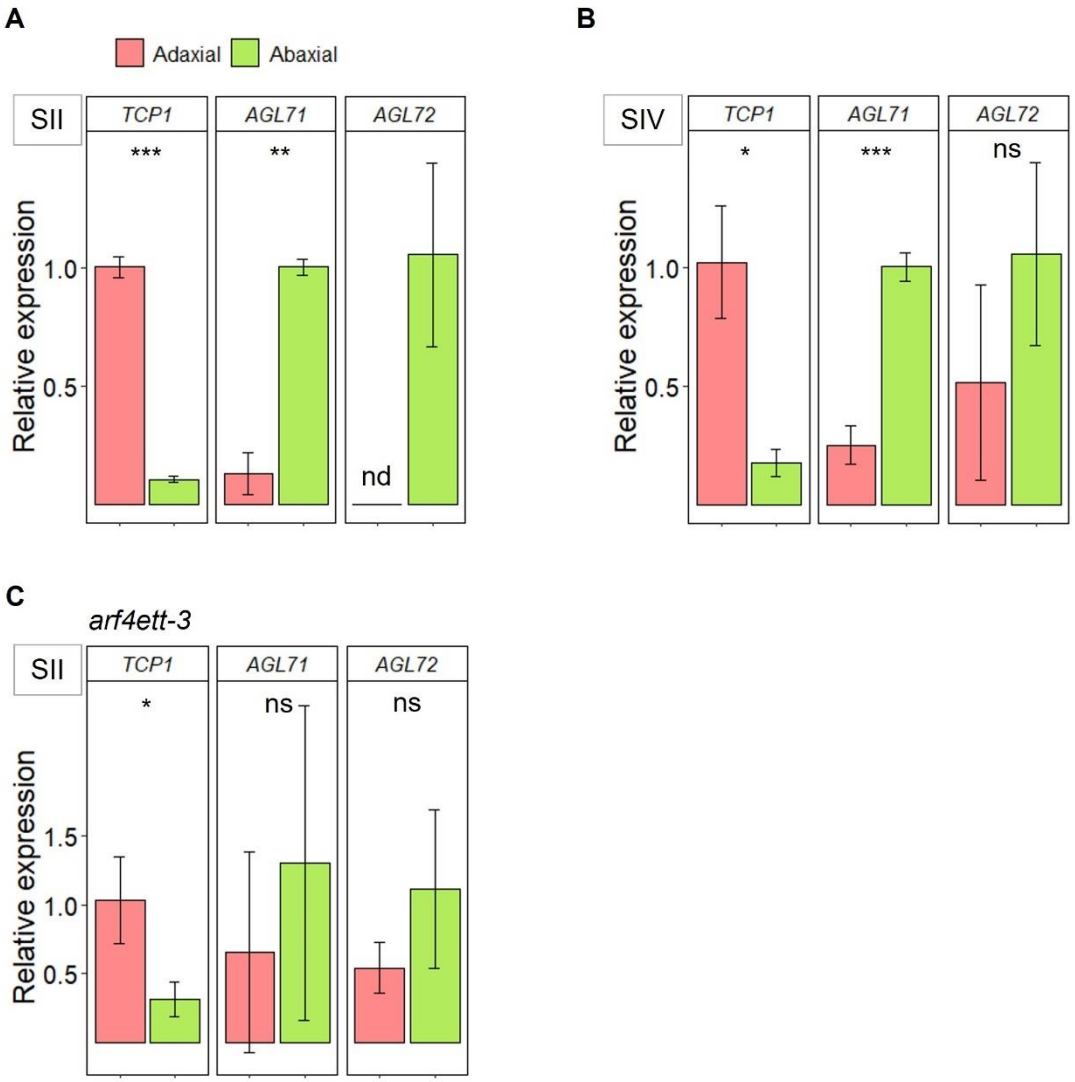

Figure 5.7: *TCP1*, *AGL71* and *AGL72* expression during lateral shoot development

A-B) Bar chart showing quantitative analysis of *TCP1*, *AGL71* and *AGL72* expression in lateral shoot early (SII) and late (SIV) development of wt (Col). C) Bar chart showing quantitative analysis of *TCP1*, *AGL71* and *AGL72* expression in *arf4ett-3* lateral shoot early development (SII). Error bars = standard deviation. The analysis was performed with three biological replicates. Statistical analysis was performed using independent t-test. (*) = $p < 0.05$, (**) = $p < 0.005$, ns = non-significant.

To gather more information around the role of the two AGLs in lateral shoot development, single loss-of-function mutants *agl71* and *agl72* were analysed. *agl71* and *agl72* show overall normal development, with SII rootward growth and SIV GSA setting comparable to wt (Fig. 5.8 A-C). Interestingly, both mutants show a mild phenotype in the transition from SIII to SIV, with lateral shoots elongating on a straight line during SIII, before bending upward and setting the characteristic sigmoid shape in SIV (Fig. 5.8 A and B).

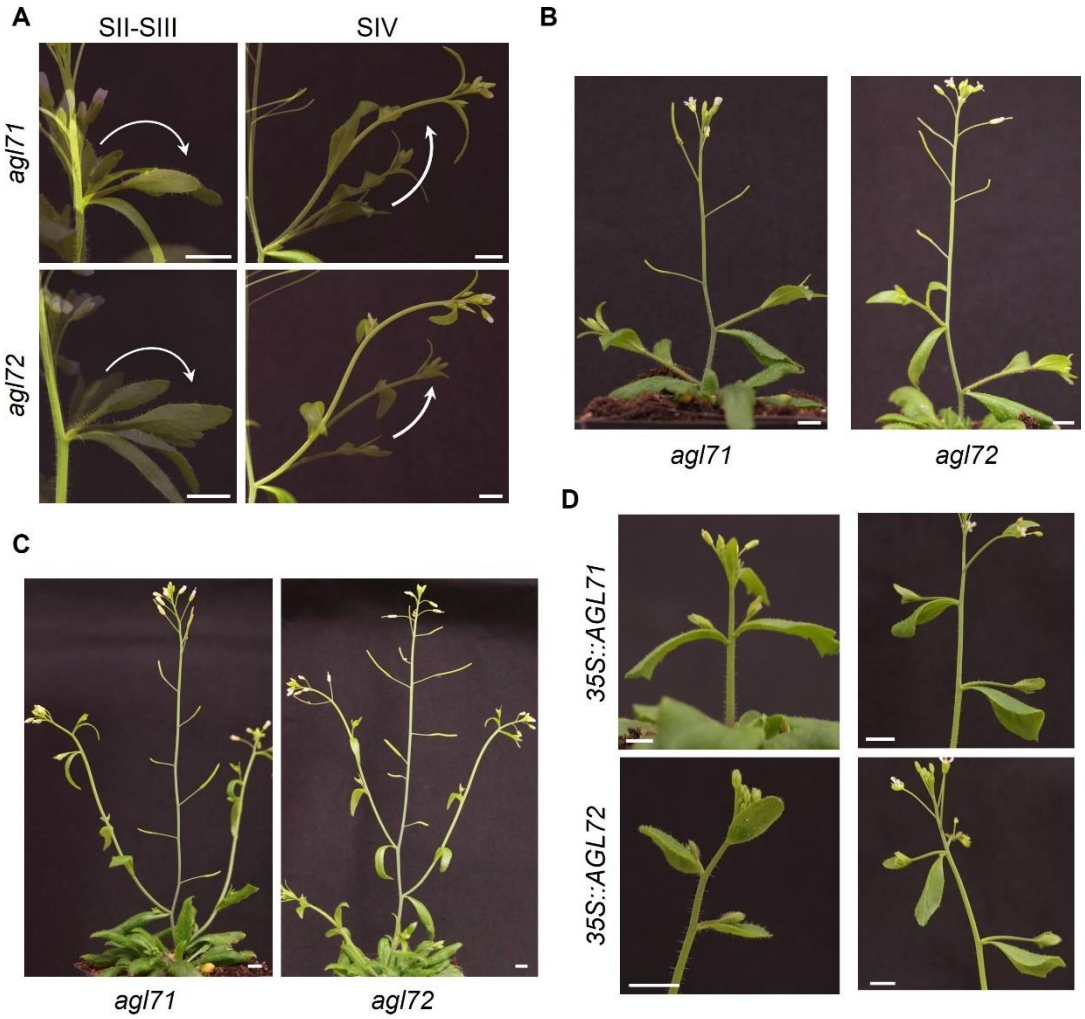

Figure 5.8: Role of AGL71 and AGL72 in lateral shoot development

A) Representative images of SII-SIII and SIV lateral shoots. Images are obtained by overlaying three pictures taken 24 hours from each other. White arrows indicate the direction of growth. B) Representative images of *agl71* and *agl72* at SIII to SIV transition. C) Representative images of ~28 days-old *agl71* and *agl72* plants. D) Representative images of SII-SIII lateral shoots of *35S::AGL71* and *35S::AGL72*. Scale bars = 0.5 cm.

In addition to the analysis loss-of-function mutants, *AGL71*, *AGL72* and *TCP1* overexpression lines were generated using the *CaMV 35S* constitutive promoter (*35S*), and the phenotype of T_1 (transformed) plants was analysed. *AGL71* and *AGL71* overexpression do not cause any particular phenotype during lateral shoot development (Fig. 5.8 D and 5.9 B). In *35S::ALG71* and *35S::AGL72* the rootward growth during SII is maintained and the GSA is set normally (Fig. 5.8 D and 5.9 B). Conversely, overexpression of *TCP1* causes a plethora of phenotypes across the shoot (Fig. 5.9 A-D). Independent T_1 lines show variable leaf and inflorescence morphologies, most likely due to different levels of *TCP1* overexpression. *35S::TCP1* rosette is overall smaller than wt, with some lines showing cup-shaped cauline leaves, and others showing leaves with elongated morphology and absence of a defined petiole (Fig. 5.9 A). The less morphologically impaired *TCP1* overexpression lines show normal shoot phenotype and set more vertical GSAs than wt (Fig. 5.9 B). Similarly, lines showing strong morphological impairments show very vertical SIV lateral shoots and a complete suppression of SII-SIII rootward growth (Fig. 5.9 C and D). Taken together the changes of *AGL71* and *AGL72* expression in *arf4ett-3* and the phenotypes shown by loss of function and overexpressing lines demonstrate a role of *TCP1*, *AGL71* and *AGL72* in lateral shoot development.

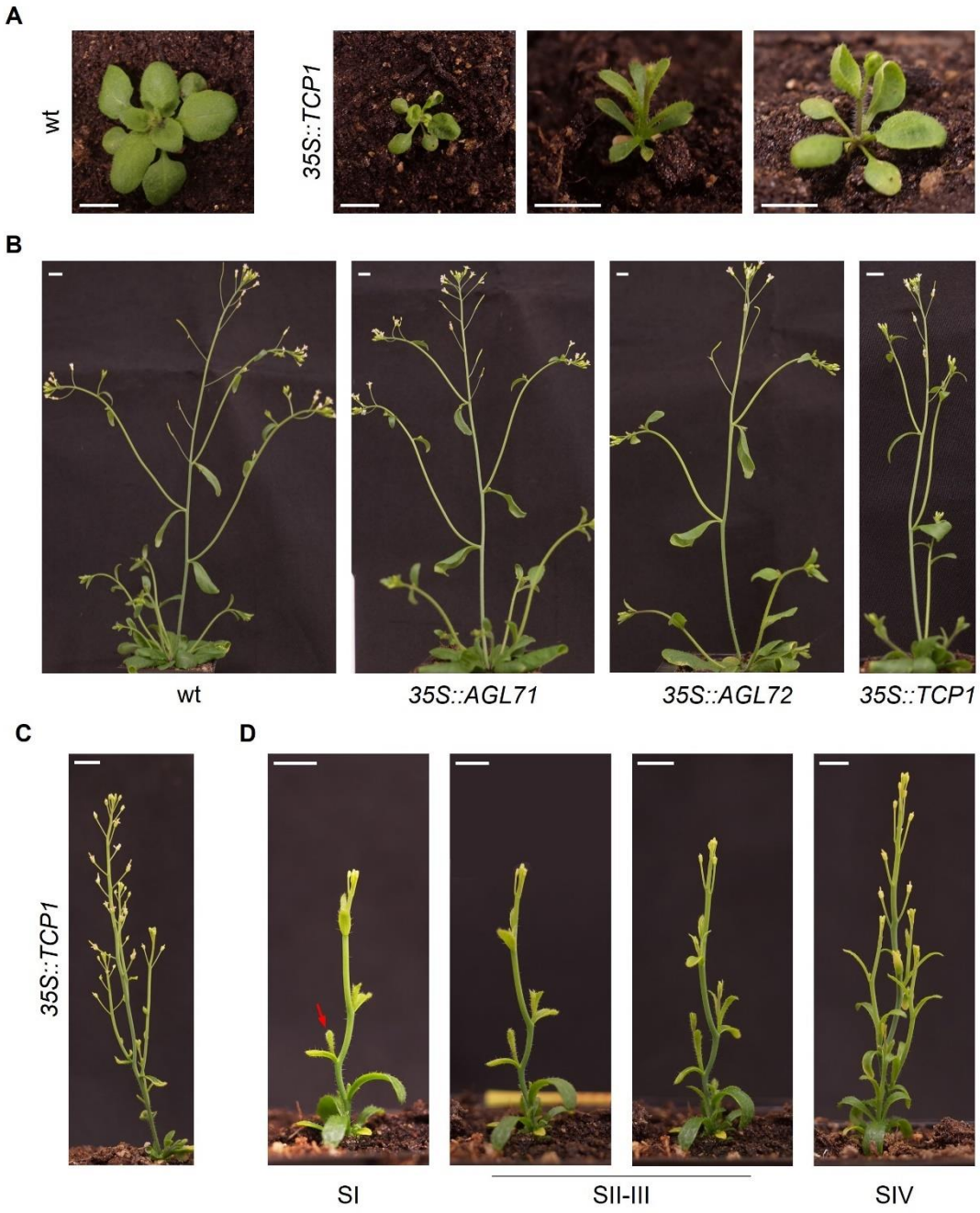

Figure 5.9: Analysis of *AGL71*, *AGL72* and *TCP1* overexpressing lines

A) Representative images of wt (Col) and three independent *35S::TCP1* T_1 lines at rosette stage and after bolting. B-D) Representative images of ~28 days old wt and 35S::*AGL71*, 35S::*AGL72* and a *TCP1* overexpressing lines with mild (B) and strong (C) phenotype. D) Representative images of lateral shoot development of one of the *TCP1* overexpressing line showing strong shoot phenotype. Red arrow indicates SI lateral shoot. Scale bars = 0.5 cm.

Discussion

Lateral shoot growth and behaviour during the early phase of development can be explained by the existence of an ad-abaxial identity developmentally set during the branch formation. Similarly to other organs such as leaves, in which the establishment of the ad-abaxial polarity is critical for the organ function, in lateral shoots the differences generated between the adaxial and abaxial side are crucial to induce the first branch elongation away from the primary shoot. The importance of branches spreading away from the plant main axis is demonstrated by the dominant effect that SII-SIII rootward growth exerts on the gravitropic response, preventing gravity-induced tropic growth to influence the young lateral shoot growth angle. The data I presented here lay the groundwork necessary to characterise the biophysical and molecular mechanisms behind the establishment of ad-abaxial polarity at the basis of lateral shoot early development.

Transition from cell proliferation to cell elongation characterises the shift from lateral shoot early to late development

The low level of differentiation along the proximal-distal axis of SII and SIII lateral shoots, together with cyclins B1 and D3 expression data demonstrate that, during early development, lateral shoot cells are still dividing. Cell elongation and differentiation, instead, start to become visible only at the proximal end of branches entering SIII. The differences observed in cell number between adaxial and abaxial side, and the absence of an evident asymmetry in cyclins expression, suggest the existence of an asymmetry in the rate of cell division along the ad-abaxial axis, rather than differences in the duration of cell proliferation between the two sides. Due to the heterogeneity of cell elongation in SIII epidermis, cell length measurements show a high degree of variation, making it difficult to estimate a possible asymmetry along the ad-abaxial axis. For this reason, the possible involvement of cell elongation in lateral shoot early development cannot be completely excluded. Integrating the observation presented here with the results discussed in the previous chapter, I propose two possible models to explain lateral shoot progression from early to late development (Fig. 5.10). In the first model, cell proliferation asymmetry is the sole mechanism driving the early phase of development. Differences in cell proliferation rate determines the adaxial side to produce more cells than the abaxial side, driving the early rootward growth observed at the start of SII. As the lateral shoot progresses to SIII, older cells

at the proximal end of the branch start to exit the cell cycle and begin to elongate. In this model cell elongation happens symmetrically across the branch but, due to the asymmetry in cell number set early on in development, it contributes to generate more overall growth on the adaxial side, driving the final rootward growth that marks the transition from SII to SIII. As cell division is turned off during SIII, cell elongation become the sole mean of growth at the proximal end of the branch. This marks the end of the early phase and the progression to the GSA setting. Gravity-dependent control of cell elongation, mediated by auxin, determines cells at the lower side to elongate more than the upper side, inducing the upward growth that shift SIII growth angles to SIV GSAs (Fig. 5.10). Once the GSA is reached, auxin symmetric distribution between the upper and lower side, controlled respectively by the AGO and the gravitropic response, determines the stable non-vertical growth shown by SIV lateral shoots. The early process at the basis of what I named “SII-growth” is rooted in the control of cell proliferation between the adaxial and abaxial side of young lateral shoots, and determines the impossibility for the gravitropic response to elicit any changes in the shoot growth angle along the ad-abaxial axis before this developmental phase is concluded. Alternatively, the rootward growth shown in early development can be the result of asymmetry in both cell proliferation and elongation between the adaxial and abaxial side of young lateral shoots (Fig. 5.10). In this second model, early and late (GSA-dependent) cell elongations are regulated by different factors with spatiotemporal expression over development. Regardless, in both models the high variation of cell length observed in adjacent cells suggests that cell elongation induction, and perhaps cell growth rate, are not synchronised events among neighbouring cells. This could be related to cell-specific dilution, accumulation and/or degradation of factors controlling the transition from cell division to cell expansion, determining some cells to exit the cell cycle while contiguous cells are still dividing (Jones, Band and Murray, 2019; D’Ario *et al.*, 2021). Both models can also explain the behaviour of lateral shoots developing under clinorotation. Here, although the duration of the early phase is extended, the shift from cell division (and early cell growth) to gravity-dependent cell elongation is responsible to terminate the branch rootward growth and, in absence of a stable reference to gravity, determines lateral shoots to straighten under the control of proprioception.

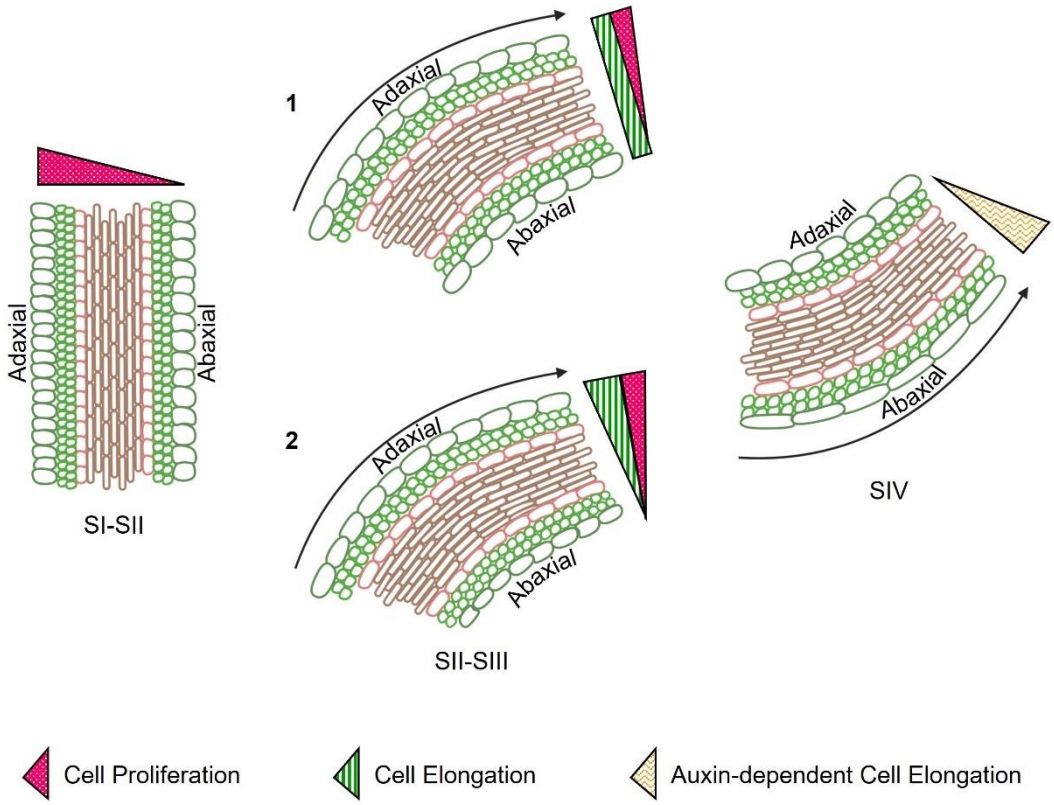

Figure 5.10: Two possible models explain lateral shoot development

Schematization of cell proliferation and cell elongation along the ad-abaxial axis during lateral shoot development. Triangles indicate the magnitude of the processes, black arrows indicate the direction of growth. After cell proliferation differences set in SI and early SII, two models are proposed to explain the subsequent rootward growth shown during SII-SIII progression. In (1) differences in cell proliferation are retained at the adaxial side while cell elongation happens symmetrically across the branch. In (2) both cell proliferation and elongation are higher at the adaxial side compared to the abaxial side. Regardless of the model, during SIV progression auxin drives cell elongation at the lower (abaxial) side of the lateral shoot and determines the setting of the GSA.

In addition to cell elongation mediated by turgor pressure and cytoplasmic growth, it has been suggested that cells can expand via endoreduplication, a mechanism in which genome duplication during cell cycle is not followed by mitosis, leading to the generation of polyploid cells. Endoreplication has been proposed to mediate cell growth in the epidermis layer of leaves and to offer a compensatory mechanism to control cell size when other cell growth processes are impaired (Dewitte *et al.*, 2007; Moreno *et al.*, 2020). Recently it has also been shown that endoreduplication participates to the auxin-mediated differential growth between the inner and outer side of the apical hook in hypocotyls, and to be required for maintaining this protective structure (Ma *et al.*, 2022). However, it is still not clear how endoreduplication influences cell size and if there is a proportional relationship between cell ploidy and size (Tsukaya, 2019). Nevertheless, it is not currently known if endoreduplication is present in epidermis cell of lateral shoots. Further analyses are needed to investigate this mechanism in branches, and determine if cell elongation happens symmetrically along the ad-abaxial axis or differential cell growth contributes to the spreading behaviour of young lateral shoots during early development.

Finally, the analysis of *CYCD3* expression across the shoot demonstrates a systemic control of cell proliferation during branch outgrowth. *CYCD3* expression reflects the acropetal direction of branch growth, with branches positioned at the base of the primary shoot expressing higher levels of *CYCD3* and elongating before branches near the primary apex. This pattern of growth is mediated by the primary shoot inhibition of branch development, a mechanism called apical dominance (Kebrom, 2017). The observations presented here indicate that cell cycle mediated by CYCD3 is under the apical dominance control, which suppresses the growth of apically positioned lateral shoots. As the primary stem elongates, distance between the branches and the primary apex increases, leading to the release of the growth inhibition over apically positioned branches. This determines the reactivation of *CYCD3* expression that in turns induces cell proliferation leading to the branch outgrowth.

The role of CK and auxin signalling during lateral shoot early development

The phenotypes shown by *ipt357* and *arf4ett-3* during early development demonstrate that CK and auxin signalling are likely involved in early lateral shoot growth. The reduced asymmetry in cell proliferation of *ipt357* suggests

that CK mediate cell division across the branch, possibly through the induction of *CYCD3* and other cell cycle regulators expression (Dewitte *et al.*, 2007). Although AHK double loss-of-function and gain-of-function mutants do not show impairments in lateral shoot development, transcriptomic data obtained in this project show that *AHK2, AHK3* and *AHK4* are all expressed across the branch, together with their targets *HISTIDINE-CONTAINING PHOSPHOTRANSMITTER 2* (*AHP2*), *AHP3* and *AHP5* (Table 7.3). Upon CK binding, AHK receptors phosphorylate AHP proteins, inducing their translocation to the nucleus where they activate CK-responsive transcription factors (Hwang, Sheen and Müller, 2012). On the other hand, genes responsible for CK biosynthesis are not expressed in the stem of young lateral shoots, suggesting that to regulate cell proliferation CK is transported to the branch rather than synthetised on site. In addition, redundancy of *AHK* genes in controlling shoot development could be responsible for the lack of phenotypes shown by *ahk* mutants.

Transcriptomic data also confirmed that *ARF4* and *ETT* are both expressed at high levels in SII branches (Table 7.3). Although their transcription is not polarised along the ad-abaxial axis, the misregulation of *AGL71* and *AGL72* expression in *arf4ett-3* mutant suggest a role of these two auxin responsive factors in the abaxial identity of young lateral shoots. In addition, the phenotype shown by *arf4ett-3* points to a possible alteration of the ratio of cell division and/or cell elongation between the adaxial and abaxial side. The transcriptomic analysis performed in this project did not include the floral meristem from which the stem originates. Asymmetry in cell number could be initiated at the meristem and then maintained during the early phase of stem development. This would determine the differential expression of polarity-setting factors along the ad-abaxial axis in the meristem (and/or in the region of the stem adjacent to it) that was not captured by the transcriptomic analysis of SII lateral stems. Furthermore, many other *ARFs* are expressed across SII branches, together with some *IAA* genes, demonstrating the overall importance of auxin signalling during branch development (Table 7.3). However, which role auxin signalling might have in the establishment of ad-abaxial polarity and early development remains an open question. Further analyses are needed to understand if auxin participate to the differential cell division and/or early cell elongation across the branch. In addition to this, other hormones such as GA and BR could be involved in regulating cell growth during the early phase, as TCP1 has already been linked to BR biosynthesis

and transcriptomic analysis presented here also revealed adaxial expression of the sucrose/GA transporters SWEET13 (Table 7.2) (Guo *et al.*, 2010; Kanno *et al.*, 2016).

The role of *TCP1, AGL71* and *AGL72* in lateral shoot development

Based on the transcriptomic data presented here, not many genes are differentially expressed between the adaxial and abaxial side of young lateral shoots. Differently from leaves, the adaxial and abaxial side of shoot branches do not show different cell composition, therefore it can be hypothesised that factors involved in cell differentiation act symmetrically at the two sides of the branch. This would explain the low number of differentially expressed genes observed in the transcriptomic data. Based on the analysis of cell number and length, factors involved in cell proliferation and/or early cell elongation, instead, are expected to be differentially expressed between the adaxial and abaxial side. *TCP1*, *AGL71* and *AGL72*, being the most significantly differentially expressed genes, are interesting to investigate as possible regulators of the ad-abaxial polarity in young lateral shoots. TCP1 has already been proposed to regulate both cell proliferation and expansion in other plant organs, such as leaves and flowers (Busch and Zachgo, 2007; Koyama, Sato and Ohme-Takagi, 2010; Busch, Horn and Zachgo, 2014). Knock-down mutants of *TCP1* generated using artificial microRNA have been reported to have no obvious phenotype in the adult plant (Guo *et al.*, 2010), suggesting that, although adaxially expressed also during SIV, this transcription factor might not be involved in SIV GSA setting. As in the case of *arf4ett3*, the absence of a phenotype during SIV does not exclude the existence of possible impairments in the mutants during branch early development. Unfortunately, no loss-of-function mutants of *TCP1* were publicly available to analyse. For this reason, using Crispr-Cas9 gene editing strategy, I generated transgenic lines targeting *TCP1* genomic sequence to produce *tcp1* knock-out mutants. The analysis of these mutants will hopefully help us to better understand the role of TCP1 during early development. Meanwhile, some information on TCP1 activity can be gathered from the observation of the overexpressing lines. The variable phenotypes produced by *TCP1* overexpression suggest a dose-dependent activity of the protein. The reduced size of the most impaired transgenic plants indicates possible defects in either cell proliferation or cell elongation. In addition, these lines shown alteration of lateral shoot growth during both early and late development, demonstrating that whatever mechanism TCP1 is regulating, its misregulation can also influence the setting

of the GSA. The quantification of *TCP1* expression levels, together with the analysis of cell size and number in the overexpressing lines will elucidate TCP1 role in the establishment of the adaxial identity in lateral shoots. Conversely to *TCP1*, *AGL71* and *AGL72* overexpression do not cause any obvious phenotype during branch development, while *agl71* and *agl72* single mutants only show a mild phenotype during the transition between SIII and SIV. However, the impaired expression of *AGL71* and *AGL72* in *arf4ett-3* suggests a role of these two MADs-box factors in branch abaxial specification. Interestingly *AGL72* does not seem to maintain its abaxial expression during SIV, pointing out a possible change in its role at later stages of branch development. AGL71 and AGL72 redundancy, already shown in their regulation of flowering transition (Dorca-Fornell *et al.*, 2011), could be the cause of the lack of phenotypes in both overexpressing lines and single mutants. Analysis of *agl71agl72* double mutants will confirm if indeed the two factors are redundantly involved in the abaxial identity of lateral shoots. In addition to this, to gather more information about the role of all three transcription factors, I generated transgenic lines expressing *TCP1* coding sequence under the control of *AGL71* promoter, and *AGL71* and *AGL72* coding sequences under the control of *TCP1* promoter. Swapping the ad-abaxial patterns of these transcription factors hopefully will not strongly impair the whole shoot (as in the case of *TCP1* overexpression), and will help us to determine the roles and importance of these factors in driving lateral shoot early growth through the setting of the adaxial and abaxial polarity.

Chapter 6. General discussion

The identification of novel regulators of lateral shoot and root growth angles offers the opportunity to discover new targets for future crop improvement. The control of lateral root growth angles, for example, has been proposed to influence drought tolerance of various crop species, such as wheat and maize, while lateral shoot growing habit is strongly connected with planting strategies (Wasson *et al.*, 2012; Comas *et al.*, 2013; Carriedo, Maloof and Brady, 2016; Hill and Hollender, 2019). For instance, lateral shoot growth angles of orchard trees highly influence planting density. While in crops grown at high density, branching can increase plant shading inducing shade avoidance syndrome (SAS) (Carriedo, Maloof and Brady, 2016; Hill and Hollender, 2019). SAS leads to a series of phenotypes, among which reduced branching, that can highly impact crop productivity (Carriedo, Maloof and Brady, 2016). For these reasons, my work is part of a bigger research effort to build a comprehensive understanding of the molecular control of plant architecture that will not only present opportunities to enhance crop resilience to environmental stresses, but will also provide new potential molecular targets to improve management practices of agronomically important species to increase yield adopting more sustainable planting strategies.

Alterations of membrane trafficking can offer new ways to modulate GSA in lateral roots

PIN protein localisation during both normal and tropic growth strongly depends on membrane trafficking (Rahman *et al.*, 2010; Rakusová *et al.*, 2011; Doyle, Haeger, Vain, Rigal, Viotti, Łangowska, Ma, Friml, N. V. Raikhel, *et al.*, 2015). In lateral roots, GSA maintenance has been proposed to solely rely on PIN-mediated auxin export from the columella cells (Roychoudhry *et al.*, 2019). In line with this, auxin's ability to modulate lateral root GSAs has been shown to depend on the columella-specific RCN1 control of PIN3 localization, through dephosphorylation of its cytoplasmic loop (Roychoudhry *et al.*, 2019). With my work I identified two novel uncharacterized factors, MAP70-2 and C2DP, involved in lateral root GSA control in antagonism to RCN1 and proposed to participate in membrane trafficking. The loss-of-function of these two factors alters lateral root GSA without impairing neither the overall root growth nor other processes in the plant, demonstrating their specificity in regulating lateral root GSAs. Due to their putative activity in membrane trafficking, it can be hypothesized that MAP70-2 and C2DP are involved downstream of PIN

phospho- and dephosphorylation by the action, respectively, of kinases and phosphatases (among which RCN1), and mediate PIN cycling between the plasma membrane and the endosomal compartments. Similarly to the proposed role of RLD and LZY proteins in determining PIN3 polarization in the direction of statolith sedimentation, MAP70-2 and C2DP activity might influence PIN3 and/or PIN7 polarity at the upper side of the columella cells. If these two factors are indeed involved in PIN localization, their loss of function does not determine a complete abolishment of auxin transport at the upper side of the root, as both mutants respond to gravistimulation in upward- and downward-bending lateral roots. This might be caused by MAP70-2 and C2DP regulation of just one of the two PINs, determining a reduction rather than a suppression of auxin transport. In addition, other trafficking factors might act redundantly with MAP70-2 and C2DP, determining the resilience of the system in the absence of either regulators. Regardless of the specific mode of action of MAP70-2 and C2DP, the identification of these two new factors determines the exciting prospective of new ways to modulate lateral root GSAs by tweaking the activity of specific factors involved in membrane trafficking, without causing strong off-target phenotypes in other regions of the plant. Although it is still early to tell how conserved and important these novel factors are outside Arabidopsis, this work has indeed advanced our knowledge on the overall understanding of lateral root GSA maintenance.

Growth angle control in lateral shoots involves more than the GSA setting

Differently from lateral roots, where a careful analysis and classification of all stages of development have long been established (Guyomarc'h *et al.*, 2012; Rosquete *et al.*, 2013), in Arabidopsis not every stage of lateral shoot development has been described. For this reason, the phenotypical characterization of the whole lateral shoot development, and the identification of the molecular factors involved in the early phase of growth, carried out during my work, have paved the way to fill this gap in our knowledge. During early development, branches grow away from the primary axis and determine a newly discovered way of branching out independently from the gravity-set GSA. Investigating the biophysical and molecular basis of this early growth is particularly important to expand our understanding of growth angles set without the gravitropic input. The role of cell proliferation during the early phase shares similarities with leaf early development, where different rates of cell division along the ad-abaxial axis determine the leaf to grow away from

the shoot apical meristem (Manuela and Xu, 2020). This suggests a conserved role of cell proliferation during the early spreading of lateral organs. It would be interesting to see if this model of growth is conserved across other organs, such as pedicels, and other species. In addition to this, the phenotype shown by *arf4ett-3* suggests that cell elongation during GSA setting can balance out the possible growth impairments happening along the ad-abaxial axis early on in development, enabling lateral shoots to retain a normal GSA. Similarly, in leaves higher levels of cell expansion can offset impairments in cell proliferation during development, demonstrating the resilience of this growth system (Dewitte *et al.*, 2007). However, the altered phenotypes in both early and late development of *ipt357* and *35S::TCP1* lateral shoots suggest that a possible systemic misregulation of cell proliferation and/or early growth can as well impact the GSA setting. In conclusion, the foundation I laid with my work will help understand the molecular mechanisms behind gravity-independent growth angles in Arabidopsis, and offers the opportunity to build a general growth model for the emergence of lateral organs across different species.

Differences between lateral root and shoot growth angle control

Previous studies in Arabidopsis demonstrated that lateral shoots maintain their GSAs similarly to SIII-SIV lateral roots (Roychoudhry *et al.*, 2013, 2019). Lateral roots emerge perpendicularly to the primary root, with an angle of ~90°, and progressively grow rootward until they set their given GSA in SIII (Guyomarc'h *et al.*, 2012). Interestingly, this progression from early angles to the GSA happens as the columella differentiates and statoliths start to sediment towards the direction of gravity (Guyomarc'h *et al.*, 2012). Lateral shoots do not have such direct relationship between a functioning gravity-sensing tissue and the setting of the GSA, as the GSA is not immediately set following the differentiation of the endodermis. The establishment of the early phase during lateral shoot development pushes back the setting of the GSA and decouples it from the organ acquisition of gravicompetence. Another interesting difference between lateral roots and shoots is the position of emersion with respect to the primary axis. As mentioned above, lateral roots emerge perpendicularly to the primary root, a position that already secures their growing away from the primary axis. Conversely, lateral shoots emerge adjacent and parallel to the primary shoot. Therefore, to spread away from the main axis, lateral shoots must grow rootward as they elongate, changing their growth angle independently from gravity. This could be the reason why lateral

shoots have maintained or evolved both an upper-lower polarity with respect to gravity and an ad-abaxial polarity with respect to the primary shoot, while lateral roots seem to rely only on the former and lack the latter. In addition, the perception of gravity in roots and shoots is substantially different. The columella is made by a small pool of cells placed at the root tip, restricting the perception of gravity to the terminal end of lateral roots. On the other hand, gravity perception above ground happens across the entire stem, as statoliths develop in the endodermis layer. This determines a more complex control of the stem position with respect to gravity, as the final GSA is determined by the integration of the gravitropic and antigravitropic responses at every point along the stem. Finally, as gravitropism (and consequently the GSA setting) has evolved during plant colonization of land, with seed plants showing the most efficient ways to quickly adjust their position with respect to gravity (Zhang *et al.*, 2019), it would be interesting to investigate how the gravity-independent growth angle control has evolved in relationship with the GSA setting.

Conclusions

In conclusion, my results show a potentially new way to control lateral root growth angles based on the regulation of membrane trafficking factors working at the upper side of the columella cells, and define a new gravity-independent mechanism behind lateral shoot development. Better characterising these two processes in Arabidopsis and other species, especially agronomically important crops, can potentially offer new ways to develop plants more resilient to drought stress and plants that can be adopted for more sustainable growing models through the increase of planting density without loss of productivity. In a future where 60% more food will need to be produced to support the growing global population, while the rise of extreme weather conditions caused by climate change is predicted to increasingly impact food security (Alexandratos and Bruinsma J., 2012; United Nations, 2015), developing new methods to control plant architecture can offer powerful tools to prepare the agricultural system to the challenges ahead.

Chapter 7. Appendix

Table 7.1: List of candidate genes containing SNPs in *rcn1sor* mutants

rcn1sor1		
Gene ID	Type of mutation	aa change
AT2G16225	start loss	p.Met1?
AT1G05490	splice donor v	/
AT1G09930	stop codon gain	p.Trp184*
AT1G30510	splice donor v	/
AT1G01600	missense	p.Ala59Val
AT1G02475	missense	p.Ala92Thr
AT1G10760	missense	p.Gly699Glu
AT1G14630	missense	p.Pro183Leu
AT1G15660	missense	p.Leu246Phe
AT1G17690	missense	p.Arg474Gln
AT1G19220	missense	p.Arg820Lys
AT1G19220	missense	p.Arg789His
AT1G19880	missense	p.Ser473Asn
AT1G21400	missense	p.Arg28Cys
AT1G22370	missense	p.Asp126Asn
AT1G24764	missense	p.Arg194Gln
AT1G29300	missense	p.Gly416Ser
AT1G29750	missense	p.Gly440Glu
AT1G31040	missense	p.Glu168Lys
AT1G33612	missense	p.Gly343Arg
AT1G48120	missense	p.Ala409Val
AT1G49520	missense	p.Glu70Lys
AT1G60140	missense	p.Leu836Phe
AT3G24780	missense	p.Arg189His
AT4G09830	missense	p.Pro101Ser
AT4G11440	missense	p.Leu59Phe
AT4G14180	missense	p.Val496Ile
AT1G26330	missense	p.Thr592Ile
AT1G27680	missense	p.Pro367Ser
AT1G42710	missense	p.Ala179Val
AT1G58100	missense	p.Ala244Val
AT2G31890	missense	p.Thr18Ile
AT2G39782	missense	p.Gly70Asp
AT4G14050	missense	p.Glu513Lys
AT1G11755	missense	p.Glu143Lys
AT1G31290	missense	p.Thr581Ile
AT1G32810	missense	p.Asp528Asn
AT3G46230	missense	p.Val152Ile
AT2G43650	missense	p.Ala275Thr
AT5G25230	missense	p.Arg508His

AT5G25230	missense	p.Gly511Arg
rcn1sor2		
Gene ID	Type of mutation	aa change
AT1G63420	missense	p.Arg305Lys
AT5G04050	missense	p.Ser341Leu
AT5G28919	missense	p.Arg158Cys
AT5G38190	missense	p.Thr78Thr
AT1G73330	missense	p.Glu183Lys
AT5G41070	missense	p.Gly305Arg
AT1G61120	missense	p.Pro864Leu

rcn1sor3

Gene ID	Type of mutation	aa change
AT2G41110	splice donor var	/
AT1G52500	stop codon gain	p.Gln310*
AT1G09930	stop codon gain	p.Trp184*
AT1G52290	splice acceptor v	/
AT4G19130	stop codon gain	p.Gln29*
AT1G04400	missense	p.Gly30Glu
AT1G34340	missense	p.Pro67Ser
AT1G66050	missense	p.Asp471Asn
AT1G68980	missense	p.Gly237Arg
AT1G37130	missense	p.Leu114Phe
AT1G31740	missense	p.Glu772Lys
AT1G30330	missense	p.Ala895Thr
AT1G17147	missense	p.Ala39Thr
AT1G22440	missense	p.Ala164Val
AT1G30700	missense	p.Pro279Leu
AT1G24070	missense	p.Gly195Asp
AT1G38131	missense	p.Ala341Thr
AT1G09720	missense	p.Ala791Thr
AT1G30490	missense	p.Ala486Thr
AT1G50120	missense	p.Ala160Thr
AT1G37000	missense	p.Leu126Phe
AT1G44910	missense	p.Ala558Val
AT1G47310	missense	p.Pro264Ser
AT1G20240	missense	p.Asp128Asn
AT1G21010	missense	p.Ala47Val
AT1G18460	missense	p.Pro124Leu
AT1G36925	missense	p.Val33Ile
AT1G53645	missense	p.Ala57Thr
AT1G20000	missense	p.Glu128Lys
AT1G49340	missense	p.Thr1811Ile
AT1G58260	missense	p.Val47Ile
AT2G44650	missense	p.His28Tyr

AT2G44180	missense	p.Gly12Glu
AT2G39340	missense	p.Val823Ile
AT2G05330	missense	p.Ser203Asn
AT2G31320	missense	p.Ala2Thr
AT2G05250	missense	p.Ala387Thr
AT2G02840	missense	p.Thr61Met
AT2G05120	missense	p.Arg438Lys
AT2G42510	missense	p.Gly14Glu
AT2G02680	missense	p.Glu52Lys
AT2G36360	missense	p.Val348Ile
AT2G04495	missense	p.Asp155Asn
AT2G39782	missense	p.Gly70Asp
AT3G29060	missense	p.Ala724Val
AT3G57410	missense	p.Ala458Thr
AT3G06030	missense	p.Pro596Leu
AT3G13410	missense	p.Ala18Val
AT3G05430	missense	p.Pro426Ser
AT3G10670	missense	p.Ser23Phe
AT3G14620	missense	p.Leu56Phe
AT3G47760	missense	p.Ser661Phe
AT3G16175	missense	p.Glu24Lys
AT3G18282	missense	p.Pro42Ser
AT3G10820	missense	p.Asp268Asn
AT3G27530	missense	p.Met508Ile
AT4G21820	missense	p.Ala12Val
AT4G34550	missense	p.Val140Ile
AT4G30460	missense	p.Ala91Val
AT4G13750	missense	p.Ala994Thr
AT4G16100	missense	p.Ser322Asn
AT4G15090	missense	p.Thr465Met
AT4G18020	missense	p.Ser432Asn
AT4G13750	missense	p.Gly1012Asp
AT4G29900	missense	p.Pro443Leu
AT4G01660	missense	p.Val94Ile
AT4G24000	missense	p.Arg656Cys
AT4G32750	missense	p.Ala218Val

rcn1sor4

Gene ID	Type of mutation	aa change
AT3G25160	stop codon gain	p.Arg18*
AT3G50950	stop codon gain	p.Trp96*
AT3G18370	splice donor var	/
AT1G68980	missense	p.Gly237Arg
AT3G19170	missense	p.Pro623Leu
AT4G36830	missense	p.Ser14Phe
AT2G28890	missense	p.Thr385Met

AT3G20015	missense	p.Thr216Met
AT1G77310	missense	p.Ala620Thr
AT1G28440	missense	p.Ser778Asn
AT3G26730	missense	p.Gly547Glu
AT3G19720	missense	p.Thr482Ile
AT3G44050	missense	p.Ala164Thr
AT4G39900	missense	p.Arg197Lys
AT2G30090	missense	p.Pro282Ser
AT4G11550	missense	p.Ala219Val
AT4G39800	missense	p.Arg398Gln

Table 7.2: List of significant differentially expressed genes in SII lateral shoots

Gene ID	Log2FoldChange	p-adjusted value	Gene info
AT1G03495	-1.615910948	5.64E-15	HXXXD-type acyl-transferase family protein
AT1G03940	-1.166501019	3.84E-10	HXXXD-type acyl-transferase family protein
AT1G04660	1.185598105	1.62E-08	glycine-rich protein
AT1G05680	-1.576872229	1.43E-05	UGT74E2 - UDP-glucosyltransferase (auxin homeostasis)
AT1G07450	-1.197071999	0.046046239	NAD(P)-binding Rossmann-fold superfamily protein
AT1G09500	-1.72902745	0.003174817	Similar to Eucalyptus gunnii alcohol dehydrogenase of unknown physiological function
AT1G13650	-1.299108814	0.005067024	hypothetical protein

AT1G19790	3.718685326	0.000613357	SRS7 - SHI gene family
AT1G45191	-1.239853828	0.003009525	BGLU1 - beta-glucosidase
AT1G64780	1.268597395	0.035767003	AMT1-2 - ammonium transporter
AT1G65880	-2.518651325	0.003673127	AAE20 - benzoate-CoA ligase
AT1G66390	-2.351410614	0.000161662	MYB90 - Production of anthocyanin pigment 2 protein (PAP2)
AT1G66540	-1.685188356	0.037594355	Cytochrome P450 superfamily protein
AT1G67260	-2.827358463	3.28E-150	TCP1 - TB1,CYC,PCF family
AT1G68500	-1.46538539	0.019607261	hypothetical protein
AT1G69260	1.562649224	0.021037857	AFP1 - ABI five binding protein
AT2G24210	1.589897562	0.000322084	TPS10 - terpene synthase 10
AT2G25810	1.965648132	0.015629206	TIP4-1 - tonoplast intrinsic protein 4
AT2G29090	-2.036619848	0.035835628	CYP707A2 - ABA catabolism
AT2G33420	2.913518791	0.020757882	CELLULOSE-RELATED DUF810
AT2G38210	-1.528929671	0.044624296	PDX1L4 - putative PDX1-like protein 4
AT3G05160	1.122416935	0.001177013	Major facilitator superfamily protein

AT3G22840	-3.096924962	2.29E-05	ELIP1 - early light-inducible protein
AT3G24460	1.009505796	0.031927594	Serinc-domain containing serine and sphingolipid biosynthesis protein
AT3G29590	-1.876060224	5.51E-07	5MAT - malonyl-CoA:anthocyanidin 5-O-glucoside-6"-O-malonyltransferase
AT4G08870	2.030462148	0.025814434	ARGAH2 - arginase
AT4G09820	-1.329294668	0.000221903	TT8 - regulation factor in flavonoid pathway
AT4G10380	1.56455199	0.002793133	NIP5-1 - Boric acid channel
AT4G11310	1.68067065	0.041782627	ATCP1 - cysteine proteinase precursor-like protein
AT4G14090	-1.669369868	4.97E-25	encodes a anthocyanidin 5-O-glucosyltransferase specifically glucosylating the 5-position of the flavonoid A-ring.
AT4G14365	1.278783296	0.040558806	XBAT34 - hypothetical protein
AT4G14690	-1.828092601	1.83E-13	ELIP2 - early light-induced protein
AT4G15620	1.220508916	0.035835628	CASP-LIKE PROTEIN 1E2 - Uncharacterized protein family

AT4G22880	-2.166080362	3.71E-38	LDOX - leucoanthocyanidin dioxygenase
AT4G25420	-1.17462382	0.000607014	GA20OX1 - GA biosynthesis
AT4G27830	-1.157860678	7.65E-18	BGLU10 - beta-glucosidase
AT4G30250	2.082068162	0.024961166	P-loop containing nucleoside triphosphate hydrolases superfamily protein
AT4G30460	1.006450687	0.034798351	glycine-rich protein
AT4G31610	3.377067444	0.001357226	REM1 - Reproductive Meristem 1
AT5G01870	-1.150097742	0.00037291	LTP10 - Predicted to encode a PR (pathogenesis-related) protein
AT5G04770	-1.763696624	0.001582209	CAT6 - cationic amino acid transporter
AT5G06570	-1.563694549	6.62E-05	alpha/beta-Hydrolases superfamily protein
AT5G07990	-1.887825379	1.07E-27	CYP75B1 - Required for flavonoid 3' hydroxylase activity
AT5G12330	2.71349687	0.002906588	LRP1 – SHI family
AT5G17220	-1.872733427	1.46E-27	GSTF12 - glutathione transferase

AT5G19100	-1.583293786	0.014631012	Eukaryotic aspartyl protease family protein
AT5G20110	-1.322360103	0.049670633	Dynein light chain type 1 family protein
AT5G24570	-2.079360716	1.46E-05	hypothetical protein
AT5G37550	-1.581856059	0.041133745	hypothetical protein
AT5G37970	2.178997749	0.045471223	SABATH family methyltransferase.
AT5G42800	-2.513676454	8.73E-26	DFRA - dihydroflavonol reductase
AT5G44050	1.30917572	0.04961085	DTX28 - MATE efflux family protein
AT5G50800	-1.964433087	1.25E-08	SWEET13 - sucrose channel
AT5G51860	4.833851462	5.03E-57	AGL72 - MADS-box transcription factor
AT5G51870	2.515800245	7.64E-62	AGL71 - MADS-box transcription factor
AT5G54060	-1.371853103	1.83E-23	A3G2XYLT - anthocyanin 3-O-glucoside
AT5G55450	2.076711585	0.003412738	Bifunctional inhibitor/lipid-transfer protein/seed storage 2S albumin superfamily protein
AT5G55570	-1.428279698	0.007787626	transmembrane protein
AT5G57785	3.601471175	0.003440286	hypothetical protein

AT5G61290	1.42582172	0.031583272	Flavin-binding monooxygenase family protein
AT5G64770	-1.073020267	3.00E-08	CLEL9/RGF9 - root meristem growth factor
AT5G66080	1.30624034	0.035954082	Type 2C protein phosphatase
AT5G66700	1.95143461	0.042689066	ATHB-53 - Member of HD-ZIP 1 family

Table 7.3: CK and auxin related genes expressed during SII

Gene ID	Base Mean	Gene Name
AT5G35750	634.7165	AHK2
AT1G27320	908.5829	AHK3
AT2G01830	1045.808	AHK4
AT3G29350	385.1245	AHP2
AT5G39340	231.8336	AHP3
AT1G03430	208.5225	AHP5
AT2G24765	1678.156	ETT/ARF3
AT5G60450	1840.99	ARF4
AT1G19220	449.4109	ARF19
AT1G19850	559.5738	ARF5/MP
AT1G30330	8267.477	ARF6
AT1G59750	1439.014	ARF1
AT1G77850	218.5685	ARF17
AT2G28350	301.0434	ARF10
AT3G61830	517.5109	ARF18
AT4G23980	680.5719	ARF9

AT4G30080	563.3447	ARF16
AT5G37020	5351.531	ARF8
AT5G62000	5230.644	ARF2
AT2G22670	5486.348	IAA8
AT3G04730	1704.465	IAA16
AT3G23050	1014.929	IAA7

Table 7.4: PCR primers

Name	**Sequence**	**Reference**
RCN1 RP	AAA CAT AGC CAC ACG CAT TTC	This project
RCN1 LP	GGC CAG CCA GTT AGG TAT AGG	This project
LB-b1.3	ATTTTGCCGATTTCGGAAC	SALK genotyping project
LB3 (SAIL)	TAGCATCTGAATTTCATAACCAATCT CGATACAC	SALK genotyping project
o8474 (GABI-KAT)	ATAATAACGCTGCGGACATCTACATT TT	Kleinboelting *et al.* (2012)
PROTON1 RP	ACTTGTTTGGGTTGTCAGGTG	This project
PROTON1 LP	ACTTACGTGGCCTTCCTCTTC	This project
MAP70-2 RP	GCTGCTCAAAAGGATGATGAC	This project
MAP70-2 LP	TTAACTGTGCCTCGGATTTTG	This project
O-GT RP	GGGTGAAGGCAGGAGATAAAC	This project
O_GT LP	GGCTTCTGTGCATAGCTCAAC	This project
DRB5 RP	CTTCCAAATTGTTCCATCAACCC	This project

DRB5 LP	ACAAACGTCATTCTCGCAAACC	This project
KUK RP	CTCGTCCACGTCTCTTATTCG	This project
KUK LP	GTTGATCTGCGATGTTGTGTG	This project
LRR-K RP	GACGCTGATACTTCGCGTTAG	This project
LRR-K LP	GATTGCATTTATTGCCTCCAC	This project
PERK15 RP	CTCGGATTATGGGAACCTTCG	This project
PERK15 LP	ATCAGGCTCATGACAGTTTCG	This project
ABHY RP	ATTTCAGATGTCGCGTCAATCTC	This project
ABHY LP	GCAGCCAACTGAGCAATATG	This project
O-FT RP	AAGAAGAGAAGGCAACGAACC	This project
O-FT LP	TGAAGTGTGTAGAATTTAGATGAGTT	This project
NET2B RP	GGCTGAAAGTGTGAGCATCTC	This project
NET2B LP	AGTAAGGTTGGTCCGGTGATC	This project
LOT-2 RP	CTCAGAATGGGTATGGCATGC	This project
LOT-2 LP	TTTACCTCGAGGCATCTTCTG	This project
ANP3 RP	CTCAAGCTTCCCAGTTCACAG	This project
ANP3 LP	TATTGGATGGCTCCTGAAGTC	This project
NOV RP	CCGTGAAGGAGAATTTACTTGC	This project
NOV LP	GTGAGGGATTTGTTGATGAAGG	This project
FAR1 RP	GTCGAGACCCTGAAAAATTGTG	This project
FAR1 RP	CAGCTTCTTGCAAATGTTTCCTG	This project
PHS RP	CTGGCCTCACTCTCATCACT	This project
PHS LP	GCCGGTTTCTGGATTGCAC	This project
ERRP RP	GAACGTCGCATAAAAGCTCTG	This project
ERRP LP	TCTGTGTAGACGCAAAACGC	This project
C2DP RP	AGTGCTTACGATTAATCTTGATC	This project
C2DP LP	CTTCGTCACTTTGACCCAG	This project

AGL71 RP	CCGATTTGTTTGAGCTAAGTC	This project
AGL71 LP	GATGGAAATTGATAGAATGGTG	This project
AGL72 RP	GCTCAAGTGGCAGCTATGATC	This project
AGL72 LP	GAAAGGAACCTGCACGTATTG	This project

Table 7.5: Primers for cloning

Name	**Sequence**	**Reference**
AGL71-topo Fw	CACCATGAATCTTGGAATGAATATCGCAG	This project
AGL71-topo Rev	TTATAGCCGAGTCACGGGCAATCC	This project
AGL72-topo Fw	CACCATGGTGAGAGGAAAGATCGA	This project
AGL72-topo Rev	TTATGGTCGGTTCTTCAGAAATCC	This project
TCP1-topo Fw	CACCATGTCGTCTTCCACCAATGA	This project
TCP1-topo Rev	TTAGTTTACAAAAGAGTCTTGAATCC	This project

Table 7.6: qPCR primers

Name	**Sequence**	**Reference**
ACT2 Fw	AATTTCCCGCTCTGCTGTT	Di Mambro *et al,* 2019
ACT2 Rev	TGCCAATCTACGAGGGTTTCT	
EF1a Fw	CTTCAAGTACGCATGGGTGT	M. Del Bianco, Kepinski lab
EF1a Rev	CTTGGTGGTCTCGAACTTCC	
TCP1 Fw	TCTTCACTCTCTGGCCATCA	This project
TCP1 Rev	CTGCTGATACCATATGGCCC	This project
AGL71 Fw	TTCGGTTCTATGCGATGCTC	This project

AGL71 Rev	CAGCTCCTGCAAGTATCGTT	This project
AGLI72 Fw	TCAAGGACGAGAGAGTCAGG	This project
AGL72 Rev	TTTCTCTTTGCTTCCCGACG	This project

References

Alexandratos, N. and Bruinsma J. (2012) 'World agriculture towards 2030/2050: the 2012 revision', *ESA Working paper*, 12(03).

Ambrose, C. *et al.* (2013) 'CLASP Interacts with Sorting Nexin 1 to Link Microtubules and Auxin Transport via PIN2 Recycling in Arabidopsis thaliana', *Developmental Cell*, 24(6), pp. 649–659. Available at: https://doi.org/10.1016/j.devcel.2013.02.007.

Barbosa, I.C.R., Hammes, U.Z. and Schwechheimer, C. (2018) 'Activation and Polarity Control of PIN-FORMED Auxin Transporters by Phosphorylation', *Trends in Plant Science*, 23(6), pp. 523–538. Available at: https://doi.org/10.1016/j.tplants.2018.03.009.

Bargmann, B.O.R. *et al.* (2013) 'A map of cell type-specific auxin responses', *Molecular Systems Biology*, 9(1), p. 688. Available at: https://doi.org/10.1038/msb.2013.40.

Bartrina, I. *et al.* (2017) 'Gain-of-Function Mutants of the Cytokinin Receptors AHK2 and AHK3 Regulate Plant Organ Size, Flowering Time and Plant Longevity', *Plant Physiology*, 173(3), pp. 1783–1797. Available at: https://doi.org/10.1104/pp.16.01903.

Baunsgaard, L. *et al.* (1998) 'The 14–3-3 proteins associate with the plant plasmamembrane H1-ATPase to generate a fusicoccin bindingcomplex and a fusicoccin responsive system', *The Plant Journal*, 13(5), pp. 661–671. Available at: https://doi.org/10.1046/j.1365-313X.1998.00083.x.

Benková, E. *et al.* (2003) 'Local, Efflux-Dependent Auxin Gradients as a Common Module for Plant Organ Formation', *Cell*, 115(5), pp. 591–602. Available at: https://doi.org/10.1016/S0092-8674(03)00924-3.

Bennett, T. *et al.* (2016) 'Connective Auxin Transport in the Shoot Facilitates Communication between Shoot Apices', *PLOS Biology*, 14(4), p. e1002446. Available at: https://doi.org/10.1371/journal.pbio.1002446.

Bérut, A. *et al.* (2018) 'Gravisensors in plant cells behave like an active granular liquid', *Proceedings of the National Academy of Sciences*, 115(20), pp. 5123–5128. Available at: https://doi.org/10.1073/pnas.1801895115.

Blancaflor, E.B. (2013) 'Regulation of plant gravity sensing and signaling by the actin cytoskeleton', *American Journal of Botany*, 100(1), pp. 143–152. Available at: https://doi.org/10.3732/ajb.1200283.

Blancaflor, E.B., Fasano, J.M. and Gilroy, S. (1998) ‘Mapping the Functional Roles of Cap Cells in the Response of Arabidopsis Primary Roots to Gravity1’, *Plant Physiology*, 116(1), pp. 213–222. Available at: https://doi.org/10.1104/pp.116.1.213.

Blilou, I. *et al.* (2005) ‘The PIN auxin efflux facilitator network controls growth and patterning in Arabidopsis roots’, *Nature*, 433(7021), pp. 39–44. Available at: https://doi.org/10.1038/nature03184.

Bonner, J. and Koepfli, J.B. (1939) ‘The Inhibition of Root Growth by Auxins’, *American Journal of Botany*, 26(7), pp. 557–566.

Busch, A., Horn, S. and Zachgo, S. (2014) ‘Differential transcriptome analysis reveals insight into monosymmetric corolla development of the crucifer Iberis amara’, *BMC Plant Biology*, 14(1), p. 285. Available at: https://doi.org/10.1186/s12870-014-0285-4.

Busch, A. and Zachgo, S. (2007) ‘Control of corolla monosymmetry in the Brassicaceae *Iberis amara*’, *Proceedings of the National Academy of Sciences*, 104(42), pp. 16714–16719. Available at: https://doi.org/10.1073/pnas.0705338104.

Carriedo, L.G., Maloof, J.N. and Brady, S.M. (2016) ‘Molecular control of crop shade avoidance’, *Current Opinion in Plant Biology*, 30, pp. 151–158. Available at: https://doi.org/10.1016/j.pbi.2016.03.005.

Chauvet, H. *et al.* (2016) ‘Inclination not force is sensed by plants during shoot gravitropism’, *Scientific Reports*, 6(1), p. 35431. Available at: https://doi.org/10.1038/srep35431.

Chen, D. *et al.* (2022) ‘Receptor-like kinase HAESA-like 1 positively regulates seed longevity in Arabidopsis’, *Planta*, 256(2), p. 21. Available at: https://doi.org/10.1007/s00425-022-03942-y.

Chen, W.-H. *et al.* (2022) ‘Regulatory network for FOREVER YOUNG FLOWER-like genes in regulating Arabidopsis flower senescence and abscission’, *Communications Biology*, 5(1), p. 662. Available at: https://doi.org/10.1038/s42003-022-03629-w.

Chen, X. *et al.* (2016) ‘Shoot-to-Root Mobile Transcription Factor HY5 Coordinates Plant Carbon and Nitrogen Acquisition’, *Current Biology*, 26(5), pp. 640–646. Available at: https://doi.org/10.1016/j.cub.2015.12.066.

Cheng, S. and Wang, Y. (2022) ‘Subcellular trafficking and post-translational modification regulate PIN polarity in plants’, *Frontiers in Plant Science*, 13. Available at: https://doi.org/10.3389/fpls.2022.923293.

Cholodny, N. (1927) ‘ Wuchshormone and Tropismen bei den Pflanzen’, *Biol Zentralbl*, 47, pp. 604–629.

Claussen, M. *et al.* (1997) ‘Auxin-induced growth and its linkage to potassium channels’, *Planta*, 201(2), pp. 227–234. Available at: https://doi.org/10.1007/BF01007708.

Comas, L.H. *et al.* (2013) ‘Root traits contributing to plant productivity under drought’, *Frontiers in Plant Science*, 4. Available at: https://doi.org/10.3389/fpls.2013.00442.

Dai, M. *et al.* (2012) ‘A PP6-Type Phosphatase Holoenzyme Directly Regulates PIN Phosphorylation and Auxin Efflux in *Arabidopsis*’, *The Plant Cell*, 24(6), pp. 2497–2514. Available at: https://doi.org/10.1105/tpc.112.098905.

Dardick, C. *et al.* (2013) ‘PpeTAC1 promotes the horizontal growth of branches in peach trees and is a member of a functionally conserved gene family found in diverse plants species’, *The Plant Journal*, 75(4), pp. 618–630. Available at: https://doi.org/10.1111/tpj.12234.

D’Ario, M. *et al.* (2021) ‘Cell size controlled in plants using DNA content as an internal scale’, *Science*, 372(6547), pp. 1176–1181. Available at: https://doi.org/10.1126/science.abb4348.

Dewitte, W. *et al.* (2007) ‘Arabidopsis CYCD3 D-type cyclins link cell proliferation and endocycles and are rate-limiting for cytokinin responses’, *Proceedings of the National Academy of Sciences of the United States of America*, 104(36), pp. 14537–14542. Available at: https://doi.org/10.1073/PNAS.0704166104/SUPPL_FILE/04166TABLE3.PDF.

Dharmasiri, N. *et al.* (2005) ‘Plant Development Is Regulated by a Family of Auxin Receptor F Box Proteins’, *Developmental Cell*, 9(1), pp. 109–119. Available at: https://doi.org/10.1016/j.devcel.2005.05.014.

Dhonukshe, P. *et al.* (2007) ‘Clathrin-Mediated Constitutive Endocytosis of PIN Auxin Efflux Carriers in Arabidopsis’, *Current Biology*, 17(6), pp. 520–527. Available at: https://doi.org/10.1016/j.cub.2007.01.052.

Dhonukshe, P. *et al.* (2010) ‘Plasma membrane-bound AGC3 kinases phosphorylate PIN auxin carriers at TPRXS(N/S) motifs to direct apical PIN recycling’, *Development*, 137(19), pp. 3245–3255. Available at: https://doi.org/10.1242/dev.052456.

Digby, J. and Firn, R.D. (1995) ‘The gravitropic set-point angle (GSA): the identification of an important developmentally controlled variable governing plant architecture*’, *Plant, Cell and Environment*, 18(12), pp. 1434–1440. Available at: https://doi.org/10.1111/j.1365-3040.1995.tb00205.x.

Dorca-Fornell, C. *et al.* (2011) ‘The Arabidopsis SOC1-like genes AGL42, AGL71 and AGL72 promote flowering in the shoot apical and axillary meristems’, *The Plant Journal*, 67(6), pp. 1006–1017. Available at: https://doi.org/10.1111/J.1365-313X.2011.04653.X.

Doyle, S.M., Haeger, A., Vain, T., Rigal, A., Viotti, C., Łangowska, M., Ma, Q., Friml, J., Raikhel, N. v., *et al.* (2015) ‘An early secretory pathway mediated by GNOM-LIKE 1 and GNOM is essential for basal polarity establishment in *Arabidopsis thaliana*’, *Proceedings of the National Academy of Sciences*, 112(7). Available at: https://doi.org/10.1073/pnas.1424856112.

Doyle, S.M., Haeger, A., Vain, T., Rigal, A., Viotti, C., Łangowska, M., Ma, Q., Friml, J., Raikhel, N. V., *et al.* (2015) ‘An early secretory pathway mediated by GNOM-LIKE 1 and GNOM is essential for basal polarity establishment in *Arabidopsis thaliana*’, *Proceedings of the National Academy of Sciences*, 112(7). Available at: https://doi.org/10.1073/pnas.1424856112.

Duarte, G.T. *et al.* (2021) ‘Plasticity of rosette size in response to nitrogen availability is controlled by an <scp>RCC1</scp> -family protein’, *Plant, Cell & Environment*, 44(10), pp. 3398–3411. Available at: https://doi.org/10.1111/pce.14146.

Duckney, P. *et al.* (2021) ‘NETWORKED2-subfamily proteins regulate the cortical actin cytoskeleton of growing pollen tubes and polarised pollen tube growth’, *New Phytologist*, 231(1), pp. 152–164. Available at: https://doi.org/10.1111/nph.17391.

Eamens, A.L. *et al.* (2012) ‘DRB2 Is Required for MicroRNA Biogenesis in Arabidopsis thaliana’, *PLoS ONE*, 7(4), p. e35933. Available at: https://doi.org/10.1371/journal.pone.0035933.

Eloy, N.B. *et al.* (2011) 'The APC/C *subunit 10* plays an essential role in cell proliferation during leaf development', *The Plant Journal*, 68(2), pp. 351–363. Available at: https://doi.org/10.1111/j.1365-313X.2011.04691.x.

Emery, J.F. *et al.* (2003) 'Radial Patterning of Arabidopsis Shoots by Class III HD-ZIP and KANADI Genes', *Current Biology*, 13(20), pp. 1768–1774. Available at: https://doi.org/10.1016/j.cub.2003.09.035.

Eshed, Y. *et al.* (2001) 'Establishment of polarity in lateral organs of plants', *Current Biology*, 11(16), pp. 1251–1260. Available at: https://doi.org/10.1016/S0960-9822(01)00392-X.

F. Baluška and K.H. Hasenstein (1997) 'Root cytoskeleton: its role in perception of and response to gravity', *Planta*, 203, pp. S69–S78.

Fendrych, M. *et al.* (2018) 'Rapid and reversible root growth inhibition by TIR1 auxin signalling', *Nature Plants*, 4(7), pp. 453–459. Available at: https://doi.org/10.1038/s41477-018-0190-1.

Fendrych, M., Leung, J. and Friml, J. (2016) 'TIR1/AFB-Aux/IAA auxin perception mediates rapid cell wall acidification and growth of Arabidopsis hypocotyls', *eLife*, 5. Available at: https://doi.org/10.7554/eLife.19048.

Friml, Jiří *et al.* (2002) 'AtPIN4 Mediates Sink-Driven Auxin Gradients and Root Patterning in Arabidopsis', *Cell*, 108(5), pp. 661–673. Available at: https://doi.org/10.1016/S0092-8674(02)00656-6.

Friml, Jiří *et al.* (2002) 'Lateral relocation of auxin efflux regulator PIN3 mediates tropism in Arabidopsis', *Nature*, 415(6873), pp. 806–809. Available at: https://doi.org/10.1038/415806a.

Fuglsang, A.T. *et al.* (1999) 'Binding of 14-3-3 Protein to the Plasma Membrane H+-ATPase AHA2 Involves the Three C-terminal Residues Tyr946-Thr-Val and Requires Phosphorylation of Thr947', *Journal of Biological Chemistry*, 274(51), pp. 36774–36780. Available at: https://doi.org/10.1074/jbc.274.51.36774.

Fukaki, H. and Tasaka, M. (1999) 'Gravity perception and gravitropic response of inflorescence stems in Arabidopsis thaliana', *Advances in Space Research*, 24(6), pp. 763–770. Available at: https://doi.org/10.1016/S0273-1177(99)00410-X.

Furutani, M. *et al.* (2020) ‘Polar recruitment of RLD by LAZY1-like protein during gravity signaling in root branch angle control’, *Nature Communications*, 11(1), pp. 1–13. Available at: https://doi.org/10.1038/s41467-019-13729-7.

Ganguly, A., Lee, S.-H. and Cho, H.-T. (2012) ‘Functional identification of the phosphorylation sites of Arabidopsis PIN-FORMED3 for its subcellular localization and biological role’, *The Plant Journal*, 71(5), pp. 810–823. Available at: https://doi.org/10.1111/j.1365-313X.2012.05030.x.

Gao, Y., Zhang, D. and Li, J. (2015) ‘TCP1 Modulates DWF4 Expression via Directly Interacting with the GGNCCC Motifs in the Promoter Region of DWF4 in Arabidopsis thaliana’, *Journal of Genetics and Genomics*, 42(7), pp. 383–392. Available at: https://doi.org/10.1016/j.jgg.2015.04.009.

Gauthier, J. *et al.* (2020) ‘DiscoSnp-RAD: de novo detection of small variants for RAD-Seq population genomics’, *PeerJ*, 8, p. e9291. Available at: https://doi.org/10.7717/peerj.9291.

Geisler, M. *et al.* (2017) ‘A Critical View on ABC Transporters and Their Interacting Partners in Auxin Transport’, *Plant and Cell Physiology*, 58(10), pp. 1601–1614. Available at: https://doi.org/10.1093/pcp/pcx104.

van Gelderen, K. *et al.* (2018) ‘Far-Red Light Detection in the Shoot Regulates Lateral Root Development through the HY5 Transcription Factor’, *The Plant Cell*, 30(1), pp. 101–116. Available at: https://doi.org/10.1105/tpc.17.00771.

Geldner, N. *et al.* (2003) ‘The Arabidopsis GNOM ARF-GEF Mediates Endosomal Recycling, Auxin Transport, and Auxin-Dependent Plant Growth’, *Cell*, 112(2), pp. 219–230. Available at: https://doi.org/10.1016/S0092-8674(03)00003-5.

Gerondopoulos, A. *et al.* (2021) ‘A signal capture and proofreading mechanism for the KDEL-receptor explains selectivity and dynamic range in ER retrieval’, *eLife*, 10. Available at: https://doi.org/10.7554/eLife.68380.

Glanc, M., Fendrych, M. and Friml, J. (2018) ‘Mechanistic framework for cell-intrinsic re-establishment of PIN2 polarity after cell division’, *Nature Plants*, 4(12), pp. 1082–1088. Available at: https://doi.org/10.1038/s41477-018-0318-3.

Goldsmith, M.H.M. (1977) ‘THE POLAR TRANSPORT OF AUXIN’, *Ann. Rev. Plant Physiol*, 28, pp. 439–478.

Gonzalez, N., Vanhaeren, H. and Inzé, D. (2012) 'Leaf size control: complex coordination of cell division and expansion', *Trends in Plant Science*, 17(6), pp. 332–340. Available at: https://doi.org/10.1016/j.tplants.2012.02.003.

Grones, P. *et al.* (2018) 'PID/WAG-mediated phosphorylation of the Arabidopsis PIN3 auxin transporter mediates polarity switches during gravitropism', *Scientific Reports*, 8(1), p. 10279. Available at: https://doi.org/10.1038/s41598-018-28188-1.

Guan, C. *et al.* (2003) 'The ARG1-LIKE2 Gene of Arabidopsis Functions in a Gravity Signal Transduction Pathway That Is Genetically Distinct from the *PGM* Pathway', *Plant Physiology*, 133(1), pp. 100–112. Available at: https://doi.org/10.1104/pp.103.023358.

Guan, P. *et al.* (2017) 'Interacting TCP and NLP transcription factors control plant responses to nitrate availability', *Proceedings of the National Academy of Sciences*, 114(9), pp. 2419–2424. Available at: https://doi.org/10.1073/pnas.1615676114.

Guo, H.-S. *et al.* (2005) 'MicroRNA Directs mRNA Cleavage of the Transcription Factor *NAC1* to Downregulate Auxin Signals for Arabidopsis Lateral Root Development', *The Plant Cell*, 17(5), pp. 1376–1386. Available at: https://doi.org/10.1105/tpc.105.030841.

Guo, Z. *et al.* (2010) 'TCP1 Modulates Brassinosteroid Biosynthesis by Regulating the Expression of the Key Biosynthetic Gene DWARF4 in Arabidopsis thaliana', *The Plant Cell*, 22(4), p. 1161. Available at: https://doi.org/10.1105/TPC.109.069203.

Guyomarc'h, S. *et al.* (2012) 'Early development and gravitropic response of lateral roots in *Arabidopsis thaliana*', *Philosophical Transactions of the Royal Society B: Biological Sciences*, 367(1595), pp. 1509–1516. Available at: https://doi.org/10.1098/rstb.2011.0231.

Harrison, B. and Masson, P.H. (2008) 'Do ARG1 and ARL2 form an actin-based gravity-signaling chaperone complex in root statocytes?', *Plant Signaling & Behavior*, 3(9), pp. 650–653. Available at: https://doi.org/10.4161/psb.3.9.5749.

Higuchi, M. *et al.* (2004) '*In planta* functions of the *Arabidopsis* cytokinin receptor family', *Proceedings of the National Academy of Sciences*, 101(23), pp. 8821–8826. Available at: https://doi.org/10.1073/pnas.0402887101.

Hill, J.L. and Hollender, C.A. (2019) ‘Branching out: new insights into the genetic regulation of shoot architecture in trees’, *Current Opinion in Plant Biology*, 47, pp. 73–80. Available at: https://doi.org/10.1016/j.pbi.2018.09.010.

Hollender, C.A. *et al.* (2020) ‘Opposing influences of TAC1 and LAZY1 on Lateral Shoot Orientation in Arabidopsis’, *Scientific Reports*, 10(1), p. 6051. Available at: https://doi.org/10.1038/s41598-020-62962-4.

Hou, G., Mohamalawari, D.R. and Blancaflor, E.B. (2003) ‘Enhanced Gravitropism of Roots with a Disrupted Cap Actin Cytoskeleton’, *Plant Physiology*, 131(3), pp. 1360–1373. Available at: https://doi.org/10.1104/pp.014423.

Huang, F. *et al.* (2010) ‘Phosphorylation of Conserved PIN Motifs Directs *Arabidopsis* PIN1 Polarity and Auxin Transport ’, *The Plant Cell*, 22(4), pp. 1129–1142. Available at: https://doi.org/10.1105/tpc.109.072678.

Huang, T. *et al.* (2014) ‘*Arabidopsis* KANADI1 Acts as a Transcriptional Repressor by Interacting with a Specific *cis* -Element and Regulates Auxin Biosynthesis, Transport, and Signaling in Opposition to HD-ZIPIII Factors’, *The Plant Cell*, 26(1), pp. 246–262. Available at: https://doi.org/10.1105/tpc.113.111526.

Hwang, I., Sheen, J. and Müller, B. (2012) ‘Cytokinin Signaling Networks’, *Annual Review of Plant Biology*, 63(1), pp. 353–380. Available at: https://doi.org/10.1146/annurev-arplant-042811-105503.

Invernizzi, M. *et al.* (2022) ‘PERKing up our understanding of the proline-rich extensin-like receptor kinases, a forgotten plant receptor kinase family’, *New Phytologist*, 235(3), pp. 875–884. Available at: https://doi.org/10.1111/nph.18166.

Ischebeck, T. *et al.* (2014) ‘Phosphatidylinositol 4,5-Bisphosphate Influences PIN Polarization by Controlling Clathrin-Mediated Membrane Trafficking in *Arabidopsis* ’, *The Plant Cell*, 25(12), pp. 4894–4911. Available at: https://doi.org/10.1105/tpc.113.116582.

Javorka, P. *et al.* (2019) ‘artMAP: A user-friendly tool for mapping ethyl methanesulfonate-induced mutations in Arabidopsis’, *Plant Direct*, 3(6), p. e00146. Available at: https://doi.org/10.1002/pld3.146.

Jia, P.-F. *et al.* (2018) ‘Golgi-localized LOT regulates *trans* -Golgi network biogenesis and pollen tube growth’, *Proceedings of the National Academy of*

Sciences, 115(48), pp. 12307–12312. Available at: https://doi.org/10.1073/pnas.1809206115.

Jia, P.-F. *et al.* (2019) 'LOT regulates TGN biogenesis and Golgi structure in plants', *Plant Signaling & Behavior*, 14(3), p. e1573100. Available at: https://doi.org/10.1080/15592324.2019.1573100.

Jones, A.R., Band, L.R. and Murray, J.A.H. (2019) 'Double or Nothing? Cell Division and Cell Size Control', *Trends in Plant Science*, 24(12), pp. 1083–1093. Available at: https://doi.org/10.1016/j.tplants.2019.09.005.

Jose, J., Ghantasala, S. and Roy Choudhury, S. (2020) 'Arabidopsis Transmembrane Receptor-Like Kinases (RLKs): A Bridge between Extracellular Signal and Intracellular Regulatory Machinery', *International Journal of Molecular Sciences*, 21(11), p. 4000. Available at: https://doi.org/10.3390/ijms21114000.

Juniper, B.E. *et al.* (1966) 'Root Cap and the Perception of Gravity', *Nature*, 209(5018), pp. 93–94. Available at: https://doi.org/10.1038/209093a0.

Kanczewska, J. *et al.* (2005) 'Activation of the plant plasma membrane H^+-ATPase by phosphorylation and binding of 14-3-3 proteins converts a dimer into a hexamer', *Proceedings of the National Academy of Sciences*, 102(33), pp. 11675–11680. Available at: https://doi.org/10.1073/pnas.0504498102.

Kanno, Y. *et al.* (2016) 'AtSWEET13 and AtSWEET14 regulate gibberellin-mediated physiological processes', *Nature Communications*, 7(1), p. 13245. Available at: https://doi.org/10.1038/ncomms13245.

Kawamoto, N. *et al.* (2020) 'Gravity-Sensing Tissues for Gravitropism Are Required for "Anti-Gravitropic" Phenotypes of lzy Multiple Mutants in Arabidopsis', *Plants*, 9(5), p. 615. Available at: https://doi.org/10.3390/plants9050615.

Kebrom, T.H. (2017) 'A Growing Stem Inhibits Bud Outgrowth – The Overlooked Theory of Apical Dominance', *Frontiers in Plant Science*, 8. Available at: https://doi.org/10.3389/fpls.2017.01874.

Kelley, D.R. *et al.* (2012) 'ETTIN (ARF3) physically interacts with KANADI proteins to form a functional complex essential for integument development and polarity determination in *Arabidopsis*', *Development*, 139(6), pp. 1105–1109. Available at: https://doi.org/10.1242/dev.067918.

Kepinski, S. and Leyser, O. (2005) 'The Arabidopsis F-box protein TIR1 is an auxin receptor', *Nature*, 435(7041), pp. 446–451. Available at: https://doi.org/10.1038/nature03542.

Kerstetter, R.A. *et al.* (2001) 'KANADI regulates organ polarity in Arabidopsis', *Nature*, 411(6838), pp. 706–709. Available at: https://doi.org/10.1038/35079629.

Kiss, J.Z., Hertel, R. and Sack, F.D. (1989) 'Amyloplasts are necessary for full gravitropic sensitivity in roots of Arabidopsis thaliana.', *Planta*, 177, pp. 198–206.

Kitakura, S. *et al.* (2011) 'Clathrin Mediates Endocytosis and Polar Distribution of PIN Auxin Transporters in *Arabidopsis* ', *The Plant Cell*, 23(5), pp. 1920–1931. Available at: https://doi.org/10.1105/tpc.111.083030.

Kjos, I. *et al.* (2018) 'Rab and Arf proteins at the crossroad between membrane transport and cytoskeleton dynamics', *Biochimica et Biophysica Acta (BBA) - Molecular Cell Research*, 1865(10), pp. 1397–1409. Available at: https://doi.org/10.1016/j.bbamcr.2018.07.009.

Kleine-Vehn, J., Dhonukshe, P., *et al.* (2008) 'ARF GEF-Dependent Transcytosis and Polar Delivery of PIN Auxin Carriers in Arabidopsis', *Current Biology*, 18(7), pp. 526–531. Available at: https://doi.org/10.1016/j.cub.2008.03.021.

Kleine-Vehn, J., Łangowski, Ł., *et al.* (2008) 'Cellular and Molecular Requirements for Polar PIN Targeting and Transcytosis in Plants', *Molecular Plant*, 1(6), pp. 1056–1066. Available at: https://doi.org/10.1093/mp/ssn062.

Kleine-Vehn, J. *et al.* (2010) 'Gravity-induced PIN transcytosis for polarization of auxin fluxes in gravity-sensing root cells', *Proceedings of the National Academy of Sciences*, 107(51), pp. 22344–22349. Available at: https://doi.org/10.1073/pnas.1013145107.

Kögl, F., Haagen-Smit, A. and Erxleben, H. (1934) 'Über den Einfluß der Auxine auf das Wurzelwachstum und über die chemische Natur des Auxins der Graskoleoptilen', *Mitteilung über pflanzliche Wachstumsstoffe. Biol Chem*, 228, pp. 1–2.

Komaki, S. and Sugimoto, K. (2012) 'Control of the Plant Cell Cycle by Developmental and Environmental Cues', *Plant and Cell Physiology*, 53(6), pp. 953–964. Available at: https://doi.org/10.1093/pcp/pcs070.

Korolev, A. V. *et al.* (2005) ‘Identification of a novel family of 70 kDa microtubule-associated proteins in Arabidopsis cells’, *The Plant Journal*, 42(4), pp. 547–555. Available at: https://doi.org/10.1111/j.1365-313X.2005.02393.x.

Koyama, T., Sato, F. and Ohme-Takagi, M. (2010) ‘A Role of TCP1 in the Longitudinal Elongation of Leaves in Arabidopsis’, *Bioscience, Biotechnology, and Biochemistry*, 74(10), pp. 2145–2147. Available at: https://doi.org/10.1271/BBB.100442.

Krysan, P.J. *et al.* (2002) ‘An Arabidopsis Mitogen-Activated Protein Kinase Kinase Kinase Gene Family Encodes Essential Positive Regulators of Cytokinesis’, *The Plant Cell*, 14(5), pp. 1109–1120. Available at: https://doi.org/10.1105/tpc.001164.

Kuhn, A. *et al.* (2020) ‘Direct ETTIN-auxin interaction controls chromatin states in gynoecium development’, *eLife*, 9. Available at: https://doi.org/10.7554/eLife.51787.

Kurihara, D. *et al.* (2015) ‘ClearSee: a rapid optical clearing reagent for whole-plant fluorescence imaging’, *Development* [Preprint]. Available at: https://doi.org/10.1242/dev.127613.

Lehman, T.A., Smertenko, A. and Sanguinet, K.A. (2017) ‘Auxin, microtubules, and vesicle trafficking: conspirators behind the cell wall’, *Journal of Experimental Botany*, 68(13), pp. 3321–3329. Available at: https://doi.org/10.1093/jxb/erx205.

Leyser, O. (2018) ‘Auxin Signaling’, *Plant Physiology*, 176(1), pp. 465–479. Available at: https://doi.org/10.1104/PP.17.00765.

Li, J. *et al.* (2010) ‘*Arabidopsis* Transcription Factor ELONGATED HYPOCOTYL5 Plays a Role in the Feedback Regulation of Phytochrome A Signaling ’, *The Plant Cell*, 22(11), pp. 3634–3649. Available at: https://doi.org/10.1105/tpc.110.075788.

Li, S.-B. *et al.* (2016) ‘A Review of Auxin Response Factors (ARFs) in Plants’, *Frontiers in Plant Science*, 7. Available at: https://doi.org/10.3389/fpls.2016.00047.

Li, Yanli *et al.* (2018) ‘The sHSP22 Heat Shock Protein Requires the ABI1 Protein Phosphatase to Modulate Polar Auxin Transport and Downstream Responses’, *Plant Physiology*, 176(3), pp. 2406–2425. Available at: https://doi.org/10.1104/pp.17.01206.

Ma, Y. *et al.* (2022) ‘Endoreplication mediates cell size control via mechanochemical signaling from cell wall’, *Science Advances*, 8(49). Available at: https://doi.org/10.1126/sciadv.abq2047.

Manuela, D. and Xu, M. (2020) ‘Patterning a Leaf by Establishing Polarities’, *Frontiers in Plant Science*, 11. Available at: https://doi.org/10.3389/fpls.2020.568730.

Marhava, P. (2022) ‘Recent developments in the understanding of PIN polarity’, *New Phytologist*, 233(2), pp. 624–630. Available at: https://doi.org/10.1111/nph.17867.

Marti, L. *et al.* (2021) ‘The intracellular <scp>ROS</scp> accumulation in elicitor-induced immunity requires the multiple organelle-targeted Arabidopsis <scp>NPK1</scp> -related protein kinases’, *Plant, Cell & Environment*, 44(3), pp. 931–947. Available at: https://doi.org/10.1111/pce.13978.

Meijón, M. *et al.* (2014) ‘Genome-wide association study using cellular traits identifies a new regulator of root development in Arabidopsis’, *Nature Genetics*, 46(1), pp. 77–81. Available at: https://doi.org/10.1038/ng.2824.

Michniewicz, M. *et al.* (2007) ‘Antagonistic Regulation of PIN Phosphorylation by PP2A and PINOID Directs Auxin Flux’, *Cell*, 130(6), pp. 1044–1056. Available at: https://doi.org/10.1016/j.cell.2007.07.033.

Mindrebo, J.T. *et al.* (2016) ‘Unveiling the functional diversity of the alpha/beta hydrolase superfamily in the plant kingdom’, *Current Opinion in Structural Biology*, 41, pp. 233–246. Available at: https://doi.org/10.1016/j.sbi.2016.08.005.

Miyawaki, K. *et al.* (2006) ‘Roles of *Arabidopsis* ATP/ADP isopentenyltransferases and tRNA isopentenyltransferases in cytokinin biosynthesis’, *Proceedings of the National Academy of Sciences*, 103(44), pp. 16598–16603. Available at: https://doi.org/10.1073/pnas.0603522103.

Monshausen, G.B. *et al.* (2011) ‘Dynamics of auxin-dependent Ca2+ and pH signaling in root growth revealed by integrating high-resolution imaging with automated computer vision-based analysis’, *The Plant Journal*, 65(2), pp. 309–318. Available at: https://doi.org/10.1111/j.1365-313X.2010.04423.x.

Moreno, S. *et al.* (2020) ‘Nitrate Defines Shoot Size through Compensatory Roles for Endoreplication and Cell Division in Arabidopsis thaliana’, *Current Biology*, 30(11), pp. 1988-2000.e3. Available at: https://doi.org/10.1016/j.cub.2020.03.036.

Moulia, B., Douady, S. and Hamant, O. (2021) ‘Fluctuations shape plants through proprioception’, *Science*, 372(6540). Available at: https://doi.org/10.1126/science.abc6868.

Mullen, J.L. *et al.* (2000) ‘Kinetics of Constant Gravitropic Stimulus Responses in Arabidopsis Roots Using a Feedback System’, *Plant Physiology*, 123(2), pp. 665–670. Available at: https://doi.org/10.1104/pp.123.2.665.

Nakamura, M., Nishimura, T. and Morita, M.T. (2019) ‘Gravity sensing and signal conversion in plant gravitropism’, *Journal of Experimental Botany*, 70(14), pp. 3495–3506. Available at: https://doi.org/10.1093/jxb/erz158.

Narasimhan, M. *et al.* (2020) ‘Evolutionarily unique mechanistic framework of clathrin-mediated endocytosis in plants’, *eLife*, 9. Available at: https://doi.org/10.7554/eLife.52067.

Noack, L.C. *et al.* (2022) ‘A nanodomain-anchored scaffolding complex is required for the function and localization of phosphatidylinositol 4-kinase alpha in plants’, *The Plant Cell*, 34(1), pp. 302–332. Available at: https://doi.org/10.1093/plcell/koab135.

O’Brien, T.P., Feder, N. and McCully, M.E. (1964) ‘Polychromatic staining of plant cell walls by toluidine blue O’, *Protoplasma*, 59(2), pp. 368–373. Available at: https://doi.org/10.1007/BF01248568.

Ohyama, K. *et al.* (2009) ‘A glycopeptide regulating stem cell fate in Arabidopsis thaliana’, *Nature Chemical Biology*, 5(8), pp. 578–580. Available at: https://doi.org/10.1038/nchembio.182.

Okamoto, K. *et al.* (2015) ‘Regulation of organ straightening and plant posture by an actin–myosin XI cytoskeleton’, *Nature Plants*, 1(4), p. 15031. Available at: https://doi.org/10.1038/nplants.2015.31.

Ottenschläger, I. *et al.* (2003) ‘Gravity-regulated differential auxin transport from columella to lateral root cap cells’, *Proceedings of the National Academy of Sciences*, 100(5), pp. 2987–2991. Available at: https://doi.org/10.1073/pnas.0437936100.

Pan, X. *et al.* (2020) ‘Auxin-induced signaling protein nanoclustering contributes to cell polarity formation’, *Nature Communications*, 11(1), p. 3914. Available at: https://doi.org/10.1038/s41467-020-17602-w.

Paponov, I.A. *et al.* (2008) ‘Comprehensive Transcriptome Analysis of Auxin Responses in Arabidopsis’, *Molecular Plant*, 1(2), pp. 321–337. Available at: https://doi.org/10.1093/mp/ssm021.

Pekker, I., Alvarez, J.P. and Eshed, Y. (2005) ‘Auxin Response Factors Mediate *Arabidopsis* Organ Asymmetry via Modulation of KANADI Activity’, *The Plant Cell*, 17(11), pp. 2899–2910. Available at: https://doi.org/10.1105/tpc.105.034876.

Petrášek, J. and Friml, J. (2009) ‘Auxin transport routes in plant development’, *Development*, 136(16), pp. 2675–2688. Available at: https://doi.org/10.1242/DEV.030353.

Pradhan Mitra, P. and Loqué, D. (2014) ‘Histochemical staining of Arabidopsis thaliana secondary cell wall elements’, *Journal of Visualized Experiments* [Preprint], (87). Available at: https://doi.org/10.3791/51381.

Prigge, M.J. *et al.* (2005) ‘Class III Homeodomain-Leucine Zipper Gene Family Members Have Overlapping, Antagonistic, and Distinct Roles in Arabidopsis Development’, *The Plant Cell*, 17(1), pp. 61–76. Available at: https://doi.org/10.1105/tpc.104.026161.

Qian, P. *et al.* (2018) ‘The CLE9/10 secretory peptide regulates stomatal and vascular development through distinct receptors’, *Nature Plants*, 4(12), pp. 1071–1081. Available at: https://doi.org/10.1038/s41477-018-0317-4.

Rahman, A. *et al.* (2010) ‘Gravitropism of *Arabidopsis thaliana* Roots Requires the Polarization of PIN2 toward the Root Tip in Meristematic Cortical Cells ’, *The Plant Cell*, 22(6), pp. 1762–1776. Available at: https://doi.org/10.1105/tpc.110.075317.

Rakusová, H. *et al.* (2011) ‘Polarization of PIN3-dependent auxin transport for hypocotyl gravitropic response in Arabidopsis thaliana’, *The Plant Journal*, 67(5), pp. 817–826. Available at: https://doi.org/10.1111/j.1365-313X.2011.04636.x.

Rakusová, H. *et al.* (2016) ‘Termination of Shoot Gravitropic Responses by Auxin Feedback on PIN3 Polarity’, *Current Biology*, 26(22), pp. 3026–3032. Available at: https://doi.org/10.1016/j.cub.2016.08.067.

Ram, H. *et al.* (2020) ‘An integrated analysis of cell-type specific gene expression reveals genes regulated by REVOLUTA and KANADI1 in the Arabidopsis shoot apical meristem’, *PLOS Genetics*, 16(4), p. e1008661. Available at: https://doi.org/10.1371/journal.pgen.1008661.

Rayle, D.L. and Cleland, R. (1970) ‘Enhancement of Wall Loosening and Elongation by Acid Solutions’, *Plant Physiology*, 46(2), pp. 250–253. Available at: https://doi.org/10.1104/pp.46.2.250.

Rayle, D.L. and Cleland, R.E. (1980) ‘Evidence that Auxin-induced Growth of Soybean Hypocotyls Involves Proton Excretion’, *Plant Physiology*, 66(3), pp. 433–437. Available at: https://doi.org/10.1104/pp.66.3.433.

Reinisch, K.M. and de Camilli, P. (2016) ‘SMP-domain proteins at membrane contact sites: Structure and function’, *Biochimica et Biophysica Acta (BBA) - Molecular and Cell Biology of Lipids*, 1861(8), pp. 924–927. Available at: https://doi.org/10.1016/j.bbalip.2015.12.003.

Riou-Khamlichi, C. *et al.* (1999) ‘Cytokinin Activation of *Arabidopsis* Cell Division Through a D-Type Cyclin’, *Science*, 283(5407), pp. 1541–1544. Available at: https://doi.org/10.1126/science.283.5407.1541.

Riou-Khamlichi, C. *et al.* (2000) ‘Sugar Control of the Plant Cell Cycle: Differential Regulation of *Arabidopsis* D-Type Cyclin Gene Expression’, *Molecular and Cellular Biology*, 20(13), pp. 4513–4521. Available at: https://doi.org/10.1128/MCB.20.13.4513-4521.2000.

Rizo, J. and Südhof, T.C. (1998) ‘C2-domains, Structure and Function of a Universal Ca2+-binding Domain’, *Journal of Biological Chemistry*, 273(26), pp. 15879–15882. Available at: https://doi.org/10.1074/jbc.273.26.15879.

Rosquete, M.R. *et al.* (2013) ‘An Auxin Transport Mechanism Restricts Positive Orthogravitropism in Lateral Roots’, *Current Biology*, 23(9), pp. 817–822. Available at: https://doi.org/10.1016/j.cub.2013.03.064.

Roychoudhry, S. *et al.* (2013) ‘Auxin controls gravitropic setpoint angle in higher plant lateral branches’, *Current biology : CB*, 23(15), pp. 1497–1504. Available at: https://doi.org/10.1016/J.CUB.2013.06.034.

Roychoudhry, S. *et al.* (2017) ‘The developmental and environmental regulation of gravitropic setpoint angle in Arabidopsis and bean’, *Scientific Reports* [Preprint]. Available at: https://doi.org/10.1038/srep42664.

Roychoudhry, S. *et al.* (2019) ‘Antagonistic and auxin-dependent phosphoregulation of columella PIN proteins controls lateral root gravitropic setpoint angle in Arabidopsis’, *bioRxiv*, p. 594838. Available at: https://doi.org/10.1101/594838.

Roychoudhry, S. and Kepinski, S. (2015) ‘Analysis of Gravitropic Setpoint Angle Control in Arabidopsis’, in, pp. 31–41. Available at: https://doi.org/10.1007/978-1-4939-2697-8_4.

Ruck, A. *et al.* (1993) ‘Patch-clamp analysis establishes a role for an auxin binding protein in the auxin stimulation of plasma membrane current in Zea mays protoplasts’, *The Plant Journal*, 4(1), pp. 41–46. Available at: https://doi.org/10.1046/j.1365-313X.1993.04010041.x.

Ruiz Rosquete, M., Barbez, E. and Kleine-Vehn, J. (2012) ‘Cellular Auxin Homeostasis: Gatekeeping Is Housekeeping’, *Molecular Plant*, 5(4), pp. 772–786. Available at: https://doi.org/10.1093/mp/ssr109.

Sabatini, S. *et al.* (1999) ‘An Auxin-Dependent Distal Organizer of Pattern and Polarity in the Arabidopsis Root’, *Cell*, 99(5), pp. 463–472. Available at: https://doi.org/10.1016/S0092-8674(00)81535-4.

Sachs, J. (1882) ‘ Über orthotrope und plagiotrope Pflanzenteille ’, *Arb Bot Inst Würzburg*, 58.

Sack, F.D. (1991) ‘Plant Gravity Sensing’, in, pp. 193–252. Available at: https://doi.org/10.1016/S0074-7696(08)60695-6.

Sageman-Furnas, K. (2016) ‘Auxin-mediated Gravitropism of Arabidopsis thaliana’, *PhD, University of Leeds* [Preprint].

Salehin, M., Bagchi, R. and Estelle, M. (2015) ‘SCF-TIR1/AFB-Based Auxin Perception: Mechanism and Role in Plant Growth and Development’, *The Plant Cell*, 27(1), pp. 9–19. Available at: https://doi.org/10.1105/tpc.114.133744.

Scheitz, K., Lüthen, H. and Schenck, D. (2013) ‘Rapid auxin-induced root growth inhibition requires the TIR and AFB auxin receptors’, *Planta*, 238(6), pp. 1171–1176. Available at: https://doi.org/10.1007/s00425-013-1941-x.

Sedbrook, J.C., Chen, R. and Masson, P.H. (1999) ‘ARG1 (Altered Response to Gravity) encodes a DnaJ-like protein that potentially interacts with the cytoskeleton’, *Proceedings of the National Academy of Sciences*, 96(3), pp. 1140–1145. Available at: https://doi.org/10.1073/pnas.96.3.1140.

Sessions, A. *et al.* (1997) ‘ETTIN patterns the Arabidopsis floral meristem and reproductive organs’, *Development*, 124(22), pp. 4481–4491. Available at: https://doi.org/10.1242/dev.124.22.4481.

Shi, B. *et al.* (2016) ‘Two-Step Regulation of a Meristematic Cell Population Acting in Shoot Branching in Arabidopsis’, *PLOS Genetics*. Edited by G.P. Copenhaver, 12(7), p. e1006168. Available at: https://doi.org/10.1371/journal.pgen.1006168.

Shih, H.-W. *et al.* (2015) ‘The Cyclic Nucleotide-Gated Channel CNGC14 Regulates Root Gravitropism in Arabidopsis thaliana’, *Current Biology*, 25(23), pp. 3119–3125. Available at: https://doi.org/10.1016/j.cub.2015.10.025.

Shinohara, H. and Matsubayashi, Y. (2013) ‘Chemical Synthesis of Arabidopsis CLV3 Glycopeptide Reveals the Impact of Hydroxyproline Arabinosylation on Peptide Conformation and Activity’, *Plant and Cell Physiology*, 54(3), pp. 369–374. Available at: https://doi.org/10.1093/pcp/pcs174.

Sievers, A., *et al.* (1991) ‘Role of cytoskeleton in gravity perception’, *In Lloyd C. W., Academic Press, London, UK.*, (The cytoskeletal basis of plant growth and form), pp. 169–182.

Simonini, S. *et al.* (2016) ‘A noncanonical auxin-sensing mechanism is required for organ morphogenesis in *Arabidopsis*’, *Genes & Development*, 30(20), pp. 2286–2296. Available at: https://doi.org/10.1101/gad.285361.116.

Simonini, S. *et al.* (2017) ‘Auxin-Induced Modulation of ETTIN Activity Orchestrates Gene Expression in Arabidopsis’, *The Plant Cell*, 29(8), pp. 1864–1882. Available at: https://doi.org/10.1105/tpc.17.00389.

Song, I. *et al.* (1988) ‘Do Starch Statoliths Act as the Gravisensors in Cereal Grass Pulvini?’, *Plant Physiology*, 86(4), pp. 1155–1162. Available at: https://doi.org/10.1104/pp.86.4.1155.

Spartz, A.K. *et al.* (2012) ‘The SAUR19 subfamily of SMALL AUXIN UP RNA genes promote cell expansion’, *The Plant Journal*, 70(6), pp. 978–990. Available at: https://doi.org/10.1111/j.1365-313X.2012.04946.x.

Spartz, A.K. *et al.* (2014) ‘SAUR Inhibition of PP2C-D Phosphatases Activates Plasma Membrane H+-ATPases to Promote Cell Expansion in *Arabidopsis* ’, *The Plant Cell*, 26(5), pp. 2129–2142. Available at: https://doi.org/10.1105/tpc.114.126037.

Stanga, J.P. *et al.* (2009) ‘A Role for the TOC Complex in Arabidopsis Root Gravitropism ’, *Plant Physiology*, 149(4), pp. 1896–1905. Available at: https://doi.org/10.1104/pp.109.135301.

Steinmann, T. *et al.* (1999) ‘Coordinated Polar Localization of Auxin Efflux Carrier PIN1 by GNOM ARF GEF’, *Science*, 286(5438), pp. 316–318. Available at: https://doi.org/10.1126/science.286.5438.316.

Strasser, R. *et al.* (2021) ‘Cracking the “Sugar Code”: A Snapshot of N- and O-Glycosylation Pathways and Functions in Plants Cells’, *Frontiers in Plant Science*, 12. Available at: https://doi.org/10.3389/fpls.2021.640919.

Swarup, R. and Bhosale, R. (2019) ‘Developmental Roles of AUX1/LAX Auxin Influx Carriers in Plants’, *Frontiers in Plant Science*, 10. Available at: https://doi.org/10.3389/fpls.2019.01306.

Szemenyei, H., Hannon, M. and Long, J.A. (2008) ‘TOPLESS Mediates Auxin-Dependent Transcriptional Repression During *Arabidopsis* Embryogenesis’, *Science*, 319(5868), pp. 1384–1386. Available at: https://doi.org/10.1126/science.1151461.

Takahashi, H. *et al.* (2013) ‘Meta-Analyses of Microarrays of Arabidopsis asymmetric leaves1 (as1), as2 and Their Modifying Mutants Reveal a Critical Role for the ETT Pathway in Stabilization of Adaxial–Abaxial Patterning and Cell Division During Leaf Development’, *Plant and Cell Physiology*, 54(3), pp. 418–431. Available at: https://doi.org/10.1093/pcp/pct027.

Takahashi, K., Hayashi, K. and Kinoshita, T. (2012) ‘Auxin Activates the Plasma Membrane H+-ATPase by Phosphorylation during Hypocotyl Elongation in Arabidopsis ’, *Plant Physiology*, 159(2), pp. 632–641. Available at: https://doi.org/10.1104/pp.112.196428.

Takei, K., Sakakibara, H. and Sugiyama, T. (2001) ‘Identification of Genes Encoding Adenylate Isopentenyltransferase, a Cytokinin Biosynthesis Enzyme, inArabidopsis thaliana’, *Journal of Biological Chemistry*, 276(28), pp. 26405–26410. Available at: https://doi.org/10.1074/jbc.M102130200.

Tan, X. *et al.* (2007) ‘Mechanism of auxin perception by the TIR1 ubiquitin ligase’, *Nature*, 446(7136), pp. 640–645. Available at: https://doi.org/10.1038/nature05731.

Taniguchi, M. *et al.* (2017) ‘The Arabidopsis LAZY1 Family Plays a Key Role in Gravity Signaling within Statocytes and in Branch Angle Control of Roots and Shoots’, *The Plant Cell*, 29(8), pp. 1984–1999. Available at: https://doi.org/10.1105/tpc.16.00575.

Taylor, S.C. *et al.* (2019) ‘The Ultimate qPCR Experiment: Producing Publication Quality, Reproducible Data the First Time’, *Trends in*

Biotechnology, 37(7), pp. 761–774. Available at: https://doi.org/10.1016/j.tibtech.2018.12.002.

Thieme, C.J. *et al.* (2015) 'Endogenous Arabidopsis messenger RNAs transported to distant tissues', *Nature Plants*, 1(4), p. 15025. Available at: https://doi.org/10.1038/nplants.2015.25.

Thomas, R.F. (2017) 'A stochastic model of root gravitropism', *PhD, University of Leeds* [Preprint].

Tiwari, S.B., Hagen, G. and Guilfoyle, T.J. (2004) 'Aux/IAA Proteins Contain a Potent Transcriptional Repression Domain', *The Plant Cell*, 16(2), pp. 533–543. Available at: https://doi.org/10.1105/tpc.017384.

Tode, K. and Lüthen, H. (2001) 'Fusicoccin- and IAA-induced elongation growth share the same pattern of K+ dependence.', *Journal of experimental botany*, 52(355), pp. 251–5.

Tsugeki, R. *et al.* (2009) 'NO VEIN Mediates Auxin-Dependent Specification and Patterning in the *Arabidopsis* Embryo, Shoot, and Root', *The Plant Cell*, 21(10), pp. 3133–3151. Available at: https://doi.org/10.1105/tpc.109.068841.

Tsugeki, R. *et al.* (2010) '*NO VEIN* facilitates auxin-mediated development in Arabidopsis', *Plant Signaling & Behavior*, 5(10), pp. 1249–1251. Available at: https://doi.org/10.4161/psb.5.10.12948.

Tsukaya, H. (2019) 'Re-examination of the role of endoreduplication on cell-size control in leaves', *Journal of Plant Research*, 132(5), pp. 571–580. Available at: https://doi.org/10.1007/s10265-019-01125-7.

Uhrig, R.G., Labandera, A.-M. and Moorhead, G.B. (2013) 'Arabidopsis PPP family of serine/threonine protein phosphatases: many targets but few engines', *Trends in Plant Science*, 18(9), pp. 505–513. Available at: https://doi.org/10.1016/j.tplants.2013.05.004.

Ulmasov, T. *et al.* (1997) 'Aux/IAA proteins repress expression of reporter genes containing natural and highly active synthetic auxin response elements.', *The Plant Cell*, 9(11), pp. 1963–1971. Available at: https://doi.org/10.1105/tpc.9.11.1963.

Ung, K.L. *et al.* (2022) 'Structures and mechanism of the plant PIN-FORMED auxin transporter', *Nature*, 609(7927), pp. 605–610. Available at: https://doi.org/10.1038/s41586-022-04883-y.

United Nations (2015) ‘ World Population Prospects: The 2015 Revision, Key Findings and Advance Tables’, *Department of Economic and Social Affairs, Population Division.* , Working paper(ESA/P/WP.241).

Uricaru, R. *et al.* (2015) ‘Reference-free detection of isolated SNPs’, *Nucleic Acids Research*, 43(2), pp. e11–e11. Available at: https://doi.org/10.1093/nar/gku1187.

Ursache, R. *et al.* (2018) ‘A protocol for combining fluorescent proteins with histological stains for diverse cell wall components’, *The Plant Journal*, 93(2), pp. 399–412. Available at: https://doi.org/10.1111/tpj.13784.

Vernoux, T. *et al.* (2011) ‘The auxin signalling network translates dynamic input into robust patterning at the shoot apex’, *Molecular Systems Biology*, 7(1), p. 508. Available at: https://doi.org/10.1038/msb.2011.39.

Vidal, E.A. *et al.* (2010) ‘Nitrate-responsive miR393/ *AFB3* regulatory module controls root system architecture in *Arabidopsis thaliana*’, *Proceedings of the National Academy of Sciences*, 107(9), pp. 4477–4482. Available at: https://doi.org/10.1073/pnas.0909571107.

Voß, U. *et al.* (2015) ‘The circadian clock rephases during lateral root organ initiation in Arabidopsis thaliana’, *Nature Communications*, 6(1), p. 7641. Available at: https://doi.org/10.1038/ncomms8641.

Waidmann, S. *et al.* (2019) ‘Cytokinin functions as an asymmetric and anti-gravitropic signal in lateral roots’, *Nature Communications*, 10(1), p. 3540. Available at: https://doi.org/10.1038/s41467-019-11483-4.

Waite, J.M. and Dardick, C. (2018) ‘TILLER ANGLE CONTROL 1 modulates plant architecture in response to photosynthetic signals’, *Journal of Experimental Botany*, 69(20), pp. 4935–4944. Available at: https://doi.org/10.1093/jxb/ery253.

Wang, Hai and Wang, Haiyang (2015) ‘Multifaceted roles of FHY3 and FAR1 in light signaling and beyond’, *Trends in Plant Science*, 20(7), pp. 453–461. Available at: https://doi.org/10.1016/j.tplants.2015.04.003.

Wang, J. *et al.* (2017) ‘Cytokinin Signaling Activates WUSCHEL Expression during Axillary Meristem Initiation’, *The Plant Cell*, 29(6), pp. 1373–1387. Available at: https://doi.org/10.1105/tpc.16.00579.

Wang, L. *et al.* (2022) ‘Connected function of PRAF/RLD and GNOM in membrane trafficking controls intrinsic cell polarity in plants’, *Nature*

Communications, 13(1), p. 7. Available at: https://doi.org/10.1038/s41467-021-27748-w.

Wang, M. *et al.* (2019) 'BRANCHED1: A Key Hub of Shoot Branching', *Frontiers in Plant Science*, 10. Available at: https://doi.org/10.3389/fpls.2019.00076.

Wang, Y. *et al.* (2014) 'The Stem Cell Niche in Leaf Axils Is Established by Auxin and Cytokinin in *Arabidopsis*', *The Plant Cell*, 26(5), pp. 2055–2067. Available at: https://doi.org/10.1105/tpc.114.123083.

Wang, Y. and Jiao, Y. (2018) 'Axillary meristem initiation — a way to branch out', *Current Opinion in Plant Biology*, 41, pp. 61–66. Available at: https://doi.org/10.1016/j.pbi.2017.09.001.

Wasson, A.P. *et al.* (2012) 'Traits and selection strategies to improve root systems and water uptake in water-limited wheat crops', *Journal of Experimental Botany*, 63(9), pp. 3485–3498. Available at: https://doi.org/10.1093/jxb/ers111.

Went, F.W. (1926) 'On Growth-Accelerating Substances in the Coleoptile of Avena sativa', *Proceedings of the Section of Sciences, Koninklijke Akademie van Wetenschappen te Amsterdam*, 30, pp. 10–18.

Wilson, A.K. *et al.* (1990) 'A dominant mutation inArabidopsis confers resistance to auxin, ethylene and abscisic acid', *Molecular and General Genetics MGG*, 222(2–3), pp. 377–383. Available at: https://doi.org/10.1007/BF00633843.

de Wit, M., Galvão, V.C. and Fankhauser, C. (2016) 'Light-Mediated Hormonal Regulation of Plant Growth and Development', *Annual Review of Plant Biology*, 67(1), pp. 513–537. Available at: https://doi.org/10.1146/annurev-arplant-043015-112252.

Xin, W. *et al.* (2017) 'Dynamic expression reveals a two-step patterning of WUS and CLV3 during axillary shoot meristem formation in Arabidopsis', *Journal of Plant Physiology*, 214, pp. 1–6. Available at: https://doi.org/10.1016/j.jplph.2017.03.017.

Yamaguchi, T., Nukazuka, A. and Tsukaya, H. (2012) 'Leaf adaxial-abaxial polarity specification and lamina outgrowth: evolution and development', *Plant and Cell Physiology*, 53(7), pp. 1180–1194. Available at: https://doi.org/10.1093/pcp/pcs074.

Yamamoto, K. and Kiss, J.Z. (2002) ‘Disruption of the Actin Cytoskeleton Results in the Promotion of Gravitropism in Inflorescence Stems and Hypocotyls of Arabidopsis’, *Plant Physiology*, 128(2), pp. 669–681. Available at: https://doi.org/10.1104/pp.010804.

Yoder, T.L. *et al.* (2001) ‘Amyloplast Sedimentation Dynamics in Maize Columella Cells Support a New Model for the Gravity-Sensing Apparatus of Roots’, *Plant Physiology*, 125(2), pp. 1045–1060. Available at: https://doi.org/10.1104/pp.125.2.1045.

Yoshihara, T. and Spalding, E.P. (2017) ‘LAZY Genes Mediate the Effects of Gravity on Auxin Gradients and Plant Architecture’, *Plant Physiology*, 175(2), pp. 959–969. Available at: https://doi.org/10.1104/pp.17.00942.

Yoshihara, T., Spalding, E.P. and Iino, M. (2013) ‘AtLAZY1 is a signaling component required for gravitropism of the *Arabidopsis thaliana* inflorescence’, *The Plant Journal*, 74(2), pp. 267–279. Available at: https://doi.org/10.1111/tpj.12118.

Yu, B. *et al.* (2007) ‘TAC1, a major quantitative trait locus controlling tiller angle in rice’, *The Plant Journal*, 52(5), pp. 891–898. Available at: https://doi.org/10.1111/j.1365-313X.2007.03284.x.

Žádníková, P. *et al.* (2010) ‘Role of PIN-mediated auxin efflux in apical hook development of *Arabidopsis thaliana*’, *Development*, 137(4), pp. 607–617. Available at: https://doi.org/10.1242/dev.041277.

Zentella, R. *et al.* (2017) ‘The Arabidopsis O-fucosyltransferase SPINDLY activates nuclear growth repressor DELLA’, *Nature Chemical Biology*, 13(5), pp. 479–485. Available at: https://doi.org/10.1038/nchembio.2320.

Zhang, Y. *et al.* (2019) ‘Evolution of fast root gravitropism in seed plants’, *Nature Communications*, 10(1), p. 3480. Available at: https://doi.org/10.1038/s41467-019-11471-8.

Zieschang, HannaE., Kohler, K. and Sievers, A. (1993) ‘Changing proton concentrations at the surfaces of gravistimulated Phleum roots’, *Planta*, 190(4). Available at: https://doi.org/10.1007/BF00224794.

Zourelidou, M. *et al.* (2014) ‘Auxin efflux by PIN-FORMED proteins is activated by two different protein kinases, D6 PROTEIN KINASE and PINOID’, *eLife*, 3. Available at: https://doi.org/10.7554/eLife.02860.

Zwiewka, M. *et al.* (2019) ‘The Nuts and Bolts of PIN Auxin Efflux Carriers’, *Frontiers in Plant Science*, 10. Available at: https://doi.org/10.3389/fpls.2019.00985.